wang

ATTENUATION OF SEISMIC WAVES IN ROCKS AND APPLICATIONS IN ENERGY EXPLORATION

A DISSERTATION

SUBMITTED TO THE DEPARTMENT OF GEOPHYSICS

AND THE COMMITTEE ON GRADUATE STUDIES

OF STANFORD UNIVERSITY

IN PARTIAL FULFILLMENT OF THE REQUIREMENTS

FOR THE DEGREE OF

DOCTOR OF PHILOSOPHY

By

Einar Kjartansson

December 1979

printed as Stanford Exploration Project Report No. 23

and as Stanford Rock Physics Project Report No. 8

ABSTRACT

One of the least understood aspects of seismic wave propagation in the earth is the absorption or dissipation of wave energy into heat. This study presents results relating to four aspects of this problem.

The first is the development of a mathematical description for the general elastic response and wave propagation in materials where the specific loss or Q factor is exactly independent of frequency. From the fundamental constraints of linearity and causality, relations for the frequency-dependence of velocity and for the evolution of transient pulses are developed. The case where Q varies slowly with frequency is also treated, as well as the effects of Q on reflection coefficients at interfaces between two different materials.

Next we take a close look at one particular mechanism for the dissipation of energy, thermal relaxation. This mechanism, which affects compressional waves more than shear waves, is highly sensitive to the state and the nature of the pore fluids. When the pore fluid is water, a rapid increase of attenuation with temperature is expected, up to the boiling point. When the pore space contains mixtures of gas and liquid phases, the attenuation is sensitive to pore pressure and gas saturation in a manner that complements the dependence of velocity on these variables. Especially large losses are expected when small amounts of gas are introduced into an otherwise liquid-saturated rock. Solubility of the gas in the liquid and phase transitions leads to an even greater absorption.

The third section deals with wave propagation in media where attenuation and velocity are spatially heterogeneous. Finite-difference solutions to the wave equation, similar to those used in the oil-exploration industry in the migration of seismic reflection data, are developed to include the effects of absorption, as well as arbitrary spatial heterogeneities. This makes it possible to model the seismic response for geologically realistic situations.

Finally, methods are developed to extract information about spatial variations of attenuation and velocities from seismic reflection data. The approach used is similar to that used in medical tomography. The application of the inversions to amplitude and traveltime data from unstacked common-

midpoint reflection data, yields detailed pictures of the subsurface. The interpreted attenuation and velocity anomalies show correlations with diffractions observed on the common-offset reflection sections.

ACKNOWLEDGMENTS

In the course of this study I have benefitted greatly from interaction with many individuals.

Amos Nur provided advice and support throughout this study; the entire thesis has benefitted from his intuition and insights.

The final two chapters are largely based on concepts originated by Jon F. Claerbout. It has been a great privilege to enjoy his advice. The advice of Robert Stolt has also been of great value in the final phase of this work.

My understanding of seismic absorption was developed through conversations with Michael Gladwin, Gary Mavko, Kenneth Winkler, Clay Harter and Roger Denlinger.

The imaging concepts in Chapter VI are based on suggestions made by Fabio Rocca while he was visiting at Stanford.

The work with the field data was made possible by Ralph Shuey of Gulf Science and Technology Company, who provided the data.

Much needed editing and general assistance in the production of this thesis was provided by Jo Ann Heydron.

Finally, I wish the express my appreciation to my wife Marcia and my son Bjarni for their patience and support throughout our stay at Stanford.

My study at Stanford was made possible by the financial support provided by the Cecil and Ida Green Fellowship in Geophysics and by the members of the Stanford Exploration Project and Stanford Rock Physics Project. Part of this work was also supported by National Science Foundation grant EAR 76-22501 and by the U.S. Department of Energy, Office of Basic Energy Sciences contract EY-76-03-0325.

TABLE OF CONTENTS

Chapter I

INTRODUCTION

One of the fundamental aspects of elastic wave propagation in all materials, and in rocks in particular, is the absorption and irreversible conversion of wave energy into heat. A large body of experimental knowledge indicates that the distance that a wave propagates in any rock is roughly proportional to the wavelength. Although the fraction of energy dissipated during each cycle is, thus, nearly independent of frequency, the loss in rocks is highly variable from one rock to another and it is also sensitive to changes in the environmental conditions. The specific loss factor, Q, has, for example, been known to change by several orders of magnitude when a nominally dry sample is placed under vacuum.

The ultimate resolution that can be achieved in any seismic experiment is related to the intrinsic attenuation. For a given signal-to-noise ratio, the resolution is basically a function of Q. As an example, it has been suggested that the use of shear waves in reflection seismology might give better resolution than obtained using P-waves, because the lower velocity of S-waves would imply shorter wavelengths. This hope was not realized since the attenuation for shear waves is usually no less than for P-waves, and the usable propagation distance is thus no greater when measured in wavelengths.

In recent years it has been recognized that attenuation and velocity are related in such a way that a full understanding of traveltimes or other observations that have traditionally been used to infer velocities requires a knowledge of the absorption properties. This applies particularly when the mechanical response of the same material is measured at widely separate frequencies or time scales. For example, information about the response of the mantle comes from plate tectonics, postglacial uplift, Chandler wobble, free oscillations and body waves. In order to relate observations in one of those bands to those in another, the effects of anelasticity must be accounted for.

A similar situation exists in exploration seismology where one wants to relate observations from reflection experiment in the range of a few tens of hertz, results from well logs at a few kilohertz and ultrasonic measurements

on cores at frequencies around one megahertz.

In order to estimate attenuation from observational data, it is necessary to make some assumptions about the velocity structures. Numerous small-scale inhomogeneities can cause apparent attenuation through scattering and intrabed multiple reflections [Schoenberger and Levin, 1978]. In estimating attenuation and velocity from observations, there is considerable trade-off between absorption and velocity in that a given set of observations may often be satisfied either by a simple attenuation structure and a complex velocity structure, or a more complex attenuation structure and a simpler velocity structure. It follows that in order to obtain optimum estimates of either velocity or attenuation, an estimate of the other is also needed.

In the first chapters of this thesis, the constraints of linearity and causality are applied to obtain fundamental relations between velocities at different frequencies when the specific loss factor, or Q, is either independent of, or slowly varying with, frequency. The implications for transient pulse propagation and reflections are explored in some detail.

Chapter V presents a close look at a particular mechanism for absorption in heterogeneous media, thermal relaxation and phase transitions involving pore fluids. This is a well-known mechanism for absorption in solids; however, our results indicate that the presence of fluids will greatly increase the effect of this loss mechanism. A review of other mechanisms is given by Mavko et al. [1979].

In Chapter VI, numerical techniques for the computation of wave propagation in inhomogeneous media are developed which include the effects of absorption. The approach chosen for this turns out to be advantageous for wavefield extrapolation in heterogeneous media even when the effects of absorption are not included, and has been extensively used to migrate reflection data collected by the Consortium for Continental Reflection Profiling (COCORP) [Lynn et al. 1979; Lynn, 1979].

In the final chapter methods are developed to determine details of the spatial variations of wave-propagation parameters above a strong reflecting horizon from multichannel seismic reflection data. The theory is equally applicable to attenuation and velocity. Application of these inversion

methods to data from a producing gas field shows a detailed pattern of amplitude and velocity variations which correlate with each other and with reflections observed on common-offset seismic sections.

Not only is it desirable from a theoretical viewpoint to consider velocity and attenuation together, but it also turns out that some of the methods that work best for modeling or inversion of attenuation also give very good results when applied to velocity data.

Chapter II

CONSTANT Q -- WAVE PROPAGATION AND ATTENUATION

A fundamental feature associated with the propagation of stress waves in all real materials is the absorption of energy and the resulting change in the shape of transient waveforms. Although a large number of papers have been written on the absorption of seismic waves in rocks, little, if any, general agreement exists about even the most fundamental properties of the processes involved. Table 2.1 shows a summary of the basic features of some of the different attenuation theories.

Early laboratory work on absorption in rocks showed the loss per cycle or wavelength to be essentially independent of frequency. Since at that time no known linear theory could fit this observation, Born [1941] proposed that the loss was due to rate-independent friction of the same kind as observed when two surfaces slide against each other. Kolsky [1956] and Lomnitz [1957] gave linear descriptions of the absorption that could account for the observed frequency-independence and were also consistent with other independent observations of the transient creep in rocks and the change in shape of pulses propagating through thin rods. Despite this and the fact that a satisfactory nonlinear friction model for attenuation has never been developed to the point where meaningful predictions could be made about the propagation of waves, nonlinear friction is commonly assumed to be the dominant attenuation mechanism, especially in crustal rocks [McDonal et al., 1958, Knopoff, 1964; White, 1966; Gordon and Davis, 1968; Lockner et al., 1977; Johnston and Toksoz, 1977].

A different type of theory for attenuation has been advocated by Ricker [1953, 1977]. In his model the absorption is described by adding a single term to the wave equation. Because of this simplicity, the theory of the propagation of transient waves has been further developed than for the other theories. For this reason, wavelets based on the Ricker theory have been commonly used in the computation of synthetic seismograms [Boore et al., 1971; Munasinghe and Farnell, 1973], although the frequency-dependence of Q that is implied by the model contradicts practically all experimental observations.

Property	Theory			
	Friction	Voigt-Ricker	NCQ Band-Limited Near-Constant Q	CQ Linear Constant Q
Linearity	Nonlinear, velocity and Q depend on amplitude	Linear	Linear	Linear
Frequency dependence of Q	Independent	$1/Q \propto \omega$	Nearly independent in a frequency band	Independent
Frequency dependence of phase velocity	Independent	Independent at low frequencies	$C/C_0 \approx 1 + (1/\pi Q) \ln (\omega/\omega_0)$	$C/C_0 = (\omega/\omega_0)^\gamma$
Transient creep	None	$\Psi(t) \propto e^{-at}$	$\Psi(t) \approx (1/M_0)[1 + (2/\pi Q) \ln (1 + at)]$	$1/Q = \tan (\pi\gamma)$ $\Psi(t) \propto t^{2\gamma}$
Pulse broadening	Distorted or acausal	$\tau \propto T^{1/3}$	$\tau \propto T$	$\tau \propto T$
References	*Born* [1941]	*Voigt* [1892]	*Kolsky* [1956]	*Bland* [1960]
	Knopoff [1964]	*Ricker* [1953, 1977]	*Lomnitz* [1957]	*Strick* [1967]
	White [1966]	*Collins* [1960]	*Futterman* [1962]	This paper
	Walsh [1966]	*Clark and Rupert* [1960]	*Azimi et al.* [1968]	
	Lockner et al. [1977]	*Jaramillo and Colvin* [1970]	*Strick* [1967, 1970]	
	Johnston and Toksöz [1977]	*Balch and Smolka* [1970]	*Liu et al.* [1976]	
	Gordon and Davis [1968]		*Kanamori and Anderson* [1977]	
			Minster [1978a]	

TABLE 2.1. Comparison of attenuation theories.

In this paper, we will discuss some of the data Ricker interpreted as in support of his theory.

Recently, there has been renewed interest in the effects of anelasticity on wave propagation in rocks. Liu et al. [1976] found that the change in the elastic moduli implied by attenuation over the frequency range covered by seismic body waves and free oscillations, was about an order of magnitude greater than the uncertainty in the measurements. The models used by Liu et al. [1976], as well as all of the other nearly constant Q (NCQ) models, have included at least one parameter that is in some way related to the range of frequencies over which the model gives Q nearly independent of frequency. How this cutoff is chosen appears to be quite arbitrary and the physical implications of the cutoff parameters are different between the models of Lomnitz [1957], Futterman [1962], Strick [1967], and Liu et al. [1976].

In this paper a linear description of the attenuation is given, that features Q exactly independent of frequency, without any cutoffs. The constant Q (CQ) model is mathematically much simpler than any of the NCQ models; it is completely specified by two parameters, i. e. phase velocity at an arbitrary reference frequency, and Q.

Most of the NCQ papers have described wave phenomena in the frequency-domain and have restricted their analysis to cases where Q is large ($Q > 30$). In contrast, the simplicity of the CQ description allows the derivation of exact analytical expressions for the various frequency-domain properties, such as the complex modulus, phase velocity, and the attenuation coefficient, that are valid over any range of frequencies and for any positive value of Q. In this paper more emphasis will be placed on the time-domain description of transient phenomena, and exact expressions for the creep and relaxation functions and scaling relations for the transient wave pulse will be given. In addition, approximate expressions will be given for the impulse response, as a function of time, that results from a delta-function excitation.

We will also show that when the frequency range is restricted and the losses are small, the results obtained from the various NCQ theories approach the same limit as those obtained from the CQ theory.

Definitions and Background

Seismic attenuation is commonly characterized by the quality parameter Q. It is most often defined in terms of the maximum energy stored during a cycle, divided by the energy lost during the cycle. When the loss is large this definition becomes impractical; O'Connell and Budiansky [1978] suggested a definition in terms of the mean stored energy W and the energy loss ΔW, during a single cycle of sinusoidal deformation.

$$Q = \frac{4\pi W}{\Delta W} \tag{2.1}$$

When this definition is used, Q is related to the phase angle between stress and strain, δ, according to

$$\frac{1}{Q} = \tan \delta \tag{2.2}$$

The fact that amplitude-dependence of the propagation velocity and Q at strains less than 10^{-6} has not been observed, strongly suggests that at these amplitudes the material response is dominated by linear effects, or in other words, the strain that results from a superposition of two stress functions is equal to the sum of the strains that result from the application of each stress function separately. When two effects are linearly related, the relationship may be expressed through a convolution. Thus the relationship between stress and strain in a linear material may be expressed as

$$\sigma(t) = m(t) * \epsilon(t) \tag{2.3}$$

$$\epsilon(t) = s(t) * \sigma(t) \tag{2.4}$$

where $\sigma(t)$ is the stress as a function of time, $\epsilon(t)$ is the strain, and m(t) and s(t) are real functions that vanish for negative time. The convolution operator * is defined by

$$f(t) * g(t) = \int_{-\infty}^{\infty} f(t-t')g(t')dt' \tag{2.5}$$

The relationship between stress and strain given in (2.3) and (2.4) was first given by Boltzmann [1876]. Our notation differs from Boltzmann's original notation only in that the functions m(t) and s(t) may include generalized functions such as the Dirac delta function or its derivatives. Combination of (2.3) and (2.4) implies that m(t) and s(t) must satisfy the condition

$$\delta(t) = m(t) * s(t) \tag{2.6}$$

where $\delta(t)$ is the Dirac delta function.

Manipulations involving convolutions are usually facilitated by the use of the Fourier transform. We will use lower case letters to designate functions of time and capital letters for their Fourier transforms according to the definition

$$F(\omega) = \int_{-\infty}^{\infty} f(t)\, e^{-i\omega t} dt \tag{2.7}$$

The inverse Fourier transform is then given by

$$f(t) = \frac{1}{2\pi} \int_{-\infty}^{\infty} F(\omega)\, e^{i\omega t} d\omega \tag{2.8}$$

Bracewell [1965] gives a discussion of the formalism required for the extension to generalized functions.

Using the convolution theorem [Bracewell, 1965; p. 108], equations (2.3), (2.4) and (2.6) may be rewritten:

$$\Sigma(\omega) = M(\omega)E(\omega) \tag{2.9}$$

$$E(\omega) = S(\omega)\Sigma(\omega) \tag{2.10}$$

$$1 = M(\omega)S(\omega) \tag{2.11}$$

where $\Sigma(\omega)$ is the Fourier transform of the stress, $E(\omega)$ is the Fourier

transform of the strain, and $M(\omega)$ and $S(\omega)$ are the Fourier transforms of $m(t)$ and $s(t)$. Thus, the stress and the strain are in the frequency-domain related through a multiplication by a modulus $M(\omega)$ or compliance $S(\omega)$ just as in the purely elastic case, the only difference being that the modulus may be complex and frequency-dependent. This relationship is commonly referred to as the correspondence principle. By the substitution of a unit step function into (2.3) and (2.4), it is easily shown that $m(t)$ and $s(t)$ are the first time derivatives of the relaxation and creep functions, where the relaxation function, $\bar{\Psi}(t)$, is the stress that results from a unit step in strain, and the creep function, $\Psi(t)$, is the strain that results from a unit step in stress.

When the stress-strain relations are combined with the equilibrium equation, the resulting one-dimensional wave equation has a solution that may be written in a form analogous to the classical case:

$$U(t,x) = \exp[i(\omega t - kx)] \tag{2.12}$$

where

$$k = \omega \left(\frac{\rho}{M(\omega)}\right)^{\frac{1}{2}} \tag{2.13}$$

and ρ is the density of the material.

The Constant Q Model

The development so far has been completely general; no assumptions other than linearity and causality have been made about the properties of the material. We will now examine a particular form for the stress-strain relationships and show that it leads to a Q that is independent of frequency. Frequency-independent Q implies that the loss per cycle is independent of the time scale of oscillation; therefore it might seem reasonable to try a material that has a creep function that plots as a straight line on a log-log plot, or

$$\Psi(t) \propto t^{b}$$

For the sake of convenience in subsequent manipulations, we will use a creep function of the form

$$\Psi(t) = \frac{1}{M_0\Gamma(1+2\gamma)}\left(\frac{t}{t_0}\right)^{2\gamma} \qquad t > 0 \qquad (2.14)$$

$$\Psi(t) = 0 \qquad t < 0$$

Γ is the gamma function which in all cases of interest to us has a value close to unity and t_0 is an arbitrary reference time introduced so that when t has the dimension of time, M_0 will have the dimension of modulus. Some of the properties of a material that has this creep function are discussed by Bland [1960, p.54]. Response functions of this form have also been used to model dielectric losses in solids [Jonscher, 1977]. Differentiation of the expression in (2.14) yields

$$s(t) = \frac{2\gamma}{M_0\Gamma(1+2\gamma)}\left(\frac{t}{t_0}\right)^{2\gamma}\frac{1}{t} \qquad t > 0 \qquad (2.15)$$

$$s(t) = 0 \qquad t < 0$$

Taking the Fourier transform we get

$$S(\omega) = \frac{1}{M_0}\left(\frac{i\omega}{\omega_0}\right)^{-2\gamma} \qquad (2.16)$$

where

$$\omega_0 = \frac{1}{t_0} \qquad (2.17)$$

Using (2.11) we get

$$M(\omega) = M_0\left(\frac{i\omega}{\omega_0}\right)^{2\gamma} = M_0\left|\frac{\omega}{\omega_0}\right|^{2\gamma}\exp[i\pi\gamma\ \mathrm{sgn}(\omega)] \qquad (2.18)$$

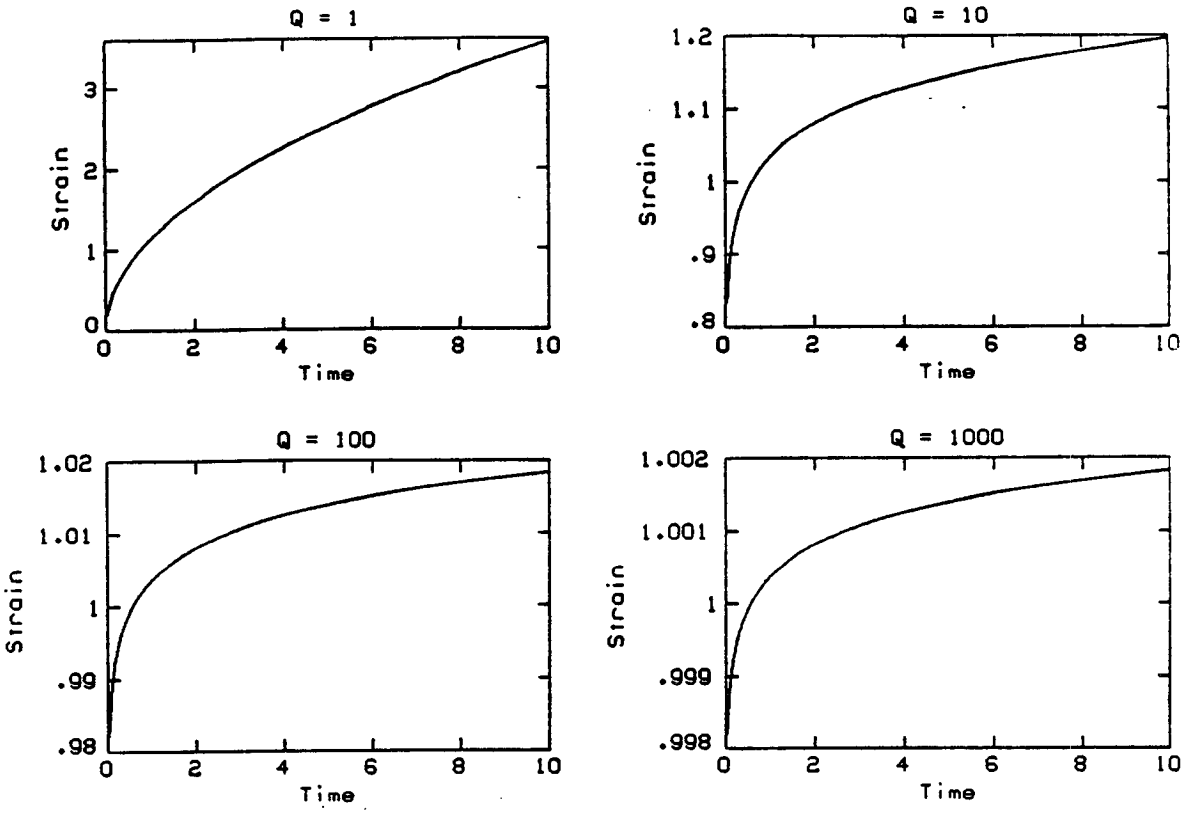

FIG. 2.1. The constant Q creep function as given by equation (2.14), in units of $1/M_0$, plotted versus time in units of t_0.

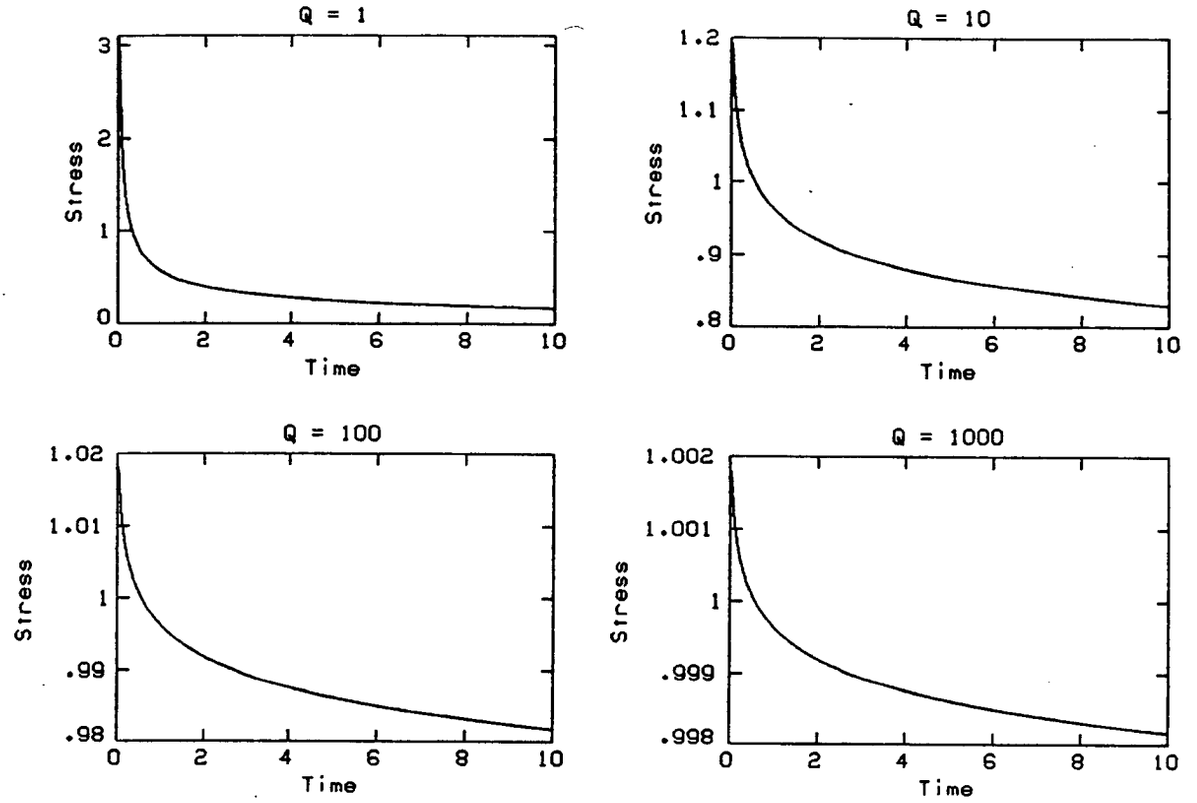

FIG. 2.2. The constant Q relaxation function as given by equation (2.20), in units of M_0, plotted versus time in units of t_0.

where

$$\mathrm{sgn}(\omega) = 1 \qquad \omega > 0 \tag{2.19}$$

$$\mathrm{sgn}(\omega) = -1 \qquad \omega < 0$$

Taking the inverse Fourier transform of $M(\omega)$ and integrating, we get the relaxation function

$$\bar{\Psi}(t) = \frac{M_0}{\Gamma(1-2\gamma)}\left(\frac{t}{t_0}\right)^{-2\gamma} \qquad t > 0 \tag{2.20}$$

$$\bar{\Psi}(t) = 0 \qquad t < 0$$

Figure 2.1 shows a plot of the constant Q creep function (2.14), and figure 2.2, of the relaxation function (2.20), for several values of Q. Equation (2.18) shows that the argument of the modulus and thus the phase angle beween the stress and the strain, is independent of frequency; therefore, it follows from the definition of Q (2.2) that Q is independent of frequency:

$$\frac{1}{Q} = \tan(\pi\gamma) \tag{2.21}$$

or

$$\gamma = \frac{1}{\pi}\tan^{-1}\left(\frac{1}{Q}\right) \simeq \frac{1}{\pi Q} \tag{2.22}$$

The approximation is valid when $Q^{-2} << 1$. Since both the creep and relaxation functions vanish for negative time, no strain can precede applied stress, nor can any stress precede applied strain; the material is causal.

To investigate the propagation of waves in the constant Q material, the modulus given by (2.18) may be substituted into the solution to the one-dimensional wave equation, given by (2.12) and (2.13); the result may be written as

$$U(t,x) = e^{-\alpha x} e^{i\omega(t-x/c)} \tag{2.23}$$

where

$$c = c_0 \left| \frac{\omega}{\omega_0} \right|^{\gamma} \tag{2.24}$$

$$\alpha = \tan\left(\frac{\pi\gamma}{2}\right) \mathrm{sgn}(\omega) \frac{\omega}{c} \tag{2.25}$$

$$c_0 = \frac{\left(\frac{M_0}{\rho}\right)^{\frac{1}{2}}}{\cos\left(\frac{\pi\gamma}{2}\right)} \tag{2.26}$$

Since c is slightly dependent on frequency, constant Q is not exactly equivalent to assuming that α is proportional to frequency, as is often assumed in the literature. It is clear from (2.24) that c_0 is simply the phase velocity at the arbitrary reference frequency ω_0. In the final section of the paper, we discuss the low- and high-frequency limits for the phase velocity and the modulus, and the short- and long-term behavior of the creep function.

An alternative to (2.23) is to write the solution to the wave equation as

$$U(x,t) = \exp\left[i\omega \left(t - \frac{x}{c_s (i\omega)^{\gamma}} \right) \right] \tag{2.27}$$

where c_s is a constant related to M_0 by

$$c_s = \left(\frac{M_0}{\rho}\right)^{\frac{1}{2}} \omega_0^{-\gamma} \tag{2.28}$$

Use of the complex velocity notation, as in (2.27), often simplifies the algebra, e.g. in the derivation of reflection coefficients or when modeling wave propagation in two or three dimensions.

As most wave phenomena encountered in seismology are transient in nature, a time-domain description of wave propagation is often more useful for modeling or comparison with data than a frequency-domain description. The waveform that results from a delta-function source, the impulse response, is particularly useful since the waveform that results from an arbitrary source is obtained by simply convolving the source with the impulse response. The Fourier transform of the impulse response, b(t), is obtained by omitting the $i\omega t$ term in (2.12) or (2.23):

$$B(\omega) = e^{-\alpha x} e^{-i\omega x/c} \tag{2.29}$$

By the substitution of (2.24) and (2.25) into (2.29), we get

$$B(\omega) = \exp\left\{ - \frac{x\omega_0}{c_0} \left| \frac{\omega}{\omega_0} \right|^{1-\gamma} \left[\tan\left(\frac{\pi\gamma}{2}\right) + i \, \mathrm{sgn}(\omega) \right] \right\} \tag{2.30}$$

The impulse response may be obtained by taking the inverse Fourier transform of $B(\omega)$ given by (2.30). Although we do not have an analytical expression for b(t), we will present a useful approximate relation and some exact scaling relations. We will rewrite (2.30) as

$$B(\omega) = B_1(\omega_1) \tag{2.31}$$

where

$$\omega_1 = t_1 \omega \tag{2.32}$$

$$t_1 = t_0 \left(\frac{x\omega_0}{c_0} \right)^{\beta} \tag{2.33}$$

$$\beta = \frac{1}{1-\gamma} \simeq 1 + \frac{1}{\pi Q} \tag{2.34}$$

and

$$B_1(\omega) = \exp\left\{ - |\omega|^{1-\gamma} \left[\tan\left(\frac{\pi\gamma}{2}\right) + i \, \mathrm{sgn}(\omega) \right] \right\} \tag{2.35}$$

It now follows from the similarity theorem [Bracewell, 1965; p. 101] that for any homogeneous material, the impulse response at any distance x from the source will be given by

$$b(t,x) = \frac{1}{t_1} b_1\left(\frac{t}{t_1}\right) \tag{2.36}$$

Equations (2.36) and (2.33) imply that in a given material, the traveltime T, the pulse width τ, and the pulse amplitude A are related according to

$$T \propto \tau \propto \frac{1}{A} \propto \left(\frac{x}{c_0}\right)^{\beta} \tag{2.37}$$

where any consistent operational definitions for the traveltime and pulse width may be used. The proportionality between traveltime and pulse width may be expressed as

$$\tau = C(Q)\frac{T}{Q} \tag{2.38}$$

where C(Q) is a function that depends only on Q. We will show that C(Q) is nearly constant for $Q > 20$. Figure 2.3 shows a plot of the function $b_1(t)$, for several values of Q.

In order to illustrate the scaling relations, seismograms due to impulsive sources at several distances are plotted on a common set of axes in figure 2.4. Figure 2.5 shows the same information but scaled according to distance, by dividing the time by the distance and multiplying the displacement by the distance. Velocity dispersion has the effect of delaying the pulses from the more distant sources more than would be expected for a constant propagation velocity. To further illustrate the dispersion, figure 2.6 shows the results of the same kind of numerical experiment as figure 2.5, for a Q of 1000 and covering a larger range of distances. It may be concluded from figures 2.5 and 2.6 that the dispersion due to the anelasticity is directly observable in the time domain when the traveltime, in a homogeneous material, can be measured to within half a pulse width over a ratio of 10 in distance. This applies to high Q as well as to low Q materials. To measure this effect

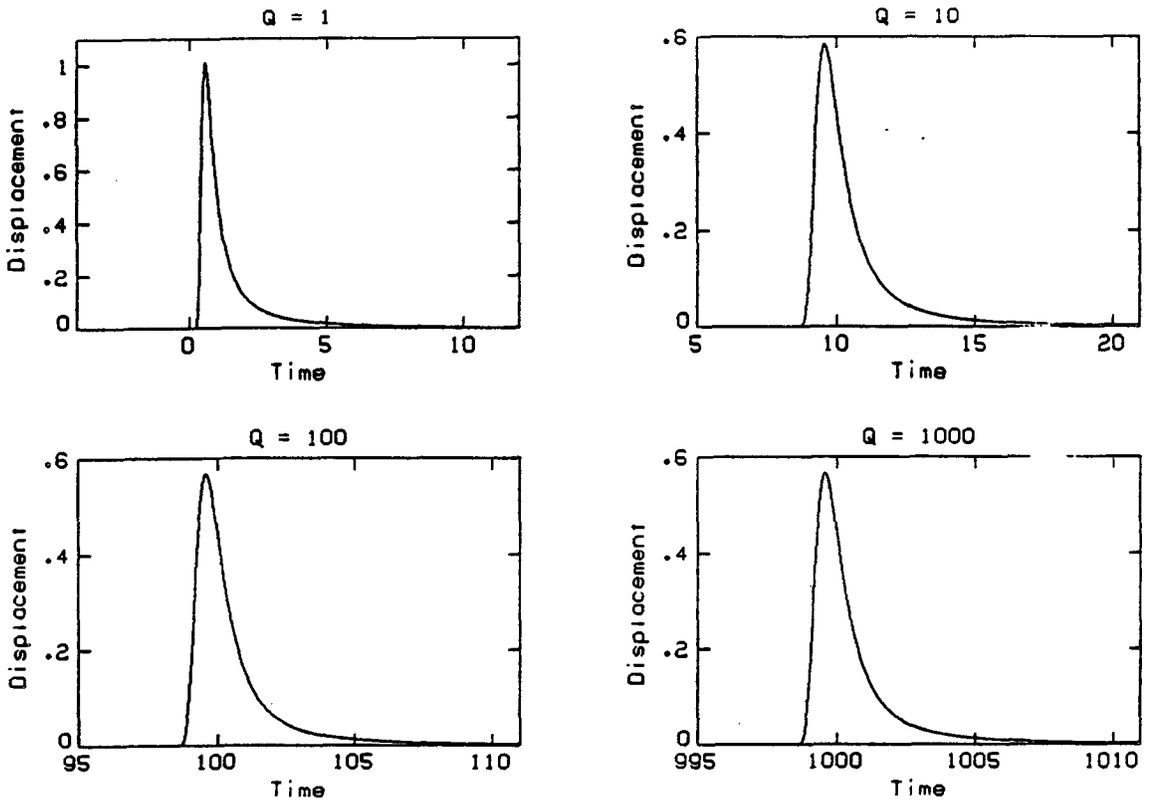

FIG. 2.3. The waveform b(t), resulting from a unit impulse plane-wave source at $x = Qc_0$, is plotted versus time in units of t_0. The waveform is computed using a numerical FFT algorithm.

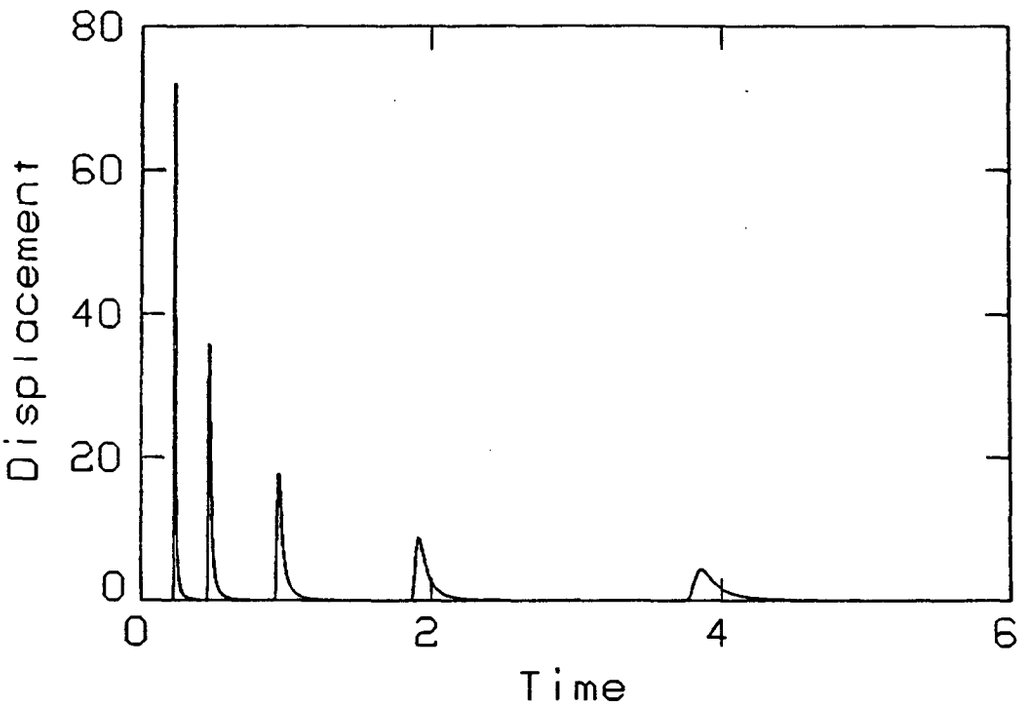

FIG. 2.4. Seismograms resulting from sources at distances of 0.25, 0.5, 1, 2 and 4 times c_0. Q is 30.

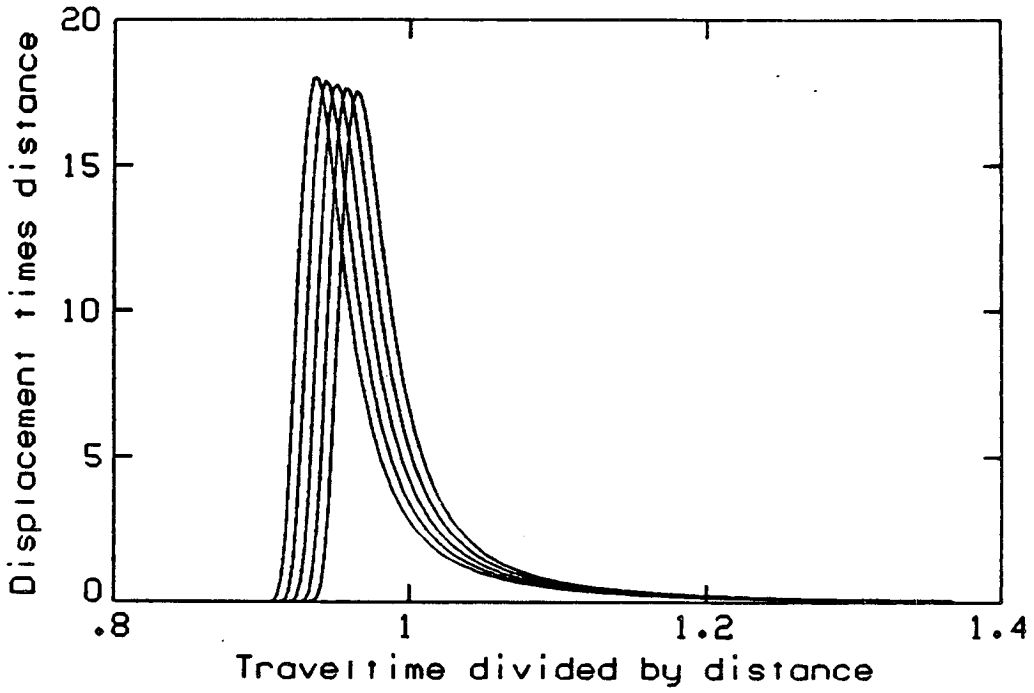

FIG. 2.5. Same seismograms as in figure 2.4, but plotted as displacement times distance versus time divided by distance. The seismograms do not overlap due to velocity dispersion.

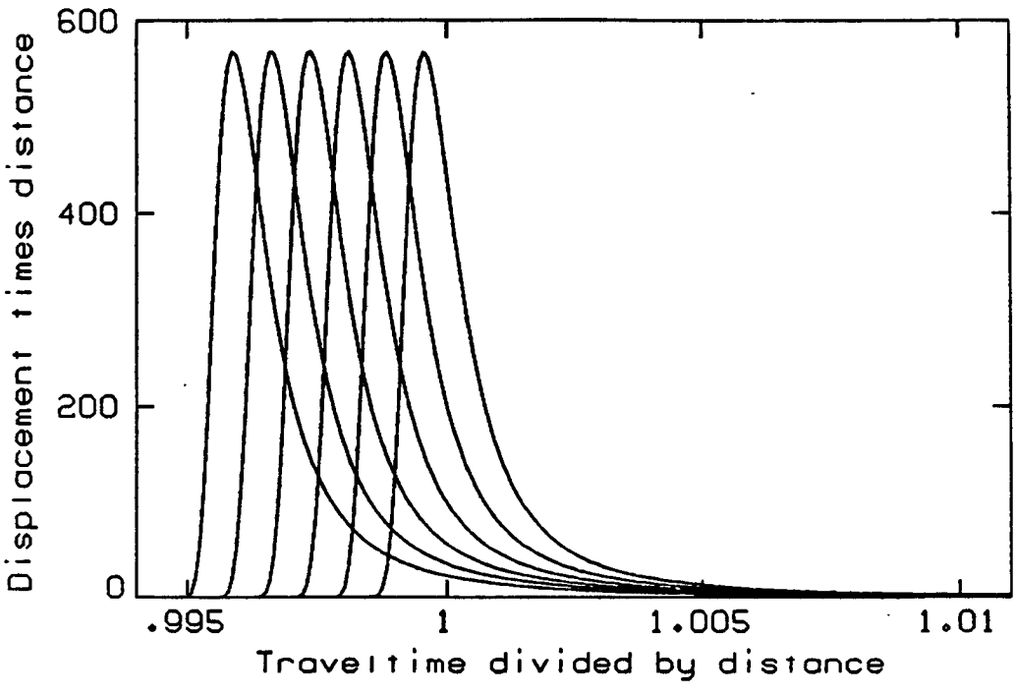

FIG. 2.6. Seismograms resulting from sources at distances of 0.01, 0.1, 1, 10, 100, and 1000 times c_0 plotted in the same manner as in figure 2.5, for Q = 1000. This shows that the dispersion effect, relative to the pulse width, is independent of Q when Q >> 1.

in the earth would, however, require a careful control over the spatial variation in velocity.

The required control may be obtained when the wave travels the same path more than once. Waves reflected off the core-mantle interface may satisfy this condition for stations near the source. Assuming an average $Q = 160$ and a traveltime of 936 seconds for one pass of ScS [Jordan and Sipkin, 1977], we obtain by a substitution into (2.34) a value for $\beta = 1.0020$. Equation (2.37) implies then that doubling the distance will result in a total traveltime of 1874.6 seconds for ScS_2, which is 2.6 seconds longer than would be expected if the dispersion were not present.

Approximations for Time-Domain Wavelets

So far we have made no assumptions about the value of Q (other than $Q > 0$), or the ranges of frequencies and traveltimes involved. Although we have been able to derive exact expressions for all frequency-domain properties of the wave propagation, we do not have exact analytical expressions for time-domain wavelets or impulse responses. While modern computer techniques (e.g. the fast-Fourier-transform algorithm) make it relatively easy to transform data to the frequency domain and back, it is still useful to study the time-domain waveform, especially since much of earthquake data is still recorded in an analog form. The need for a convenient time-domain representation is demonstrated by the fact that wavelets based on the Voigt-Ricker model are often used by workers who do not accept the frequency-dependence of Q implied by that model [e.g. Boore et al., 1971; Munasinghe and Farnell, 1973].

Strick [1967] applied the causality requirement to the propagation of a wave pulse, and found a form for the propagation function that satisfies this requirement. The constant Q transfer function (2.23), is a special case of Strick's function. Later Strick [1970] used the method of steepest descent to approximate the time-domain impulse response. His expression has, in the notation used in this paper, the form

$$b_s(t,x) = \left\{2\pi\gamma t\left[\frac{(1-\gamma)x}{c_s t}\right]^{-1/\gamma}\right\}^{-\frac{1}{2}} \exp\left\{-\frac{\gamma}{(1-\gamma)}t\left[\frac{(1-\gamma)x}{c_s t}\right]^{1/\gamma}\right\}$$

where $b_s(t,x)$ denotes Strick's approximation to the impulse response, and c_s is defined by (2.28). By rearranging this expression, it may be written as

$$b_s(t,x) = \left(\frac{x}{c_s}\right)^{-\beta} t_s^{-(\gamma+1)/2\gamma} [2\pi\gamma(1-\gamma)^{-1/\gamma}]^{-\frac{1}{2}}$$

$$\exp[-\gamma(1-\gamma)^{(1-\gamma)/\gamma} t_s^{1-1/\gamma}] \qquad (2.39)$$

where

$$t_s = t\left(\frac{x}{c_s}\right)^{-\beta}$$

By differentiation we get the approximation for the differentiated impulse response, $b_{sv}(t,x)$:

$$b_{sv}(t,x) = \left(\frac{x}{c_s}\right)^{-\beta} b_s(t,x)\left[(1-\gamma)^{1/\gamma} t_s^{-1/\gamma} - \frac{\gamma+1}{2\gamma t_s}\right] \qquad (2.40)$$

It is evident from inspection of these expressions that they do obey the correct scaling relations given by (2.37). Figures 2.7 and 2.8 show a comparison between the waveshapes computed by the fast-Fourier-transform-method and those computed using the steepest-descent approximation. They show an excellent agreement for the early part of the pulse, which includes most of the higher-frequency information, while the steepest-descent approximation underestimates the low-frequency amplitudes in the later part of the pulse. This is not surprising since the assumptions involved in the steepest descent approximation break down at very low frequencies. This agreement contrasts with the result of Minster [1978a], who in his Figure 3 shows significant differences between arrivals computed using FFT methods and those computed using analytical expansions.

So far we have only considered the pulse propagation in homogeneous materials and given scaling relations applicable to materials with the same value of Q. As the waveshapes plotted in figure 2.3 show a great deal of similarity for different values of Q, it should be possible to give scaling

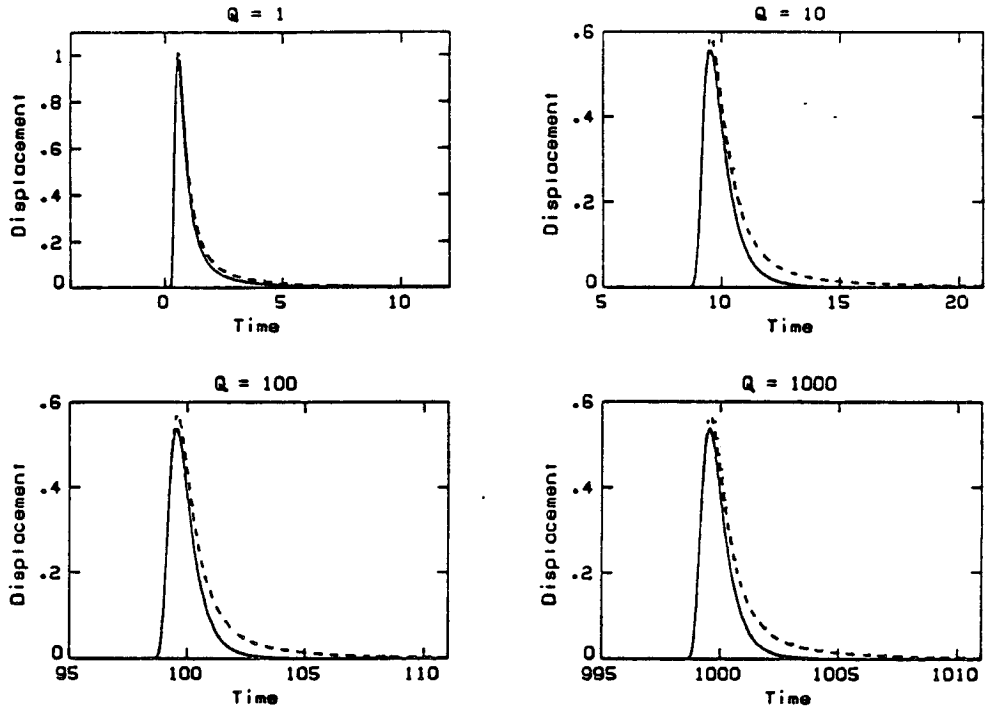

FIG. 2.7. Comparison of waveforms computed using equation (2.39) (solid line), to the waveforms from figure 2.3 (dashed).

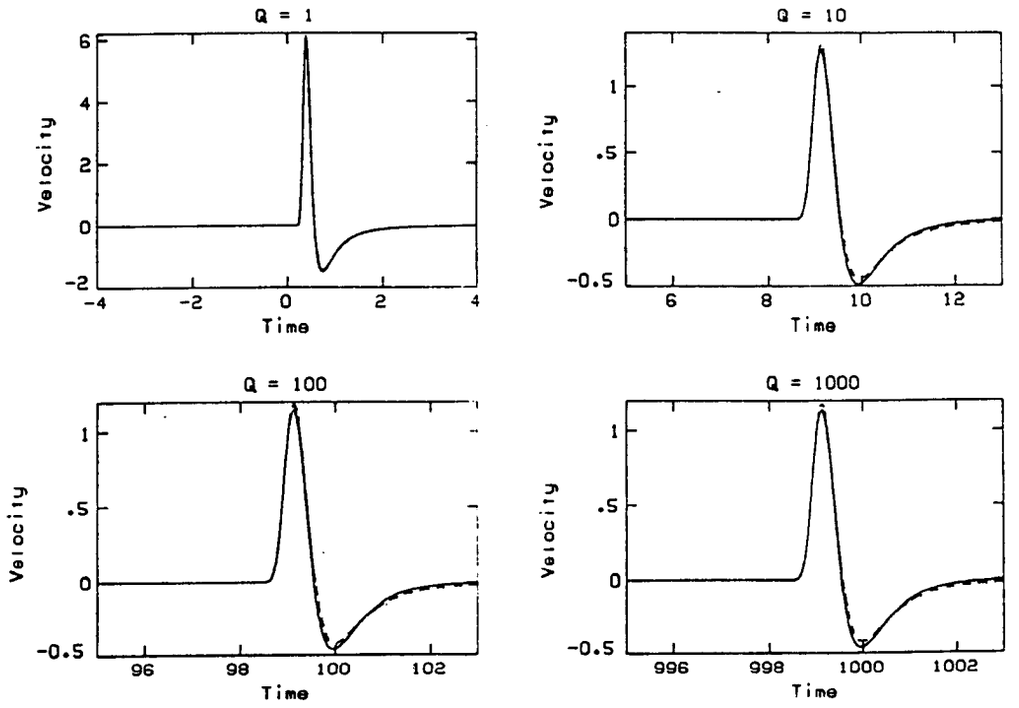

FIG. 2.8. Comparison of waveforms computed using equation (2.40) (solid line), to waveforms computed using numerical FFT algorithms (dashed).

relations for different values of Q as well as for different distances.

When $Q^{-2} << 1$, the tangents in (2.22) and (2.25) may be replaced by their arguments. Thus (2.23) and (2.25) may be written as

$$B(\omega) \simeq \exp\left\{ - \frac{x|\omega|}{2Qc} - i\omega \frac{x}{c} \right\} \tag{2.41}$$

where

$$c \simeq c_0 \left| \frac{\omega}{\omega_0} \right|^{1/\pi Q} \tag{2.42}$$

By use of the Maclaurin-series expansion of the exponential function, equation (2.42) may be written as

$$\frac{c}{c_0} = 1 + \frac{1}{\pi Q} \ln\left|\frac{\omega}{\omega_0}\right| + \frac{1}{2!}\left[\frac{1}{\pi Q} \ln\left|\frac{\omega}{\omega_0}\right|\right] + \ldots\ldots \tag{2.43}$$

When all the frequencies of interest satisfy the condition

$$\frac{1}{\pi Q} \ln\left|\frac{\omega}{\omega_0}\right| << 1 \tag{2.44}$$

sufficient precision may be maintained by only including the first two terms of the expansion given in (2.43). The result is the dispersion relation given by many of the NCQ papers [e.g. Kanamori and Anderson, 1977]. Using the approximation indicated in (2.43), and dropping all terms involving the second or higher powers of 1/Q, equation (2.41) becomes

$$B'(\omega) = \exp\left\{ - \frac{x\omega}{c_0}\left[\frac{\mathrm{sgn}(\omega)}{2Q} + i - \frac{i}{\pi Q} \ln\left|\frac{\omega}{\omega_0}\right|\right]\right\} \tag{2.45}$$

The similarity and shift theorems [Bracewell, 1965; p. 101] may now be used to relate the approximate impulse response b'(t) that has $B'(\omega)$ as its Fourier transform, as indicated by the following relations:

$$b'(t) = r b_1'(t') \tag{2.46}$$

where

$$t' = rt - Q + \frac{1}{\pi} \ln \frac{r}{\omega_0} \tag{2.47}$$

$$r = \frac{c_0 Q}{x} \tag{2.48}$$

and $b_1'(t)$ is the inverse Fourier transform of

$$B_1'(\omega') = \exp\left\{ -\omega' \left[\frac{1}{2} \operatorname{sgn}(\omega') - \frac{i}{\pi} \ln|\omega'| \right] \right\} \tag{2.49}$$

As long as the condition given by (2.44) holds, it is possible to obtain waveshapes for materials with different Q as well as different traveltimes by a combination of scaling and shifting of a single pulse shape. In particular, it follows from (2.46) and (2.48) that the amplitude of the pulse will be approximately proportional to Q. This result, combined with the exact scaling relations (2.37), implies that the function C(Q), defined by (2.38), approaches a constant value as Q becomes large. In order to test the usefulness of (2.38), we have evaluated numerically the value of C(Q). The results are plotted in figure 2.9, for two pulse-width definitions and three different traveltime definitions. These curves show that the value of C(Q) is practically independent of Q, for Q greater than about 20. The similarity of the pulse shape for different values of Q implies that the pulse broadening along the wave path may be summed and (2.38) written as

$$\tau \simeq \int C(Q) \frac{dT}{Q} \simeq C \int \frac{dt}{Q} \tag{2.50}$$

This relation may provide the basis for a practical method for inverting models for the anelastic properties of rocks *in situ* when the wave sources are sufficiently impulsive and the waves are recorded on broadband instruments. The ambiguities involved in using the pulse breadth in this manner, are far less than those involved in the use of amplitudes in a narrow

frequency band, since a number of purely elastic effects, such as focusing from curved interfaces, can have large effects on the amplitudes of seismic signals. This approach also has the advantage over spectral methods that the measurement may be done on a clearly defined phase of the waveform [Gladwin and Stacey, 1974]. It should be noted that equations (2.38) and (2.50) apply for other pulse-width measures than rise time, but the value of C(Q) will of course be different.

Field Measurements of Attenuation

There have been relatively few field studies of the propagation of transient wave pulses in rocks. Gladwin and Stacey [1974] found that the rise time τ, which they defined as the maximum amplitude divided by the maximum slope on the seismogram, could be fitted by an expression of the form

$$\tau = \tau_0 + C\frac{T}{Q} \tag{2.51}$$

where τ_0 indicates the rise time of the source and C was a constant with a value of 0.53 ± 0.04 This value is in reasonably good agreement with the value of 0.485 for large Q predicted on the basis of the CQ theory (figure 2.9).

McDonal et al. [1958] performed experiments in wells drilled into the Pierre shale formation near Limon, Colorado. Fourier analysis of their data indicated that individual Fourier components of the waveforms decayed exponentially in amplitude with distance and that this decay was proportional to frequency. The attenuation per 1000 feet was given in decibels as 0.12 times frequency. Substituting this value into (2.41) and using a velocity of 7000 feet/s gives Q equal to 32. This result was obtained at depths of several hundred feet. Deep reflections indicated that the attenuation decreased with depth with the average attenuation down to a depth of 4000 feet corresponding to a Q of approximately 100. Their waveforms did not show a large amount of broadening over a ratio of 5 in traveltimes; this indicates that the sources were long compared to the impulse response of the wave path so the assumption of a delta function source is not appropriate. However, if the rise times of the waveforms shown in figures 2.3 and 2.6 of McDonal et al. [1958], are

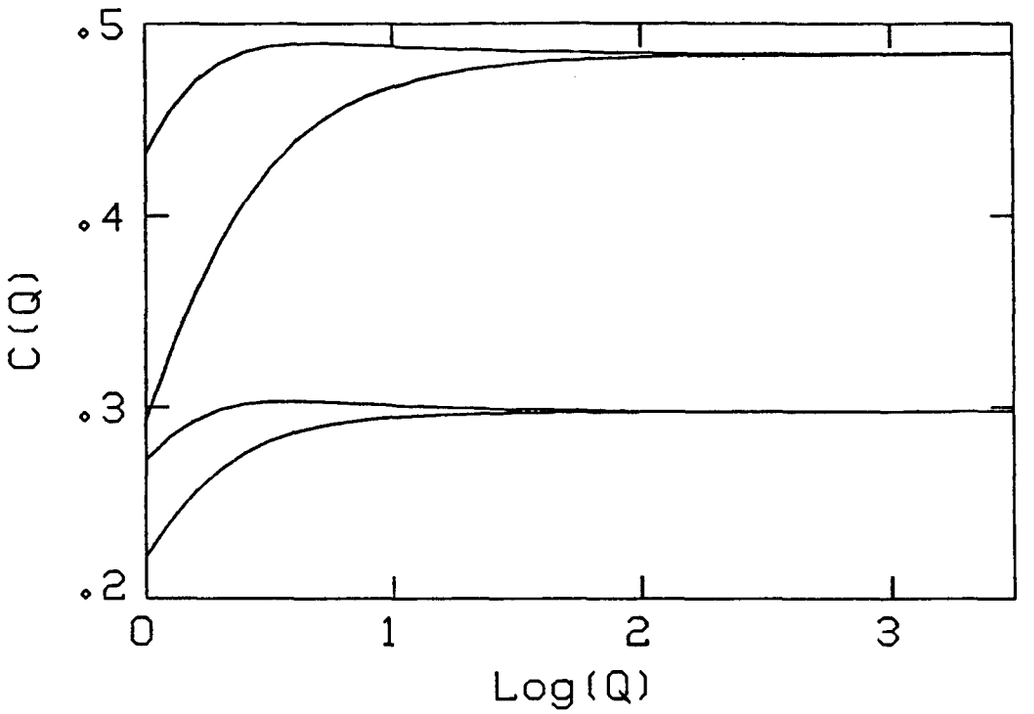

FIG. 2.9. Plot of the function C(Q) defined by equation (2.39). Each pair of curves was computed using a pulse-width measure: the rise-time definition of Gladwin and Stacey [1974], i.e. maximum amplitude divided by maximum slope. The top pair of curves applies to the impulse response b(t), and the lower curve applies to its derivative. The lower curve in each pair was computed using as traveltime T the arrival time of the peak of the pulse, and the upper was computed using the arrival time of maximum slope. The asymptotic values are 0.485 and 0.298.

fitted to the expression (2.51), a reasonable fit may be obtained using C = .5 and Q = 30. This is consistent with the first part of the source being approximately a delta function in velocity or a step function in displacement.

Ricker [1953, 1977] described experiments done in 1948 in the same formation. Waveforms were recorded by three geophones at depths of 422, 622 and 822 feet, for shots at depths less than 300 feet in adjacent wells. Figure 2.10 shows a plot of pulse width vs. traveltime [Ricker 1977; Figure 15.23]. Ricker fitted this data by a function of the form

$$\tau = at^{\frac{1}{2}} \tag{2.52}$$

This relation is in direct conflict with equation (2.37), as well as the experimental result of Gladwin and Stacey [1974]. According to Ricker [1977, p198], this observation is the strongest, if not the only evidence supporting the applicability of his theory to seismic waves. By inspection of figure 2.10 it appears that the data could just as well be fitted by a function of the form (2.51) used by Gladwin and Stacey [1974]. McDonal et al. [1958] criticized Ricker's experiment on the basis that each shot was recorded by no more than three geophones, and that waveforms from different shots were not comparable because, "One cannot shoot a second time in the same hole because the same hole is not there any more." This is probably the reason for some of the scatter in Ricker's data, particularly from the 300-foot shots. This error can be reduced, however, by adjusting the parameter τ_0 in (2.51) for each shot, provided that it is recorded by at least two geophones. Thus we have fitted the wavelet breadth data to a model given by

$$\tau = \tau_{01} + C \int \frac{dT}{Q} \tag{2.53}$$

In order to facilitate the integration, the traveltime data were fitted to the form

$$T = a(x_g - x_s) + b(x_g^2 - x_s^2) \tag{2.54}$$

where x_g is the depth to the geophone and x_s is the depth to shot. This expression implies that the velocity as a function of depth will be given by

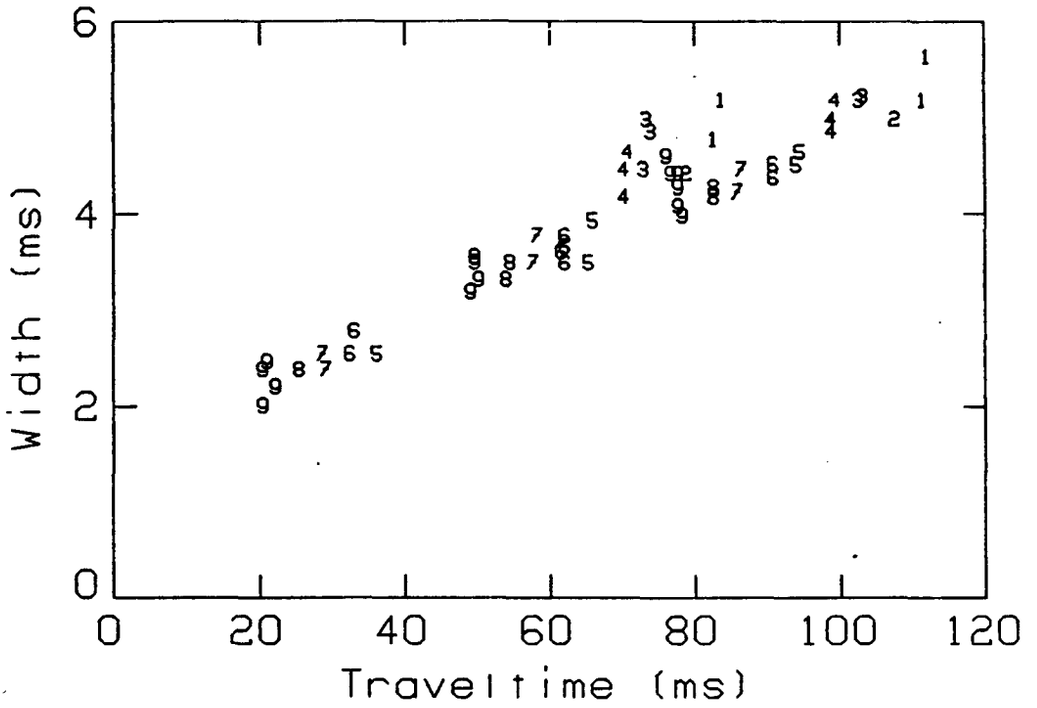

FIG. 2.10. Pulse width as a function of traveltime in Pierre shale. Data from Figure 15.23 in Ricker [1977]. Geophones are at depths of 422, 622, and 822 feet. Sources are at 25-foot intervals at depths from 100 to 300 feet. Numbers indicate sources, 1 for 100 feet, to 9 for 300 feet.

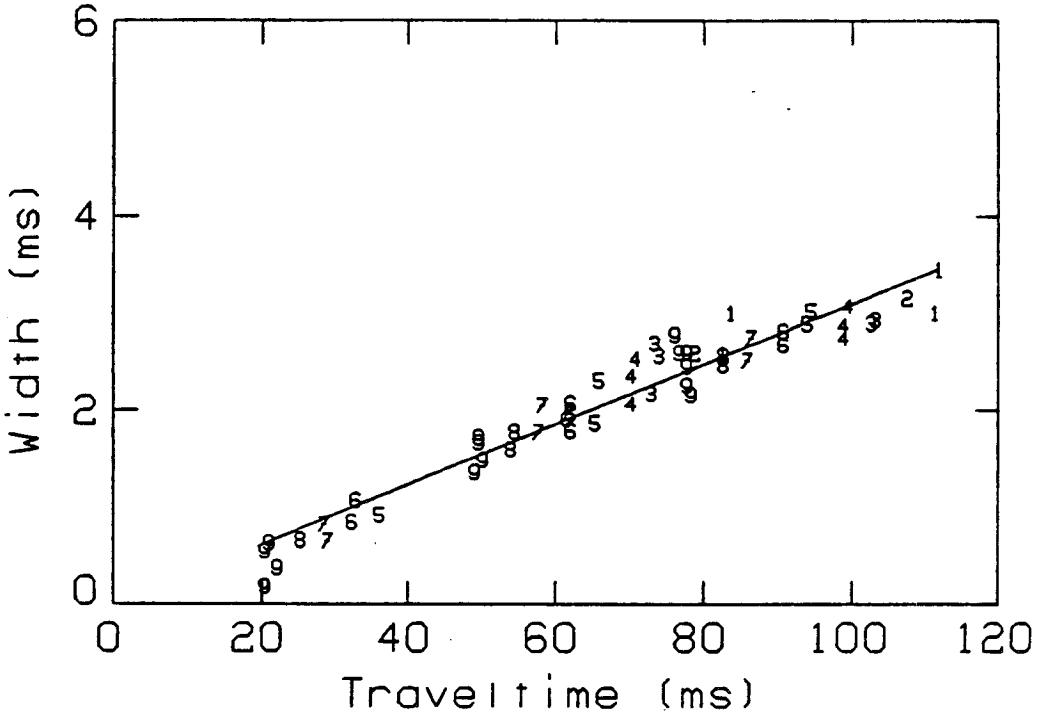

FIG. 2.11. The data in figure 2.10, after subtraction of the initial pulse widths, compared with predicted pulse widths for Q = 32. Both Q and the source widths were determined by simultaneous least-square inversion.

$$V = \frac{1}{a + 2bx} \tag{2.55}$$

As Ricker did not specify which of the data points were obtained from the same shot, it was only possible to determine the source widths for each shot depth. For the pulse-width measure used by Ricker, the value of the parameter C in (2.53) is approximately unity. Figure 2.11 shows a plot of the data from figure 2.10, with the source width subtracted, compared to a straight line with a slope of $1/Q = 1/32$. The data points for the geophone at 622 feet tend to be above the curve; this can be explained by attenuation decreasing with depth. This result implies that both Ricker's data and the data of McDonal et al. are consistent with the linear constant Q model, and both give the same value for Q. This is particularly significant in light of the fact that they interpreted their data very differently, and that neither of them considered a constant or near constant linear attenuation in the interpretation of their data. The apparent conflict between the observations of Ricker [1953] and McDonal et al. [1958] has been noted by many authors including Gladwin and Stacey [1974], Reiter and Monfort [1977], and Bless and Ahrens [1977].

Comparison with Nearly Constant Q Theories

Lomnitz [1956] investigated the transient creep in rocks at low stress levels. He found that the shear strain resulting from a step in applied stress could be described to within the experimental error with a creep function of the form

$$\Psi(t) = \frac{1}{M_0}[1 + q \ln(1+at)] \tag{2.56}$$

where a is a frequency much greater than the sample rate or the time resolution of the experiment. He found that the fit to the data was insensitive to the value of a, as long as it was large. For Q greater than about 20, (2.56) is approximately equal to the CQ creep function (2.14). By using the first two terms from the MacLaurin series expansion of the exponential function, (2.14) may be rewritten

$$\Psi(t) = \frac{1}{M_0}\exp[2\gamma \ln(\frac{t}{t_0})] \simeq \frac{1}{M_0}\left[1 + \frac{2}{\pi Q}\ln\left(\frac{t}{t_0}\right)\right]$$

When $t_0 \ll t$ this is approximately equal to

$$\psi(t) = \frac{1}{M_0}\left[1 + \frac{2}{\pi Q}\ln\left(1+\frac{t}{t_0}\right)\right] \tag{2.57}$$

Later, Lomnitz [1957,1962] used his creep law and the superposition principle to derive a model for wave attenuation with Q approximately independent of frequency for large Q. Pandit and Savage [1973] measured Q for several rock samples with Q ranging from 30 to 300 and found good agreement between values determined at sonic frequencies and those derived from transient creep measurements over several tens of seconds.

Kolsky [1956] did experiments on the propagation of ultrasonic pulses in polymers and found the pulse width to be proportional to traveltime. To model his data, he used a viscoelastic model with Q approximately independent of frequency and with a phase velocity that varied according to

$$\frac{c}{c_0} = 1 + \frac{1}{\pi Q}\ln\left(\frac{\omega}{\omega_0}\right) \tag{2.58}$$

Equation (2.58) follows from (2.43) when the condition given in (2.44) is satisfied. Futterman [1962] arrived at the same formula by imposing causality on the wave pulse and assuming the parameter α in (2.29) to be exactly proportional to frequency over a restricted range of frequencies.

There are two difficulties inherent in Futterman's approach, which necessitate limits on the range where Q is nearly constant, at both low and high frequencies. Collins and Lee [1956] showed that the assumption of a nonzero limit for the phase velocity as frequency approaches zero, implies that Q must approach infinity at zero frequency. Futterman's formulation was based on a finite value of the refractive index at zero frequency and is thus incompatible with constant Q, where the phase velocity has no nonzero limit as frequency approaches zero. It can also be shown [e.g. Azimi et al. 1968], that α proportional to frequency at high frequencies leads to a violation of causality.

It appears that these limitations, which are peculiar to Futterman's approach, have led many workers to assume that a physically realizable formulation with Q exactly independent of frequency was not possible. Liu et al. [1976] and Kanamori and Anderson [1977] have used viscoelastic distributions to derive dispersion relations of the form shown in equation (2.58). Viscoelastic density functions are discussed in appendix A, and it is shown how the constant Q model can be derived from distributions of dashpots and springs.

Discussion

Of the two assumptions that provide the basis for the constant Q model, linearity is the more fundamental, and it has also been more frequently questioned in the literature than the frequency-independence of Q. Nonlinear, rate-independent friction was originally proposed [e.g. Born, 1941] to explain the frequency-independence of Q, since at that time no simple linear models were available that could account for this observation. As summarized in table 2.1, all of the nonlinear friction mechanisms that have been proposed have several features in common. These include the dependence of the effective elastic moduli on strain amplitude, the proportionality of 1/Q to strain at low amplitudes, the frequency-independence of both Q and the moduli, the distortion of waveforms and cusped stress-strain loops, and the absence of any transient creep or relaxation. Mindlin and Deresiewicz [1953] analyzed the losses due to friction between spheres in contact, and found the attenuation to be proportional to amplitude at low amplitudes. White [1966] claimed that the introduction of static friction into this model had the effect of making Q independent of amplitude. This claim cannot be correct since it may be shown [Mavko, 1978] that static friction cannot increase the loss. Walsh [1966] considered the sliding across barely closed elliptical cracks and found the loss for closed cracks with zero normal force to be independent of amplitude. However, this model cannot, as shown by Savage [1969], explain loss independent of amplitude for the whole rock. The required distributions of elliptical cracks would imply that the effective elastic moduli of the rock, as functions of confining pressure, are discontinuous at all values of confining pressure. Mavko [1978] has considered a more general case of non-elliptical cracks and found the attenuation to depend on amplitude in much the same manner as in the contact sphere model of Mindlin and Deresiewicz. All of the above models

feature a decrease in the effective moduli with strain amplitude due to the increase in area of the sliding surfaces. Decrease of both velocity and Q, similar to what would be expected on the basis of the above models, has been observed in laboratory studies of rocks, [Gordon and Davis, 1968; Winkler et al., 1979], but only at strains greater than about 10^{-6} to 10^{-5}. At lower strains both Q and wave velocities are found to be independent of amplitudes.

The dependence of the wave velocity on frequency is such that it is difficult to separate it from the effects of spatial heterogeneities. There is, however, an increasing amount of evidence in support of the frequency-dependence of the elastic moduli. Seismic models for the whole earth show much improved agreement with the free oscillation data, when the frequency-dependence of the elastic moduli is taken into account [Anderson et al., 1977]. It is also well established that for many rocks the elastic moduli derived from ultrasonic pulse measurements are significantly greater than the moduli derived from low-frequency deformation experiments [Simmons and Brace, 1965]. This difference is generally larger for lossy materials. Gretner [1961] analyzed well logging data from several oil wells in Canada and found statistically significant differences between observed traveltimes from surface sources to geophones in wells and traveltimes predicted on the basis of high-frequency continuous velocity logs. Strick [1971] showed that these differences could be explained by the dispersion associated with linear attenuation with Q nearly independent of frequency.

Brennan and Stacey [1977] measured both Q and elastic moduli in low-frequency deformation experiments, at strains of 10^{-6}, and found the moduli to vary with frequency as predicted by linearity. The stress-strain loops were elliptical although earlier experiments at larger amplitudes showed cusped stress-strain loops [McKavanagh and Stacey, 1974].

Because the principle of superposition does not apply to the nonlinear solid friction models, it is difficult to predict their effects on the propagation of transient stress pulses. Walsh [1966] pointed out that the losses due to friction cannot be described through the use of complex moduli although this is frequently attempted [e.g. Johnston and Toksoz, 1977]. It is easily shown [e.g. Gladwin and Stacey, 1974] that the use of complex frequency-independent moduli leads to acausal waveforms that arrive before they are

excited. Savage and Hasegawa [1967] used the stress-strain hysteresis loops implied by several different friction models, to model wave propagation. The results showed significant amounts of distortion, which have never been observed experimentally.

From these observations it may be concluded that at strain amplitudes of interest in seismology, the propagation and attenuation of waves are dominated by linear effects, with some nonlinear effects showing up at strains of 10^{-5} or greater. This amplitude corresponds to a stress amplitude of 5 bars, since the ambient seismic noise level is on the order of 10^{-11} in strain, and studies of earthquake source mechanisms indicate stress changes of 1 - 100 bars [Hanks, 1977]; it is evident that nonlinear effects can only be significant very near the source.

While a good case can be made for the linearity of the absorption of seismic energy at low amplitudes, no such simple answer can be given to the question of the frequency-dependence of the attenuation. Theoretical models of specific attenuation mechanisms are often formulated in terms of relaxation times, each of which implies a creep function that is a decaying exponential. A model that has a single relaxation time is often referred to as the standard linear solid and has Q proportional and inversely proportional to frequency at high and low frequencies, respectively. Cases where inertial effects may play a role, such as in the flow of low-viscosity fluids [Mavko and Nur, 1979], feature even stronger variation of attenuation with frequency. It may be shown [Kjartansson, 1978] that in materials with sharply defined heterogeneities (e.g. grain boundaries or pores), that absorption due to processes controlled by diffusion, such as phase transformations or thermal relaxation, leads to Q proportional to $\omega^{\frac{1}{2}}$ and $\omega^{-\frac{1}{2}}$ at high and low frequencies, even for uniform distributions of identical pores or crystals.

For these types of mechanisms, the approximate frequency-independence of Q that is observed indicates distributions of time constants, associated with the individual absorbing elements. It may be shown, for example, that the frequency at which maximum absorption occurs for mechanisms involving the diffusion of heat, is inversely proportional to the square of the minimum dimension of the inhomogeneities involved. The empirical observation that Q, in solids, varies much more slowly than even the square root of frequency, is thus an

expression of the statistical nature of the inhomogeneities. It is interesting that dielectric losses in solids show the same type of frequency-dependence as do the energy losses in stress waves [Jonscher, 1977].

While Q is probably not strictly independent of frequency, there is no reason to believe that any of the band-limited near-constant Q theories better approximate the wave propagation in real materials than the constant Q model. Therefore, nothing is gained in return for the mathematical complexity and potential inconsistency in using, for example, the absorption band model of Liu et al. [1976].

Strick [1967] obtained a transfer function for wave propagation, of which the constant Q is a special case. He rejected the CQ case, however, on the basis that the lack of an upper bound for the phase velocity was in violation of causality. Strick's three-parameter model is equivalent to the CQ model, with an additional time delay applied to the waveform. Strick [1970] computed waveforms for his models, and found that the detectable onset of the signal always arrived significantly later than the applied time shift. He termed this delay "pedestal" and attributed to it significance that has been subject to some controversy. For the CQ case, the "pedestal" arrives when the source is excited. Minster [1978b] argued that the presence of the "pedestal" was an indication of the need for a high-frequency cutoff of the type built into the model of Liu et al. This "pedestal" controversy points to a limitation shared by all of continuum mechanics; no continuum model, including the CQ model, can have any significance at wavelengths shorter than the molecular separation nor at periods longer than the age of the universe. This covers approximately 32 orders of magnitude in frequency, which for a Q of 100 implies a change in velocity of about 26%. The possibility that some "calculable" energy might arrive 26% earlier than any detectable energy, is hardly a sufficient reason to introduce a high-frequency cutoff. Calculable values of physical parameters, outside the observable range are common in other fields, such as in solutions to the diffusion equation and in statistics. Minster [1978b] and Lundquist [1977] suggest that the cutoff should be at periods between 0.1 and 1 seconds for the mantle. Such cutoffs have never been observed for any of the rocks that have been studied in the laboratory, where the range of frequencies extends up to about one megahertz.

Lomnitz's [1957] attenuation model has often been criticized [Kogan, 1966; Liu et al., 1976; Kanamori and Anderson, 1977] on the basis that the lack of an upper bound for the transient creep would not permit mountains or large-scale gravity anomalies to last through geologic time. Since the Lomnitz creep function is practically equivalent to the constant Q creep function for large values of time and Q, this criticism applies equally to the constant Q model. However, it does not pass the test of substituting numbers into the expressions (2.56) or (2.14). For example, for a material with a Q of 100, the strain that results from the application of a unit stress is only about 33% larger over a period of one billion years, than for the first millisecond of applied stress. Thus, neither the constant Q theory, nor any of the NCQ theories can explain the large strains required by plate tectonics. The fact that brittle deformation only takes place in the uppermost part of the crust, with the exception of localized areas of unusually rapid tectonic activity, may indicate that over geologic time most of the earth deforms as a viscous fluid with Q for shear near zero. The assumption, implicit in the band-limited NCQ model of Liu et al. [1976], that Q approaches infinity outside the range of observations, is thus particularly inappropriate for low-frequency shear deformations in the mantle.

Conclusions

Contrary to what has often been assumed in the past, it is possible to formulate a description of wave propagation and attenuation with Q exactly independent of frequency, that is both linear and causal. The wave propagation properties of materials can be completely specified by only two parameters, for example, Q and phase velocity, at an arbitrary reference frequency. This simplicity makes it practical to derive exact expressions describing, in the frequency-domain, the wave propagation for any positive value of Q. The dispersion that accompanies any linear energy absorption leads to a propagation velocity of any transient disturbance that is not only a function of the material, but also of the past history of the wave. Review of available data indicates that the assumption of linearity is well justified for seismic waves, but it is likely that Q is weakly dependent on frequency. There is, however, no indication that any of the NCQ theories that we have discussed provide a better description of the attenuation in actual rocks than the constant Q theory does.

Chapter III

MODELS FOR FREQUENCY-DEPENDENT Q

An internally consistent model for the anelasticity and wave propagation of a linear material with Q exactly independent of frequency has been given. The constant Q model fits the properties of most rocks well, especially over the two or three orders of magnitude in frequency involved in most experiments. Considering the complexity of solids, and rocks in particular, there is, however, no reason to believe that the Q of all rocks is exactly independent of frequency, nor that there is any other simple universal law that describes it. All of the previous nearly constant Q models (except for Strick's 3- and 4-parameter models [Strick, 1967]) had sharp cutoffs on Q, that have never been observed in rocks. In this chapter I will show how the constant Q (CQ) model may be generalized to include the effects of arbitrarily weak variations of Q with frequency. This generalization should be useful in correlating data over wide ranges of frequency, such as from ultrasonic pulse measurements to the seismic band or from the seismic range to the time scales involved in the Chandler wobble, post-glacial and post-seismic rebound, and tectonics.

Theory

Figure 3.1 shows four simple viscoelastic models that are treated in most standard texts on viscoelasticity. Table 3.1 gives a summary of the properties of those models, and 1/Q is plotted in figure 3.2. We have used the definition of Q as the ratio between the real and imaginary parts of the complex modulus function [O'Connell and Budiansky, 1978]. The Voigt and the Maxwell models are specified by two parameters and the other two by three. All the models feature a 1/Q that is proportional to either frequency or inverse frequency over most of the frequency ranges shown.

The CQ model can be specified by a modulus function of the form

$$M(\omega) = M_0 (i\omega)^{\beta} \qquad (3.1)$$

where β is related to Q by

$$Q = \cot\left(\frac{\pi\beta}{2}\right) \tag{3.2}$$

and β is in the range

$$0 \leq \beta \leq 1 \tag{3.3}$$

The limiting cases are classical elasticity and Newtonian viscosity. It is clear that physical realizability is maintained if the viscous elements in the models shown in figure 3.1 are replaced by constant Q elements. Table 3.2 lists a summary of the resulting 3- and 4-parameter models. The expressions in table 3.2 reduce to those in table 3.1 when $\beta = 1$. Examples of the frequency-dependence for these models are shown in figures 3.2 through 3.5.

It is apparent from the figures that a wide range of data with Q smoothly varying with frequency can be fitted with these simple models. Should these be insufficient to fit a particular set of observations the models can be expanded as needed but given the experimental difficulties in measuring Q it is unlikely that this will happen often.

Property / Model	Modulus $M(\omega)$ $M(\omega)$	Q	Limit $\omega \to 0$	Limit $\omega \to \infty$
Maxwell	$M_o \frac{i\omega_1}{1 + i\omega_1}$	ω_1	Viscous	Elastic $M(\omega) = M_o$
Voigt	$M_o[1 + i\omega_1]$	$\frac{1}{\omega_1}$	Elastic $M(\omega) = M_o$	Viscous
3 parameter solid	$M_o \frac{1 + (1+\varepsilon) i\omega_1}{1+ \varepsilon + i\omega_1}$	$\frac{1 + \varepsilon}{\varepsilon}(\omega_1 + \omega_1^{-1})$	Elastic $M(\omega) = \frac{M_o}{1 + \varepsilon}$	Elastic $M(\omega) = (1 + \varepsilon)M_o$
3 parameter fluid	$M_o \frac{i\omega_1 - \varepsilon\omega_1^2}{\varepsilon + i\omega_1}$	$\frac{1 - \varepsilon^2}{\varepsilon} \frac{1}{(\omega_1 + \omega_1^{-1})}$	Viscous	Viscous

TABLE 3.1. A summary of the properties of the viscoelastic models shown in figure 3.1. Expressions are given in terms of $\omega_1 = \omega/\omega_0$ where ω_0 is the transition frequency from viscous to elastic behavior for the Maxwell and Voigt models and from Voigt to Maxwell for the other two.

Property / Model	Modulus $M(\omega)$	Q	Limit $\omega \to 0$	Limit $\omega \to \infty$
Generalized Maxwell Model	$M_o \dfrac{(i\omega_1)^\beta}{1 + (i\omega_1)^\beta}$	$Q_0 + \omega_1^{\beta}$	CQ $Q = Q_0$	Elastic $M(\omega) = M_o$
Generalized Voigt Model	$M_o[1 + (i\omega_1)^\beta]$	$Q_0 + \omega_1^{-\beta}$	Elastic $M(\omega) = M_o$	CQ $Q = Q_0$
Generalized 3 parameter solid model	$M_o \dfrac{1 + (1+\epsilon)(i\omega_1)^\beta}{1 + \epsilon + (i\omega_1)^\beta}$	$\dfrac{2+\epsilon}{\epsilon} Q_0 + \dfrac{1+\epsilon}{\epsilon}(Q_0^2 + 1)^{1/2}(\omega_1^{\beta} + \omega_1^{-\beta})$	Elastic $M(\omega) = \dfrac{M_o}{1 + \epsilon}$	Elastic $M(\omega) = (1+\epsilon)M_o$
Generalized 3 parameter fluid model	$M_o \dfrac{(i\omega_1)^\beta + \epsilon(i\omega_1)^{2\beta}}{\epsilon + (i\omega_1)^\beta}$	$\dfrac{\dfrac{(Q_0^2 + 1)^{1/2}}{\epsilon} + Q_0(\omega_1^{\beta} + \omega_1^{-\beta}) + \dfrac{\epsilon(Q_0^2 - 1)}{(Q_0^2 + 1)^{1/2}}}{\omega_1^{\beta} + \omega_1^{-\beta} + 2\epsilon(Q_0^{-2} + 1)^{-1/2}}$	CQ $Q = Q_0$	CQ $Q = Q_0$

$Q_0 = \cot \frac{\pi\beta}{2}$ $\quad \omega_1 = \frac{\omega}{\omega_0}$ $\quad$ *for $\epsilon \ll 1$ this reduces to $\dfrac{(Q_0^2 + 1)^{1/2}}{\epsilon(\omega_1^{\beta} + \omega_1^{-\beta})} + Q_0$

TABLE 3.2. A summary of the properties of the generalized model when the viscous element has been replaced by a constant Q element.

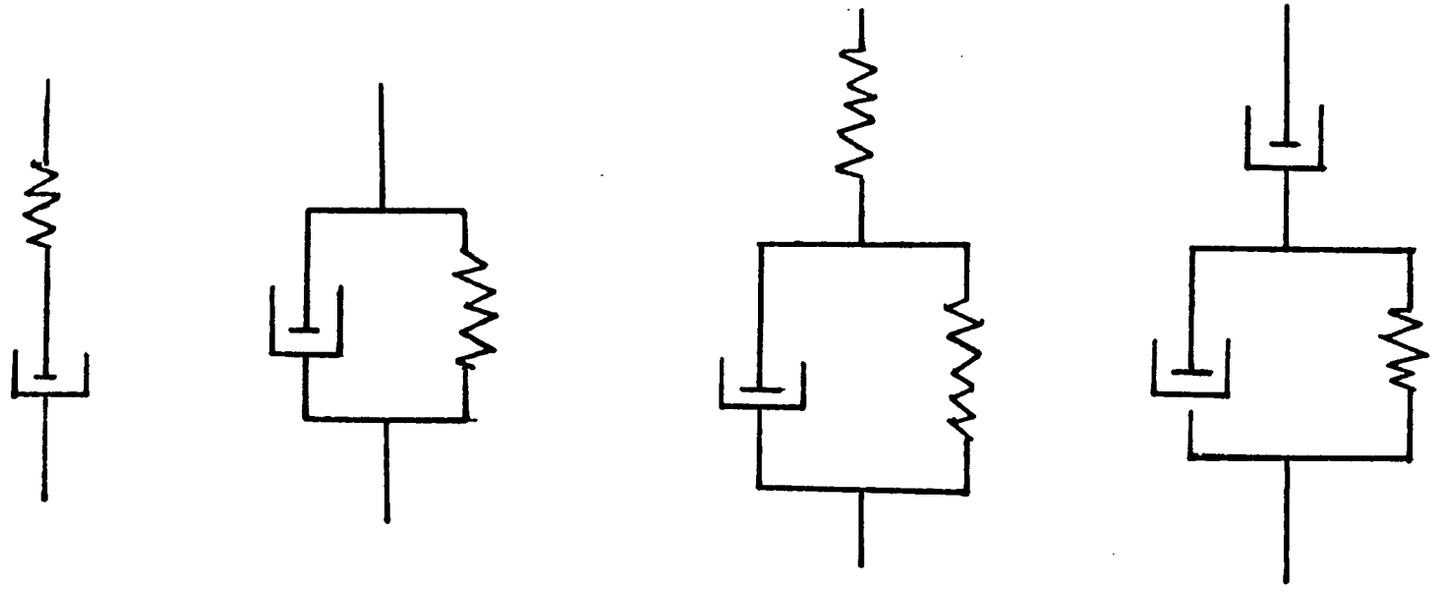

FIG. 3.1. Schematic diagrams of four simple viscoelastic models: (a) Maxwell's solid; (b) Voigt's solid; (c) 3-parameter "standard linear" solid; (d) 3-parameter fluid.

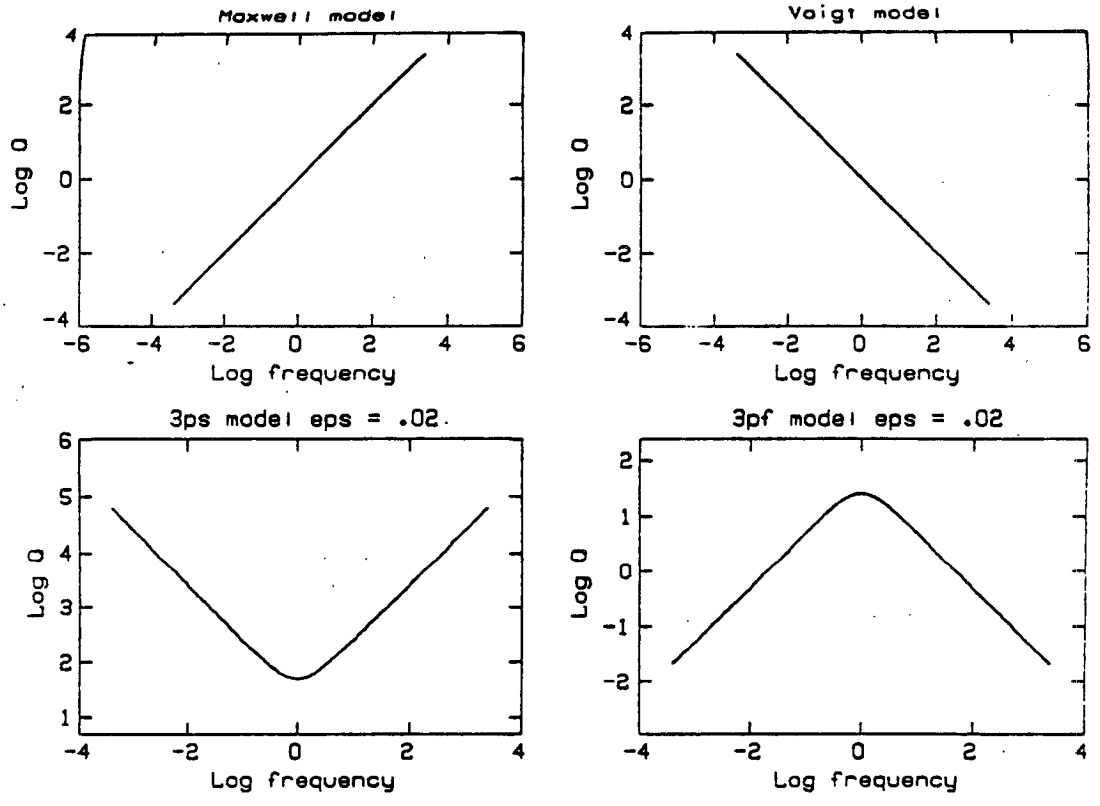

FIG. 3.2. Logarithmic plots of Q as a function of frequency relative to the transition frequency for the models shown in figure 3.1.

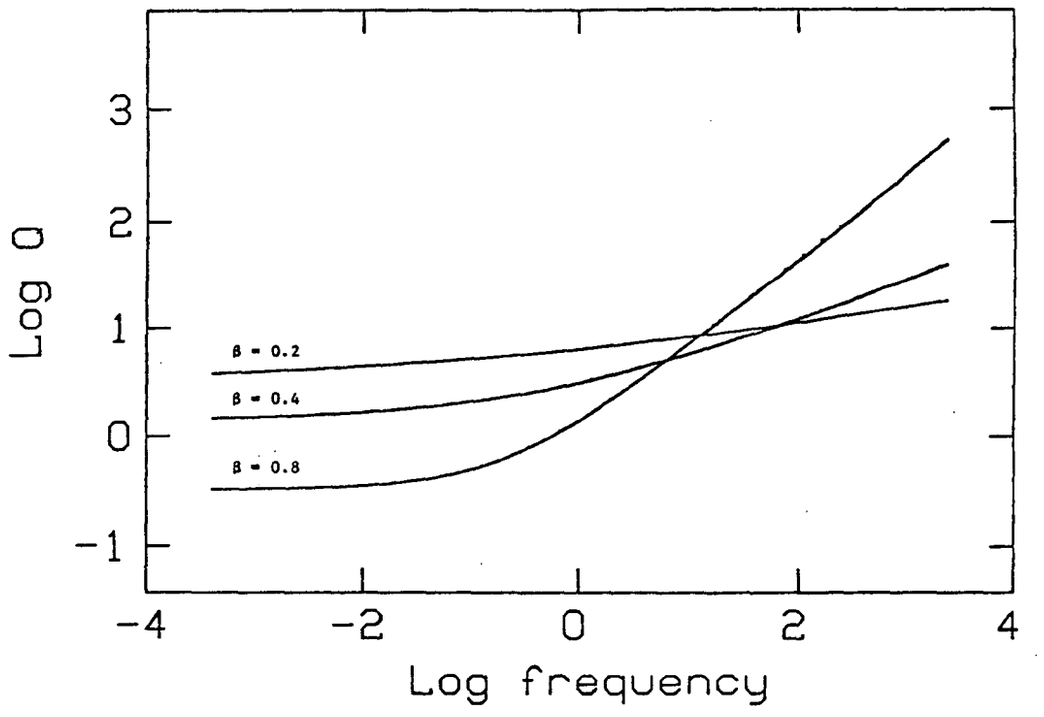

FIG. 3.3. Logarithmic plot of Q for a generalized Maxwell's model for values of β equal to 0.8, 0.4 and 0.2.

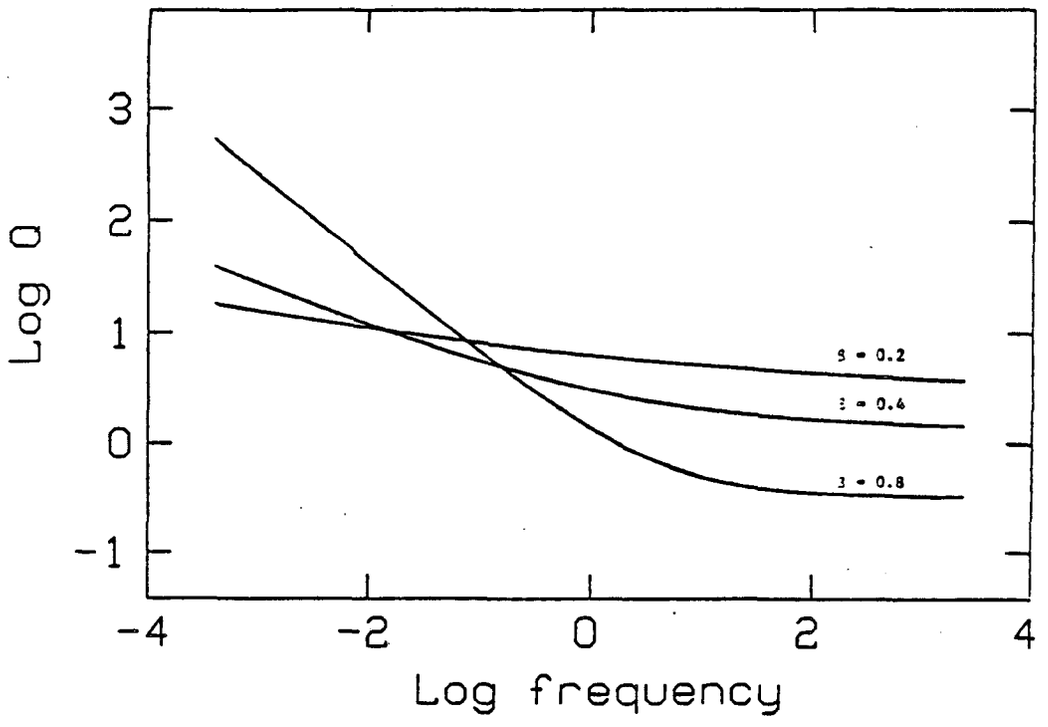

FIG. 3.4. Logarithmic plot of Q for a generalized fluid model for values of β equal to 0.8, 0.4 and 0.2.

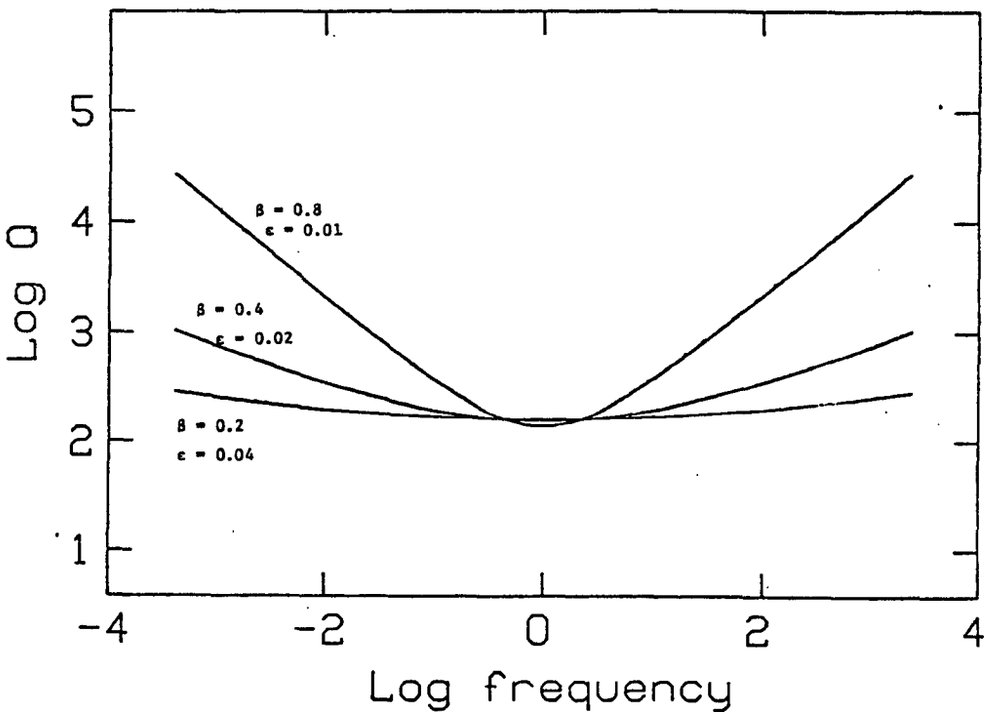

FIG. 3.5. Logarithmic plot of Q for the generalized 3-parameter solid model for β = 0.8 and ϵ = 0.01, β = 0.4 and ϵ = 0.02 and β = 0.02 and ϵ 0.04.

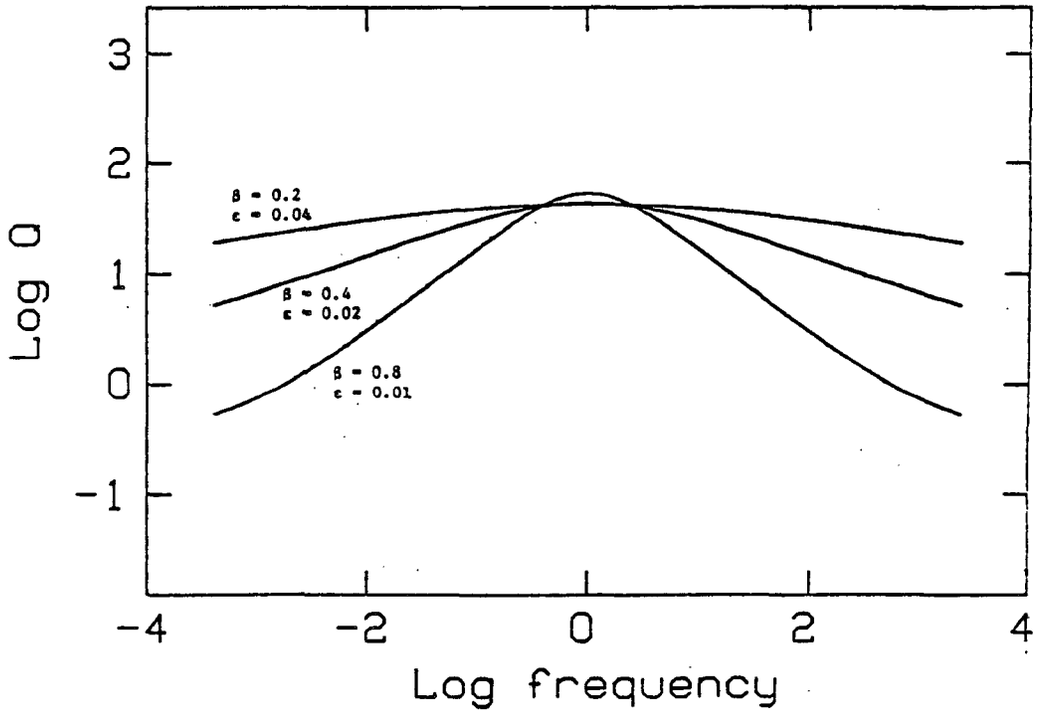

FIG. 3.6. Logarithmic plot of Q for a generalized fluid model for values of β = 0.8 and ε = 0.01, β = 0.4 and ε = 0.02, and β = 0.2 and ε = 0.04.

Chapter IV

REFLECTIONS DUE TO CONTRAST IN Q

Reflection and transmission coefficients are derived for anelastic materials by matching displacements and tractions across the interfaces just as in the elastic case. The stress at any point in a linear material may be found by convolving the strain with a modulus filter; the requirements of causality and physical realizability are satisfied when the integral of the modulus is an impedance function [Claerbout, 1976]. Specializing to monochromatic plane waves at normal incidence, with an interface at z = 0, we have

$$\sigma(\omega) = m(\omega) * \epsilon(\omega) = -\rho c^2 \frac{\partial U(\omega, z)}{\partial z} \tag{4.1}$$

where σ is stress, ϵ is strain, U is displacement, m is the modulus filter, ρ is density, and c is a velocity-like quantity, defined by

$$c^2(\omega) = \frac{m(\omega)}{\rho} \tag{4.2}$$

Equation (4.1), when combined with the equilibrium equation, leads to a wave equation, which has the same form as the usual wave equation, except c enters as a filter in the time domain or as a frequency-dependent complex function in the frequency domain. Plane-wave solutions to the wave equation may be written as the incident, reflected, and transmitted wave displacements:

$$U_i = \exp\left[i\omega\left(t - \frac{z}{c_1}\right)\right] \tag{4.3a}$$

$$U_r = R \exp\left[i\omega\left(t + \frac{z}{c_1}\right)\right] \tag{4.3b}$$

$$U_t = T \exp\left[i\omega\left(t - \frac{z}{c_2}\right)\right] \tag{4.3c}$$

At the interface, z=0, continuity of the displacements implies that

$$U_i + U_r = U_t \tag{4.4}$$

or

$$T = 1 + R \tag{4.5}$$

Substituting equation (4.1) into (4.2), and imposing continuity on the stresses, we get

$$\rho_1 c_1 - R\rho_1 c_1 = T\rho_2 c_2 \tag{4.6}$$

This combined with (4.5) gives

$$R = \frac{\rho_1 c_1 - \rho_2 c_2}{\rho_1 c_1 + \rho_2 c_2} \tag{4.7}$$

The form of c depends on the particular material. The response of most rocks is well approximated by the constant Q formulation [Kjartansson, 1979], where c has the form

$$c = c_0 \left(\frac{i\omega}{\omega_0}\right)^{\gamma} \tag{4.8}$$

where ω_0 is an arbitrary reference frequency and γ is related to Q by

$$\frac{1}{Q} = \tan(\pi\gamma) \tag{4.9}$$

Substitution of (4.8) into (4.7) gives

$$R = \frac{\frac{\rho_1 c_{01}}{\rho_2 c_{02}} \left(\frac{i\omega}{\omega_0}\right)^{\gamma_1 - \gamma_2} - 1}{\frac{\rho_1 c_{01}}{\rho_2 c_{02}} \left(\frac{i\omega}{\omega_0}\right)^{\gamma_1 - \gamma_2} + 1} \tag{4.10}$$

This shows that when the Q for both media are the same, the reflection

coefficient is real and independent of frequency. The power series expansion for the natural logarithm, given by

$$\frac{1}{2}\ln x = \frac{1-x}{1+x} + \frac{1}{3}\left(\frac{1-x}{1+x}\right)^3 + \frac{1}{5}\left(\frac{1-x}{1+x}\right)^5 + \ldots\ldots \qquad (4.11)$$

may be used to rewrite (4.10):

$$\frac{1}{2}\ln\left(\frac{\rho_1 c_{01}}{\rho 2 c_{02}}\right) + \frac{1}{2}(\gamma_1-\gamma_2)\ln\left(\frac{i\omega}{\omega_0}\right) = R + \frac{1}{3}R^3 + \frac{1}{5}R^5 + \ldots\ldots \qquad (4.12)$$

When R is small we can neglect third and higher powers of R. Then equation (4.12) reduces to

$$R = \frac{\rho_1 c_{01} - \rho_2 c_{02}}{\rho_1 c_{01} + \rho_2 c_{02}} + \frac{1}{2}(\gamma_1-\gamma_2)\ln\left(\frac{\omega}{\omega_0}\right) + i\frac{\pi}{4}(\gamma_1-\gamma_2)\,\mathrm{sgn}(\omega) \qquad (4.13)$$

Thus the reflection may be treated as a sum of two contributions: a real frequency-independent part and a frequency-dependent part that depends on the Q contrast and is similar to a Hilbert transform of the incident wave, except that it is one-sided (causal) in the time domain.

Discussion

McDonal et al. [1958] measured attenuation in water-saturated shale *in situ*. They observed Q values of about 30 for P-waves and 10 for S-waves. The laboratory results of Winkler and Nur [1979] indicate that Q may be an order of magnitude more sensitive than velocity to changes in conditions such as saturation or pore and confining pressures, and that P-wave attenuation in partially saturated rocks may be much greater than in fully saturated or dry rocks. This raises the possibility that a substantial portion of the reflections observed in some areas are caused by changes in Q rather than elastic impedance.

Chapter V

ATTENUATION DUE TO THERMAL RELAXATION IN POROUS ROCKS

Thermal relaxation is a well-known mechanism for the absorption of elastic energy in solids. Zener [1948] presents a review of its effects on the anelasticity of metals. Savage [1965] and Armstrong [1979] have treated seismic attenuation due to thermal relaxation in dry granular rocks. A closely related effect is the energy conversion caused by stress-induced phase transitions. Vaisnis [1968] has applied this mechanism to seismic absorption in areas of the mantle containing partial melt.

In this paper we will extend the results of these authors. The frequency dependence will be discussed in greater detail and the magnitude of the loss will be estimated for several cases, such as porous rocks where the pore volume is occupied by gases or liquids, or mixtures of both, with and without phase transitions. Particularly large losses are predicted for rocks containing mixtures of liquid and gas at high pore pressures, water-saturated rocks at high temperatures and rocks containing partial melt. Each of those cases is of interest in the exploration for energy resources.

In the last few years it has been established that pore fluids play a major role in determining seismic velocities [Nur and Simmons, 1969; Domenico, 1976]. It has also been discovered that even minute amounts of volatiles can dramatically increase the absorption in rocks [Pandit and Tozer, 1970; Tittman et al., 1972; Tittman, 1978]. Winkler and Nur [1979] have investigated the effects of a number of variables - including pore and confining pressures, the degree of saturation, and the nature of the pore fluid - on attenuation for both shear and compressional modes of deformation. They found that the introduction of small amounts of gas phases in water-saturated rocks led to a large increase in the attenuation associated with compressional deformations. We will investigate the role of thermal relaxation in these observations.

The magnitude of thermoelastic effects is closely related to the thermal expansivity of the material. The thermal expansivity of gases is typically

about an order of magnitude greater than the thermal expansivity of liquids, which is about an order of magnitude greater than that of solids. Since thermal relaxation is known as a mechanism responsible for significant absorption in metals [Zener, 1948], it would not be surprising to find it playing some role in the absorption in porous fluid or gas-saturated rocks. In contrast to previous investigations of thermal relaxation in rocks, which have considered its effects on dry rocks, we will examine in detail the role of pore fluids.

Physical Principles of the Thermoelastic Effect

It is known from elementary thermodynamics that any material with a nonzero thermal expansivity will be less compressible under adiabatic conditions, when it is thermally isolated, than under isothermal conditions. Adiabatic compression is accompanied by a temperature change, which depends on the thermal and elastic properties of the material. Because for all wavelengths and frequencies of interest in seismology the flow of heat from the peak to the trough of a wave traveling in a homogeneous medium may be neglected [Savage, 1965], wave propagation is controlled by the adiabatic properties of the rock.

In contrast, in a heterogeneous medium such as a porous rock, we can distinguish between two or three kinds of adiabatic responses. When a sudden pressure change is applied to a material with heterogeneous thermoelastic properties, each pore of grain responds adiabatically, producing a spatially heterogeneous temperature change. This results in local heat flow from regions of higher than average stress or greater than average thermal expansivity to regions of lesser stress or expansivity. As the temperature differences relax, some additional strain takes place. The deformation may still be considered adiabatic, now based on the average properties rather than on the local microscopic properties. Furthermore, when more then two phases of the same component, e.g. steam and water, are present, thermal equilibrium is not a sufficient condition for thermodynamic equilibrium, as one of the phases may have become unstable. Equilibrium in response to a pressure increase implies some mass transfer from the less dense phase to the denser phase, accompanied by a release or absorption of the latent heat for the transformation.

We will first derive an exact solution for the mechanical response of an idealized heterogeneous medium, that is, a rock with a random distribution of flat pores of uniform thickness. The result enables us to draw some conclusions about the frequency dependence of the attenuation in rocks with more complicated structures and about the relationships between the magnitude of the absorption and the modulus defect. The modulus defect is defined as the relative change in modulus between the high-frequency unrelaxed and the low-frequency relaxed limits.

An Exact Solution

The process of conversion of wave energy into heat may be described in detail when the geometry of the inhomogeneity is known. For simple geometries this may be done analytically. Here we consider the case of a flat inclusion in an otherwise homogeneous medium. A random distribution of such inclusions will show similar behavior when the inclusions are uncorrelated.

The geometry is illustrated in figure 5.1. Notation and definitions of the parameters we will be using are given in table 5.1. An instantaneous application of a small pressure change P implies a proportional change in temperature $\bar{T}$ by an amount

$$\bar{T} = b\,P \tag{5.1}$$

throughout the rock. If $\bar{T}$ varies in space, flow of heat across finite temperature gradients will take place, with a resulting increase in entropy and an irreversible conversion of mechanical energy into heat. Spatial variations in $\bar{T}$ can result either from inhomogeneities in P or b, or both. In a dry rock with an irregular distribution of pores and cracks, one might expect inhomogeneities in P to dominate since stress concentrations will be present at grain boundaries and the edges of cracks. This case has been considered by Savage [1965]. In fluid-saturated rocks the fluid will support much of the compressional stress in the vicinity of flat cracks. Since the stress heating coefficient b is typically an order of magnitude greater for liquids than solids, we might expect inhomogeneities in b to play a significant role here.

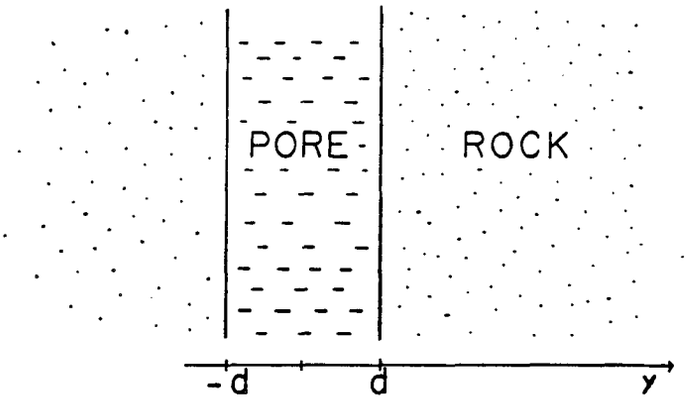

FIG. 5.1. Geometry of rock model used in diffusion solution.

parameter	symbol	definition
isothermal bulk modulus	K	$-V\left(\frac{\partial P}{\partial V}\right)_T$
heat capacity	c	$T\left(\frac{\partial S}{\partial T}\right)_P$
thermal expansivity	α	$\frac{1}{V}\left(\frac{\partial V}{\partial T}\right)_P$
adiabadic bulk modulus	K'	$-V\left(\frac{\partial P}{\partial V}\right)_S$
stress heating	b	$V\left(\frac{\partial T}{\partial P}\right)_S$
diffusivity	D	$\frac{dT}{dt} / \frac{\partial^2 T}{\partial y^2}$
thermal conductivity	h	$D\rho c$

TABLE 5.1. Notation and definitions for thermal parameters.

For the geometry in figure 5.1 both the material properties as well as the strain ϵ and the temperature depend only on y. For flat inclusions the pressure is uniform. The heat flow will thus be described by the one-dimensional diffusion equation, which has the form

$$\frac{dT}{dt} = D \frac{\partial^2 T}{\partial y^2} + b \frac{dP}{dt} \tag{5.2}$$

when the adiabatic heating effect is included. Equation (5.2) may be used to solve for the temperature when the diffusivity D is locally constant. At interfaces, continuity of temperature and heat flow must also be satisfied. Given the temperature, the strain ϵ is obtained from

$$\epsilon = \frac{1}{K} P + \alpha(T-T_0) \tag{5.3}$$

Thus, from a knowledge of the diffusivity, heating coefficient, and thermal expansivity, we can determine the temperature and strain response to any applied stress function, P(t).

When the applied pressure is a sinusoidal function of time

$$P = P_0 e^{i\omega t} \tag{5.4}$$

Equation (5.2) becomes

$$i\omega \hat{T} = D \frac{\partial^2 \hat{T}}{\partial y^2} + i\omega b \tag{5.5}$$

where

$$\hat{T} = \frac{T-T_0}{P} \tag{5.6}$$

Similarly, equation (5.3) becomes

$$S(\omega) = \frac{1}{K} + \alpha\hat{T} \tag{5.7}$$

where $S(\omega)$ is a complex, frequency-dependent compliance, ϵ/P. When $S(\omega)$ is known the attenuation parameter Q is obtained from

$$\frac{1}{Q} = \tan\delta = \frac{-Im[S(\omega)]}{Re[S(\omega)]} \tag{5.8}$$

where δ is the phase angle between stress and strain. O'Connell and Budiansky [1978] discuss the relationship between this and various other definitions for Q that have been used in the literature.

A general solution to (5.5) has the form

$$\hat{T} = A_1 \cos h\left[\frac{y}{d}(i\omega\tau_1)^{\frac{1}{2}}\right] + A_2 \exp\left[-\frac{y}{d}(i\omega\tau_2)^{\frac{1}{2}}\right] + b \tag{5.9}$$

where

$$\tau_1 = \frac{d^2}{D_1} \tag{5.10}$$

$$\tau_2 = \frac{d^2}{D_2} \tag{5.11}$$

Symmetry considerations imply that $A_2 = 0$ for $|y| < d$. The condition that T be bounded for large y implies that $A_1 = 0$ for $y > d$. The solution may therefore be written as

$$T = A_1 \cos h\left[\frac{y}{d}(i\omega\tau_1)^{\frac{1}{2}}\right] + b_1 \quad \ldots\ldots \quad |y| < d \tag{5.12}$$

$$T = A_2 \exp\left[-\frac{|y|}{d}(i\omega\tau_2)^{\frac{1}{2}}\right] + b_2 \quad \ldots\ldots \quad |y| > d \tag{5.13}$$

A_1 and A_2 are determined by imposing continuity of temperature and heat flow at the interface. Continuity of temperature implies

$$A_1 \cos h\left[(i\omega\tau_1)^{\frac{1}{2}}\right] A_2 \exp\left[-(i\omega\tau_2)^{\frac{1}{2}}\right] = b_2 - b_1 \qquad (5.14)$$

and continuity of heat flow:

$$\frac{h_1 A_1}{d}(i\omega\tau_1)^{\frac{1}{2}} \sin h\left[(i\omega\tau_1)^{\frac{1}{2}}\right] = -\frac{h_2 A_2}{d}(i\omega\tau_2)^{\frac{1}{2}} \exp\left[-(i\omega\tau_2)^{\frac{1}{2}}\right] \qquad (5.15)$$

where h_1 and h_2 are the thermal conductivities. Solving (5.14) and (5.15) we get:

$$A_1 = \frac{b_2 - b_1}{\cos h\left[(i\omega\tau_1)^{\frac{1}{2}}\right] + \frac{h_1}{h_2}\left(\frac{\tau_1}{\tau_2}\right)^{\frac{1}{2}} \sin h\left[(i\omega\tau_2)^{\frac{1}{2}}\right]} \qquad (5.16)$$

$$A_2 = -A_1 \frac{h_1}{h_2}\left(\frac{\tau_1}{\tau_2}\right)^{\frac{1}{2}} \frac{\sin h\left[(i\omega\tau_1)^{\frac{1}{2}}\right]}{\exp\left[-(i\omega\tau_2)^{\frac{1}{2}}\right]} \qquad (5.17)$$

By subtracting the initial adiabatic strain from the total strain given in Equation (5.7), and integrating over y, we obtain the total displacement, U, per unit of applied pressure caused by the relaxation of temperature differences.

$$U = \frac{2d\left[\alpha_1 - \alpha\frac{h_1\tau_1}{h_2\tau_2}\right](b_2 - b_1)}{(i\omega\tau_1)^{\frac{1}{2}} \cot h\left[(i\omega\tau_1)^{\frac{1}{2}}\right] + r(i\omega\tau_1)^{\frac{1}{2}}} \qquad (5.18)$$

where r is given by

$$r = \frac{h_1}{h_2}\left(\frac{\tau_1}{\tau_2}\right)^{\frac{1}{2}} \qquad (5.19)$$

Equation (5.18) may be rearranged to get

$$U = \frac{-2d}{T\rho_1 C_1} \frac{(b_1 - b_2)^2}{(i\omega\tau_1)^{\frac{1}{2}} \cot h\left[(i\omega\tau_1)^{\frac{1}{2}}\right] + r(i\omega\tau_1)^{\frac{1}{2}}} \qquad (5.20)$$

where use has been made of the relation

$$b = \frac{\alpha T}{\rho c} \tag{5.21}$$

The Taylor-series expansion of the hyperbolic cotangent function implies

$$s \cot h(s) = 1 + \frac{s^2}{3} + \frac{s^4}{45} \quad ..... \tag{5.22}$$

It follows from equations (5.20) and (5.22) that the displacement U ranges from

$$\Delta U = \frac{2d}{T\rho_1 c_1} (b_1 - b_2)^2 \tag{5.23}$$

to zero as frequency goes from zero to infinity, and that the imaginary component vanishes at both limits.

From our definition for Q, equation (5.8), it follows that when

$$\Delta U << U_o \tag{5.24}$$

where U_o is the initial displacement, the attenuation is approximately given by

$$\frac{1}{Q} = \frac{ImU(\omega)}{U_o} \tag{5.25}$$

The ratio

$$\frac{\Delta M}{M} = - \frac{\Delta U}{U_o} \tag{5.26}$$

is often referred to as the modulus defect. It follows from (5.8) that the attenuation, as a function of frequency, may be obtained by multiplying the imaginary part of the inverse of the denominator in equation (5.20) by the modulus defect.

Frequency dependence. Figure 5.2 shows the normalized attenuation $M/Q\Delta M$, as a function of frequency, for three different values of r. One may approximate the response of a more complicated rock by adding the creep due to each crack thickness; a result for three different crack thicknesses is shown in figure 5.3.

Inspection of equations (5.20), (5.22) and (5.25) shows that the attenuation is proportional to the square root of frequency at frequencies much less than $1/\tau_1$ and is inversely proportional to the square root of frequency at high frequencies. Most previous work on linear attenuation mechanisms in rocks [Vaisnis, 1968; Savage, 1966; White, 1975; Dutta and Ode, 1979] has assumed that diffusion-controlled mechanisms could be treated as either a single exponential decay (relaxation time), or a limited distribution of relaxation times, referred to as absorption bands [Kanamori and Anderson, 1977; Minster, 1978]. Figure 5.4 shows the curve from figure 5.2 for r = 1. For comparison a plot of the attenuation due to a single relaxation of the standard linear solid [Zener, 1948] is also shown. The comparison shows clearly that the attenuation for this idealized rock model is spread out over a much wider range of frequencies than is the attenuation due to a single relaxation time, and the maximum attenuation is just about half the attenuation for the standard linear solid model. The diffusion solution has the attenuation decreasing with square root of frequency, $\omega^{\frac{1}{2}}$, away from the peak, while the standard linear solid goes as frequency to the first power, ω. Strictly speaking, it can therefore be concluded that an infinite distribution of standard linear solid elements would be required in order to describe the loss caused by any mechanism controlled by diffusion, even in a rock where all the inhomogeneities are of the same size and shape. An actual rock will of course contain a wide range of sizes and shapes; consequently an even broader range of relaxation times would be required to describe its mechanical response.

Thermal parameters for different materials of interest in seismology are listed in table 5.2. All of the materials listed have diffusivities of the order of 1 mm^2/s; this implies that inhomogeneities with dimensions on the order of one millimeter will contribute most to the absorption of seismic waves. As the characteristic time constants, τ_1 and τ_2, are proportional to the crack thickness squared, a relatively narrow distribution of pore sizes will cause loss over a wide range of frequencies.

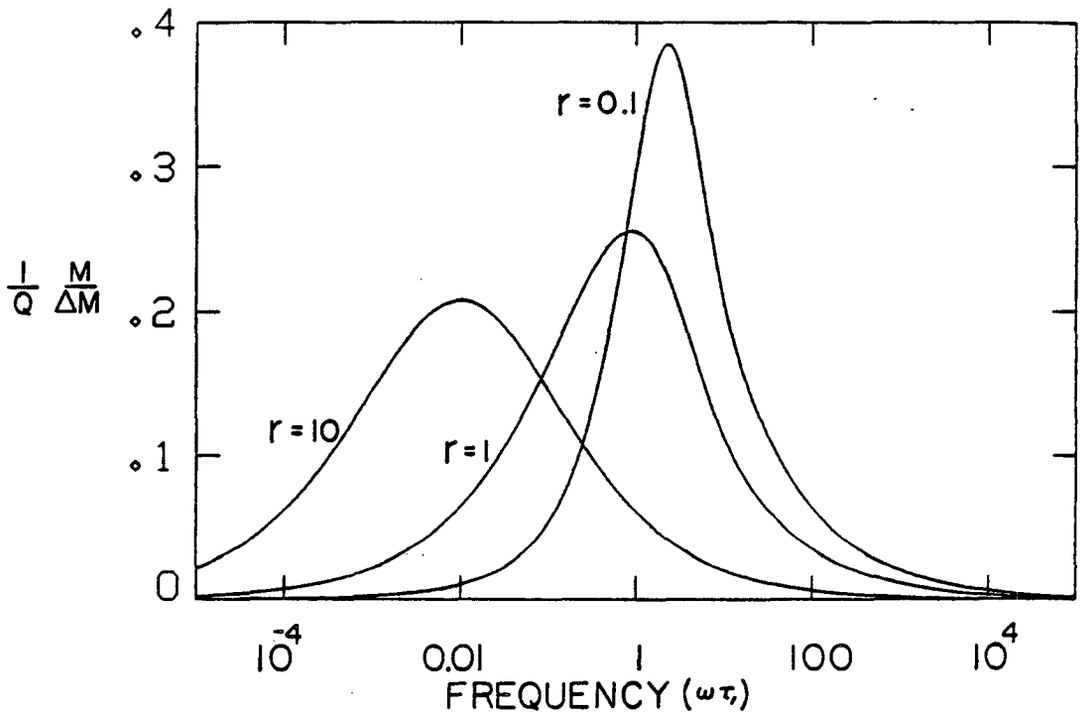

FIG. 5.2. Normalized attenuation $M/Q\Delta M$, as a function of normalized frequency $\omega\tau_1$. Curves for three different values of the thermal-impedance ratio r (5.19) are shown.

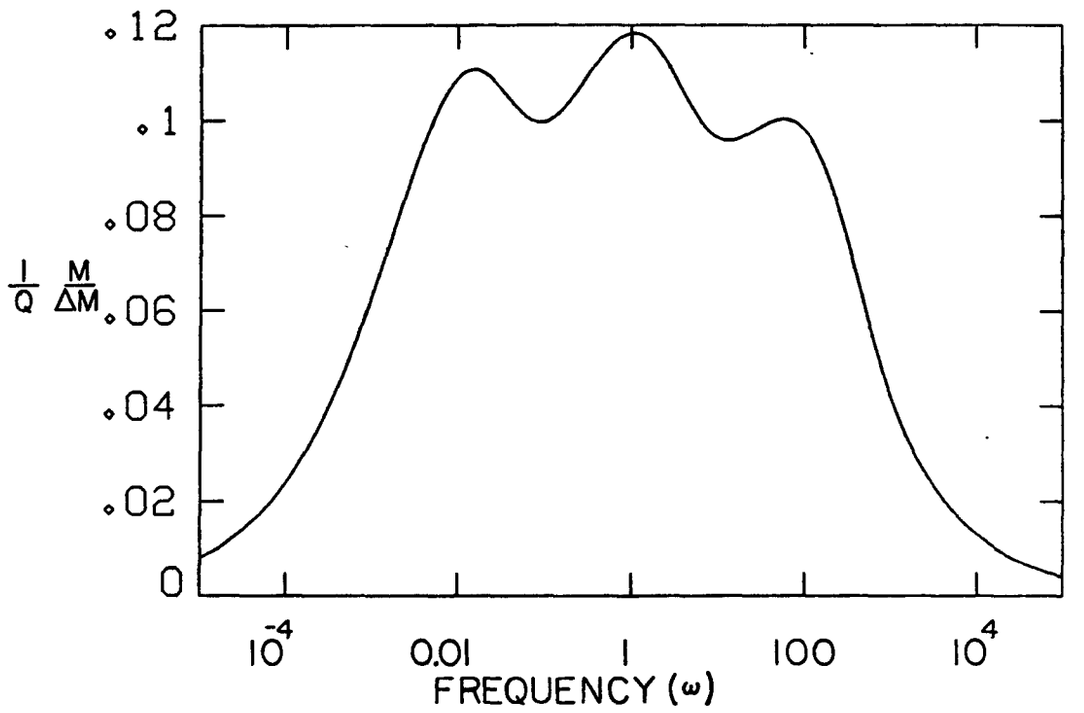

FIG. 5.3. Normalized attenuation, as a function of frequency for a rock where the pore space is equally divided between cracks with τ_1 equal to 0.1, 1 and 10 seconds. The value of r is unity.

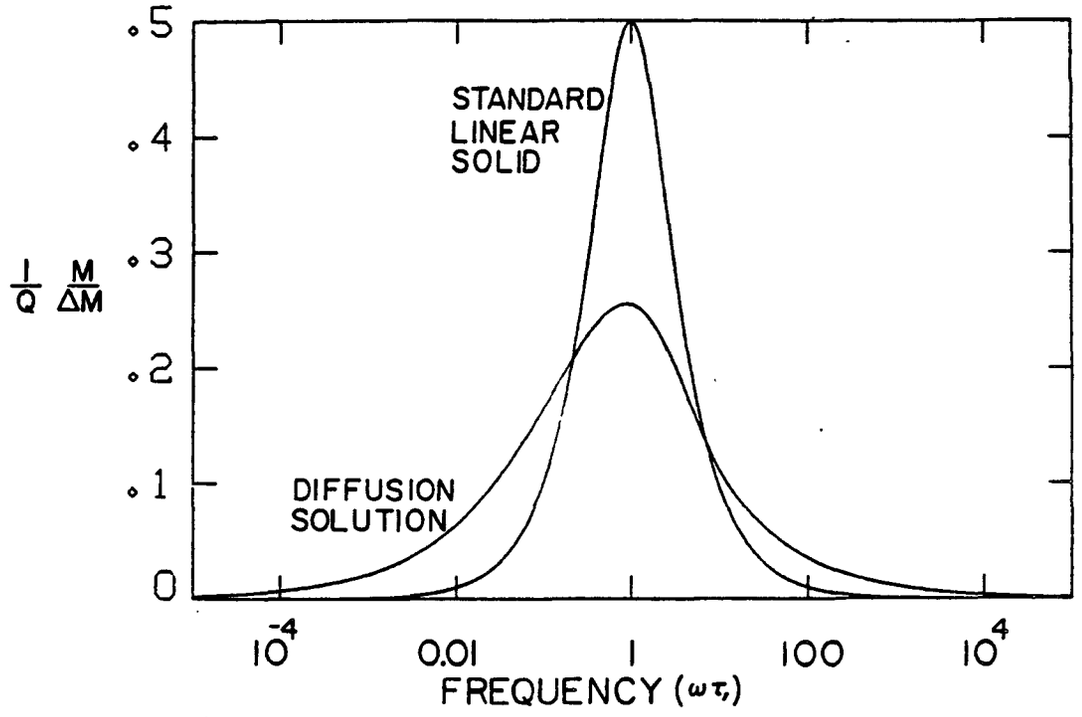

FIG. 5.4. Comparison between the standard linear solid and the diffusion solution.

	T ^oK	P Mpa	ρ $\frac{Kg}{m^3}$	$\alpha \cdot 10^6$ $^oK^{-1}$	K Pa	c $\frac{J}{^oKKg}$	h $\frac{J}{^oKms}$	b $\frac{^oK}{Pa}$	$\frac{K' - K}{K}$	D $\frac{mm^2}{s}$
limestone	300	300	2710	3.4	$76 \cdot 10^9$	840	3.85	$4.5 \cdot 10^{-10}$	$1.2 \cdot 10^{-4}$	1.7
quartzite	300	300	2640	1.1	$42 \cdot 10^9$	750	8.16	$1.6 \cdot 10^{-9}$	$7.1 \cdot 10^{-4}$	4.1
granite	300	100	2650	7.7	$46 \cdot 10^9$	590	-	$1.5 \cdot 10^{-9}$	$5.2 \cdot 10^{-4}$	-
water	293	0.1	990	202	$2.2 \cdot 10^9$	4190	0.6	$1.4 \cdot 10^{-8}$	$6.2 \cdot 10^{-3}$	0.14
water	554	10	773	2200	$5.5 \cdot 10^8$	5030	0.59	$3.2 \cdot 10^{-7}$	0.38	0.15
steam	373	0.1	0.6	2900	$1.0 \cdot 10^5$	2030	0.024	$9.0 \cdot 10^{-4}$	0.26	19
nitrogen	300	0.1	1.2	3330	$1.0 \cdot 10^5$	717	0.026	$1.2 \cdot 10^{-4}$	0.4	31

TABLE 5.2. Thermal properties of selected materials. Symbols are as defined in table 5.1. Thermodynamic data for rocks are from Simmons and Brace [1965] and Wong and Brace [1979]. Thermodynamic data for water and steam are obtained by differentiating the equation of state given by Keenan et al. [1969]. Thermodynamic parameters for nitrogen are those for a diatomic ideal gas. Conductivities for rocks are obtained by averaging values given by Clark [1966] for calcite and quartz. Conductivities for water, steam and nitrogen are from Weast [1964].

Magnitude estimation. The problem of determining the loss caused by any particular physical mechanism may be split into two parts, the estimation of the modulus defect, and the frequency dependence. It is often possible to estimate the modulus defect quite accurately, while a deterministic solution for the frequency dependence requires a detailed knowledge of the distribution and dimensions of the inhomogeneities responsible for the loss. In the remaining sections of this paper reversible thermodynamics will be used to estimate the modulus defect. A rough estimate of the range of frequencies involved may then be used to estimate the magnitude of the attenuation by a superposition of several loss peaks, as in figure 5.3. An alternative is to use the known general relationships between frequency dispersion and attenuation. For example, the assumption of a frequency-independent Q [Kjartansson, 1979] implies that

$$\frac{M(\omega)}{M(\omega_0)} = \left[\frac{\omega}{\omega_0}\right]^{2\gamma} \tag{5.27}$$

where

$$\frac{1}{Q} = \tan(\pi\gamma) \tag{5.28}$$

In the case where $Q >> 1$, this may be rewritten:

$$\frac{M(\omega)-M(\omega_0)}{M(\omega_0)} = \frac{2}{\pi Q} \ln\left(\frac{\omega}{\omega_0}\right) \tag{5.29}$$

Thus a change in modulus when the attenuation is approximately independent of frequency over six orders of magnitude is related to 1/Q by

$$\frac{1}{Q} = \frac{\pi}{2 \ln\left[10^6\right]} \frac{\Delta M}{M} \simeq \frac{1}{8} \frac{\Delta M}{M} \tag{5.30}$$

This result could also have been derived from figure 5.3.

The Magnitude of Thermoelastic Effects

In this section relations for the effective bulk modulus of rocks under various conditions will be developed and used to estimate the magnitude of loss due to thermoelastic effects. The high-frequency unrelaxed case is the simplest, as it implies periods too short for any thermal interactions to take place. Effects of porosity on the mechanical response of rocks have been treated by many authors. This includes both treatments where the pore space is assumed to be a distribution of elliptical inclusions or voids [Eshelby, 1957; Walsh, 1965; O'Connell and Budiansky, 1974], cracks of more general shapes [Mavko and Nur, 1978], or voids left between contacting spheres [Gassmann, 1951b; Mindlin and Deresewich, 1953]. These treatments all have it in common that the effective rock properties are derived from a detailed knowledge of the pore geometry as well as the intrinsic rock properties. Many of the models feature a strong dependence on poorly constrained parameters, for example aspect ratios.

In the present context we are interested in how the effective properties change as the response of the pore fluid changes, rather than in the absolute value of the effective moduli. A simple and elegant result derived by Gassmann [1951a] is ideally suited to this purpose. Gassmann's expression gives the effective bulk modulus in terms of the intrinsic bulk modulus of the rock matrix $\hat{K}$, the bulk modulus of the dry rock frame $\bar{K}$, the bulk modulus of the fluid $\tilde{K}$, and the porosity ϕ:

$$K = \frac{\hat{K}(\bar{K}+R)}{\hat{K}+R} \tag{5.31}$$

where

$$R = \frac{\tilde{K}(\hat{K}-\bar{K})}{\phi(\hat{K}-\tilde{K})} \tag{5.32}$$

The pore geometry enters into this expression only through its effect on the frame modulus ($\bar{K}$) and the porosity. Both parameters can be measured directly, as well as the intrinsic moduli of the pore fluid and the rock matrix.

In our use of Gassmann's relations, two assumptions are implicit. We will assume that the rock matrix has a zero thermal expansivity. As shown in table 5.2, the thermal expansivity of the rocks is at least an order of magnitude less than the thermal expansivity of the fluids, except for water at temperatures near 4°C. Attenuation due to thermal effects is so small when the rock and fluid have comparable thermal expansivities, that it will probably be masked by other mechanisms, such as viscous dissipation. When the expansivities are greatly different, however, attenuation may be substantial.

Shear effects. Equation (5.31) gives only relations for the bulk modulus, and is derived on the assumption that the rock is isotropic on a macroscopic scale and that the pore-fluid pressure is uniform throughout the pore volume. This implies that all the pores are connected and neglects the viscosity of the pore fluid. These assumptions are probably quite good for rocks where well-connected round pores are dominant. Gassmann's theory has been used successfully in the interpretation of seismic data for sedimentary materials [Brown and Korringa, 1975].

Winkler [1979] found that both the shear velocity and the attenuation in a porous Vycor glass are much less sensitive to changes in the pore fluid than compressional velocity and attenuation. In contrast, experiments with granite samples showed significant dependence of both shear and compressional properties on the state of the pore contents. For a rock that contains an isotropic random distribution of ***isolated*** flat cracks, both shear and bulk moduli will depend on the bulk modulus of the pore fluid [Korringa et al., 1979]. Mavko and Nur [1979] have estimated that the effects of the pore fluids on the shear response in rocks containing flat crack may be about half the effect on compressional deformations.

Estimation of effective bulk moduli. We seek expressions for the adiabatic bulk modulus of pore fluids under various conditions. We have chosen to express the results in terms of parameters that may be measured under conditions of either constant pressure or temperature. Thus we will express the adiabatic bulk modulus K' and the rate of temperature increase with pressure b in terms of the isothermal bulk modulus K, the density ρ or the specific volume V, the heat capacity at constant pressure c, and the coefficient of thermal expansivity α. The parameters are defined in table 5.1.

One of Maxwell's relations [Kelly, 1973, p. 142] enables us to write the stress heating coefficient, b, as

$$b = \left(\frac{\partial T}{\partial P}\right)_S = \left(\frac{\partial V}{\partial S}\right)_P \tag{5.33}$$

In the absence of any phase transitions this becomes

$$b = \frac{\left(\frac{\partial V}{\partial T}\right)_P}{\left(\frac{\partial S}{\partial T}\right)_P} = \frac{T\alpha V}{c} = \frac{T\alpha}{\rho c} \tag{5.34}$$

In order to get the adiabatic bulk modulus K' we may write

$$\left(\frac{\partial V}{\partial P}\right)_S = \left(\frac{\partial V}{\partial P}\right)_T + \left(\frac{\partial V}{\partial T}\right)_P \left(\frac{\partial T}{\partial P}\right)_S \tag{5.35}$$

Using the definitions in table 5.1, this reduces to

$$\frac{1}{K'} = \frac{1}{K} - \alpha b \tag{5.36}$$

Equations (5.34) and (5.36) may be applied to heterogeneous systems, as long as no phase transitions take place. The isothermal bulk modulus and the isobaric expansivity and heat capacity are not defined in the presence of phase transitions: this case will be treated separately. The parameters used will now be the effective parameters, K_e, α_e, c_e and V_e, for the system that is being analyzed. For a porous rock where the matrix has no thermal expansivity, a specific volume V_r, heat capacity c_r, and porosity ϕ, and a pore space containing a mixture of two fluids, indicated by subscripts 1 and 2 where the mass fraction of the first fluid is x, we have the following relations for the effective parameters of the pore mixture:

$$V_e = xV_1 + (1-x)V_2 \tag{5.37}$$

$$\frac{1}{K_e} = \frac{1}{V_e}\left[\frac{xV_1}{K_1} + \frac{(1-x)V_2}{K_2}\right] \tag{5.38}$$

$$\alpha_e = \frac{1}{V_e}\left[xV_1\alpha_1 + (1-x)V_2\alpha_2\right] \tag{5.39}$$

$$c_e = xc_1 + (1-x)c_2 + \frac{V_e(1-\phi)c_r}{V_r\phi} \tag{5.40}$$

Water-saturated rock. We will first consider a rock saturated with liquid water. In this case $x = 1$, $V_e = V_1$, $K_e = K_1$, $\alpha_e = \alpha_1$ and

$$c_e = c_1 + \frac{V_1}{V_r}\frac{1-\phi}{\phi}c_r \tag{5.41}$$

Thus the only difference between the unrelaxed high-frequency limits, where there is no thermal interaction, and the fully relaxed limit, is an increase in the effective heat capacity of the liquid; the rock matrix acts as a heat sink. The second term in equation (5.41) will tend to dominate when $\phi << 1$. For low-porosity rocks the relaxed case is well-approximated by using the isothermal bulk modulus for the fluid.

Keenan et al. [1969] give an empirical equation of state that fits the observed behavior of liquid water and steam at pressures less than 100 Mpa (1000 bar) and at temperatures less than 1000°C. Differentiation of this equation yields an internally consistent set of thermodynamic parameters for water and steam. Figure 5.5 shows a plot of the isothermal and adiabatic bulk moduli of water, as functions of temperature, at the boiling pressure. At room temperature there is little difference between the two curves, but the difference increases rapidly at higher temperatures. Another noteworthy feature on this plot is the rapid decrease of both the isothermal and adiabatic bulk moduli at temperatures above 100°C.

Figure 5.6 shows P-wave velocities for three different rocks as functions of temperature at a pore pressure of 10 Mpa (100 bar). The rocks have the same intrinsic matrix velocity (6.5 km/s) and the same dry P-velocity (1.5 km/s), with Poisson ratios of .25 and .2, respectively. Porosities were chosen so as to give saturated velocities of 2, 3, and 4 km/s. Two curves are shown for each rock, one for the unrelaxed case and one for the relaxed case.

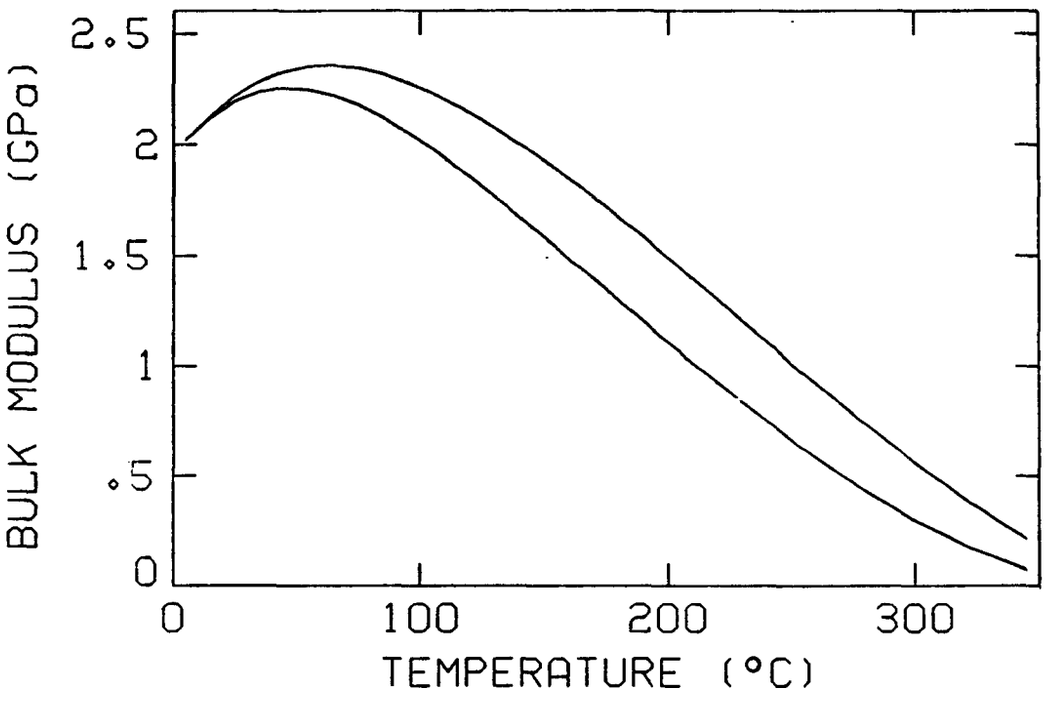

FIG. 5.5. Adiabatic and isothermal bulk moduli of water, as functions of temperature, at boiling pressure.

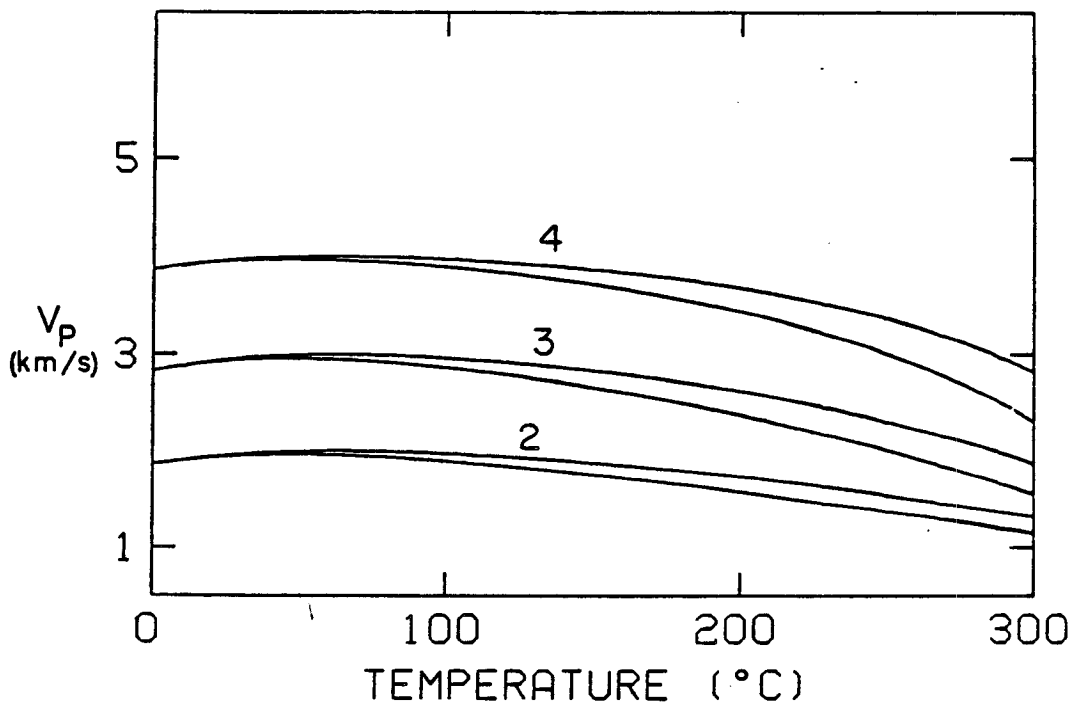

FIG. 5.6. P-wave velocities for three different rocks saturated with liquid water, plotted vs. temperature. The upper curve in each pair is the unrelaxed, the lower is the relaxed velocity. The three rocks have the same dry velocity, 1 km/s, and the same matrix material with a P-velocity of 6.5 km/s. Porosities were chosen to give maximum saturated velocities of 2, 3 and 4 km/s. Pore pressure is 10 MPa.

Figure 5.7 shows the attenuation obtained by applying equation (5.30) to the results from figure 5.6. All three curves show a strong increase in attenuation with temperature. The example with the lowest porosity and the highest saturated velocity shows stronger temperature dependence than the other; this is due to an increase in the fraction of the total strain energy that is stored in the pore fluid as its compressibility increases.

The examples in figures 5.6 and 5.7 were computed for specified values of the dry and saturated velocities. For comparison with *in-situ* observations, it may sometimes be more desirable to specify porosity rather than dry velocity since the latter may be more readily estimated. Figure 5.8 shows a contour plot of the attenuation, predicted as a function of porosity and temperature, for a rock with a saturated velocity of 4 km/s and an intrinsic velocity of 6.5 km/s. As before, a strong dependence of attenuation on temperature is indicated, but at high temperatures the attenuation increases as porosity (and the dry velocity) decreases.

Gas and liquid. The second example that we will consider is for rock where the pore space contains a mixture of a gas phase and liquid water, such that the two materials do not interact except through the flow of heat from one to the other. Figure 5.9 shows relaxed and unrelaxed velocities for three different rocks, chosen to have properties similar to those used by Domenico [1974], as representative of sand reservoir rocks at depths of 600, 1800 and 3000 meters (2000, 6000, and 10000 feet). The corresponding attenuation values are plotted in figure 5.10. The gas is assumed to be an ideal gas with the ratio between the adiabatic and isothermal bulk moduli $\gamma = 1.4$, the theoretical value for a diatomic gas. The density was assumed to be that of air, $a = 0.029 kg/mol$. The other parameters are given by

$$V = \frac{RT}{aP} \tag{5.42}$$

$$K = P \tag{5.43}$$

$$\alpha = \frac{1}{T} \tag{5.44}$$

$$c = \frac{R}{(\gamma-1)a} \tag{5.45}$$

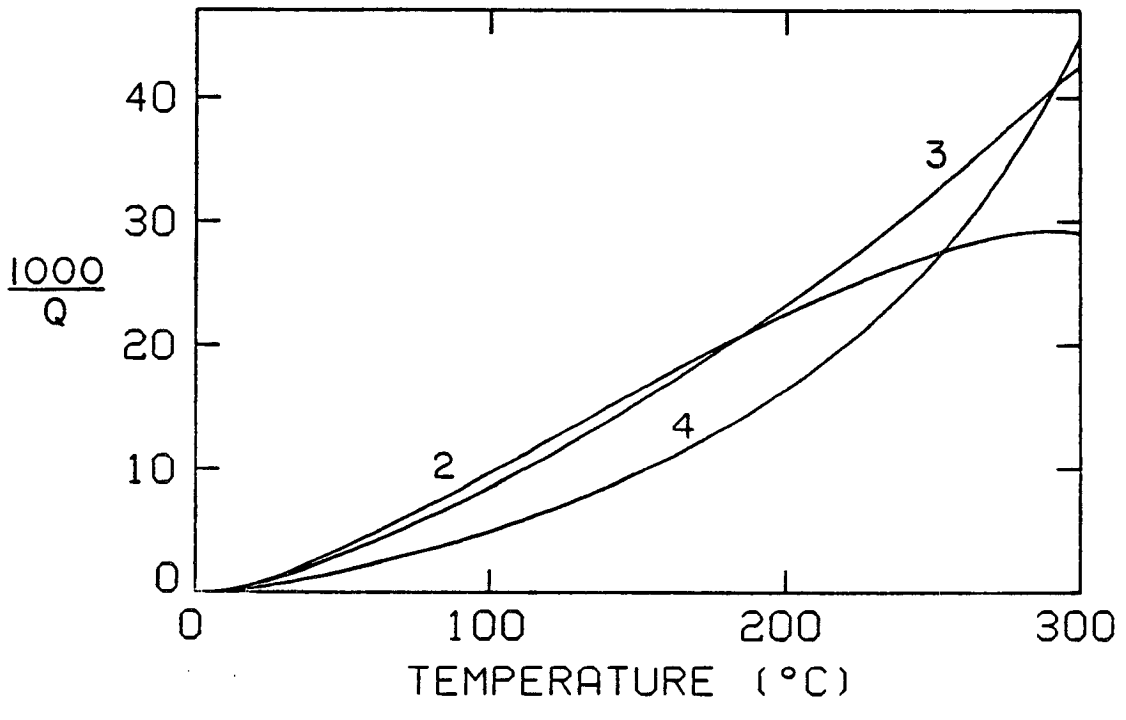

FIG. 5.7. Attenuation as a function of temperature for the conditions in figure 5.6.

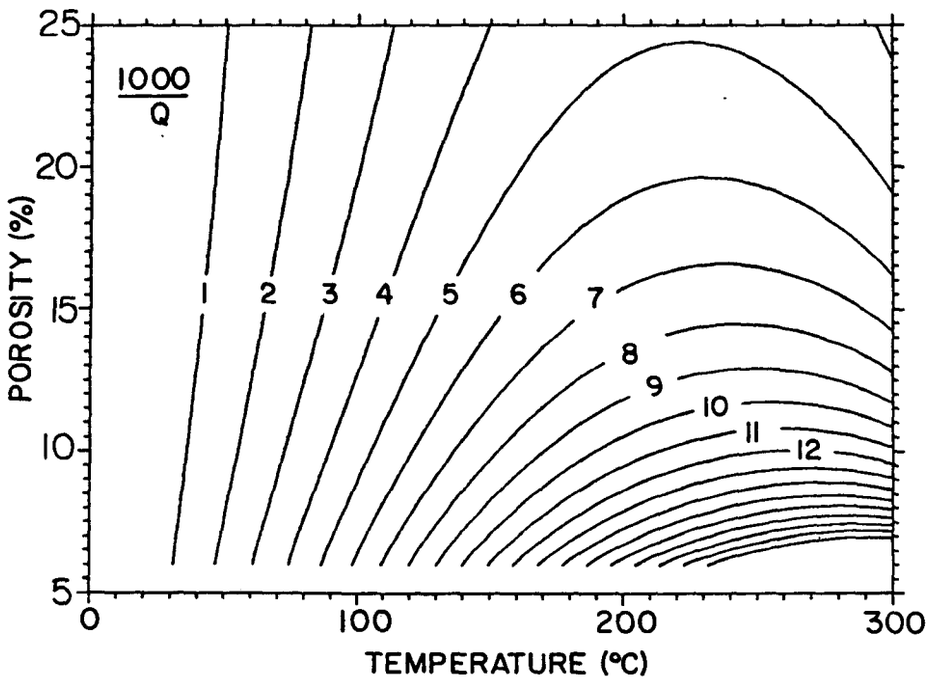

FIG. 5.8. Attenuation for water-saturated rocks, as a function of temperature and porosity, for rocks with a P-wave velocity of 3.5 km/s at 65°C and an intrinsic matrix velocity of 6.5 km/s.

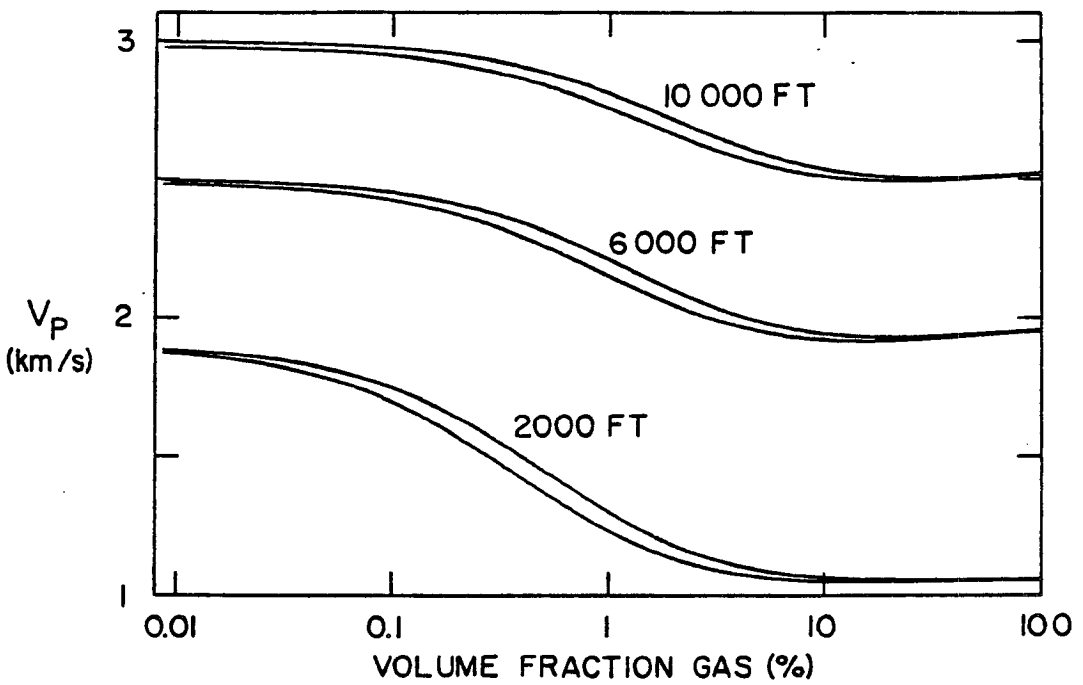

FIG. 5.9. Computed relaxed and unrelaxed P-wave velocities for rocks containing a mixture of gas and water. Rock parameters are the same as used by Domenico [1974], as representative of conditions in sand reservoirs at depths of 2000, 6000 and 10,000 feet.

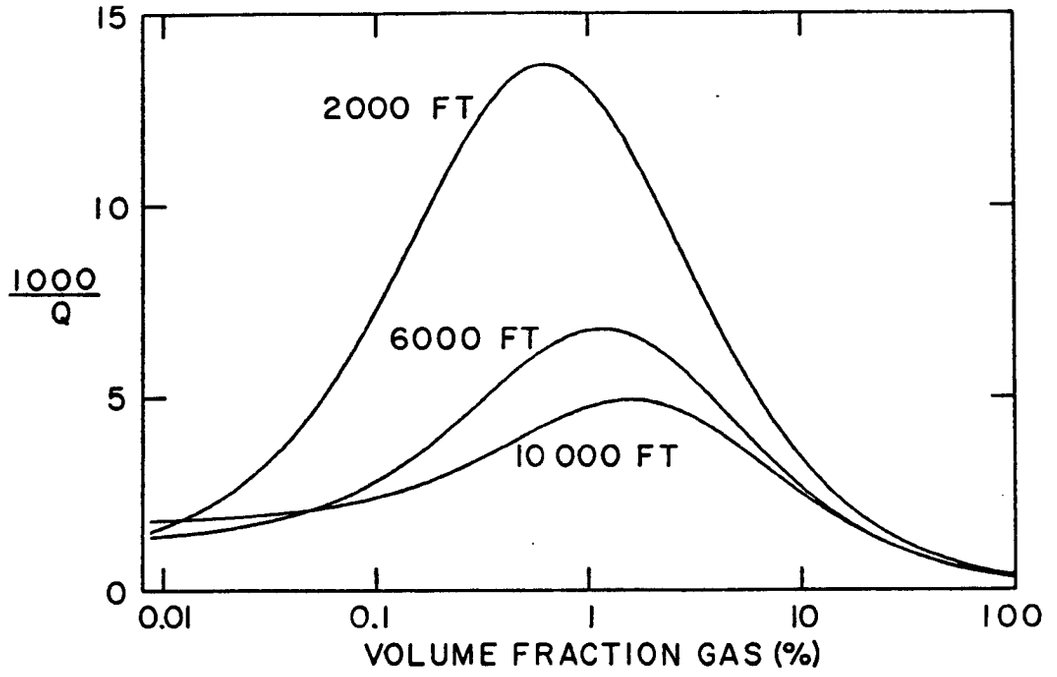

FIG. 5.10. Attenuation for the rocks in figure 5.9.

where R is the gas constant, 8.314 J/mol. The gas parameters are combined with those for water using equations (5.37)-(5.40) and then substituted into Gassmann's formula (5.31).

Our results show the same qualitative dependence of velocity on gas saturation as was reported by Domenico [1974], while there is a substantial drop in velocity as small amounts of gas are introduced into water-saturated rock; there is little difference in velocity between rocks with 10% and 100% of the pore volume gas, for all of the cases shown. Attenuation increases as gas is introduced into the pore space, reaches a peak, and then falls off and is minimum when no water is left in the pores. The gas saturation at the peak is roughly proportional to the pore pressure. The examples in figure 5.10 show a large change in attenuation as the gas fraction changes from 5% to 100%, while the velocity is virtually unchanged over this range. This may be of interest in exploration for natural gas and geothermal resources.

Winkler and Nur [1979] and Frisillo and Stewart [1979] present laboratory results showing the same qualitative features, but with the attenuation peak occurring when the gas saturation is between 10% and 30%. This discrepancy between our theoretical and these experimental results may be caused by microscopic inhomogeneities in the pore space. The pore space may consist of both wide pores and relatively flat cracks, which are not all connected at the sonic and ultrasonic frequencies used in these experiments.

Systems with more than one phase. In the presence of phase transitions we can no longer use equation (5.35) since $(\partial V/\partial P)_T$ is not finite. To get the effective adiabatic bulk modulus we may write

$$\left[\frac{\partial V}{\partial P}\right]_S = \left[\frac{\partial V}{\partial T}\right]_S \left[\frac{\partial T}{\partial P}\right]_S \tag{5.46}$$

Use of the Maxwell's relation (5.33) yields the Clausius-Clapeyron equation

$$b = \frac{dT}{dP} = \frac{T(V_1 - V_2)}{L_{12}} \tag{5.47}$$

where L_{12} is the latent heat released in the transition from state 1 to state 2. The other factor on the left side of (5.46) is obtained by writing

$$\left(\frac{\partial V}{\partial T}\right)_S = \left(\frac{\partial V}{\partial T}\right)_{P,x} + \left(\frac{\partial V}{\partial P}\right)_{T,x}\left(\frac{\partial P}{\partial T}\right)_S + \left(\frac{\partial V}{\partial x}\right)_{P,T}\left(\frac{\partial x}{\partial T}\right)_S \qquad (5.48)$$

The first term in (5.48) is obtained from equations (5.39) and the second term from (5.38) and (5.47). For the final term we have

$$\left(\frac{\partial V}{\partial x}\right)_{P,T} = (V_2 - V_1) \qquad (5.49)$$

The final factor, $(\partial x/\partial T)_S$, is obtained by writing

$$\left(\frac{\partial S}{\partial T}\right)_S = 0 = \left(\frac{\partial S}{\partial x}\right)_{P,T}\left(\frac{\partial x}{\partial T}\right)_S + \left(\frac{\partial S}{\partial T}\right)_{P,x} + \left(\frac{\partial S}{\partial P}\right)\left(\frac{\partial P}{\partial T}\right)_S \qquad (5.50)$$

Through the use of Maxwell's fourth relation [Kelly, 1973], this becomes

$$\left(\frac{\partial x}{\partial T}\right)_S = \frac{-\left(\frac{\partial S}{\partial T}\right)_{P,x} + \left(\frac{\partial V}{\partial T}\right)_{P,x}\left(\frac{\partial P}{\partial T}\right)_S}{\left(\frac{\partial S}{\partial x}\right)_{P,T}} \qquad (5.51)$$

Substitution of equations (5.48) and (5.51) into (5.46) and the definition of the bulk modulus give the result

$$\frac{1}{K'} = \frac{1}{K_e} - 2b\alpha_e + \frac{b^2 c_e}{V_e T} \qquad (5.52)$$

where b is given by equation (5.47) and V_e, α_e, and c_e are given by equations (5.37), (5.39), and (5.40).

We have applied equation (5.52) to two cases. One is a porous rock where the pore space contains a mixture of water and steam. The relaxed and unrelaxed velocities are shown as functions of mass fraction steam in figure 5.11. Figure 5.12 shows the corresponding attenuation. The introduction of any steam into a water-saturated rock results in a drop of the effective relaxed modulus, to a value that is essentially the same as the modulus of the dry rock. This results in attenuation that is much greater than when phase transitions are absent.

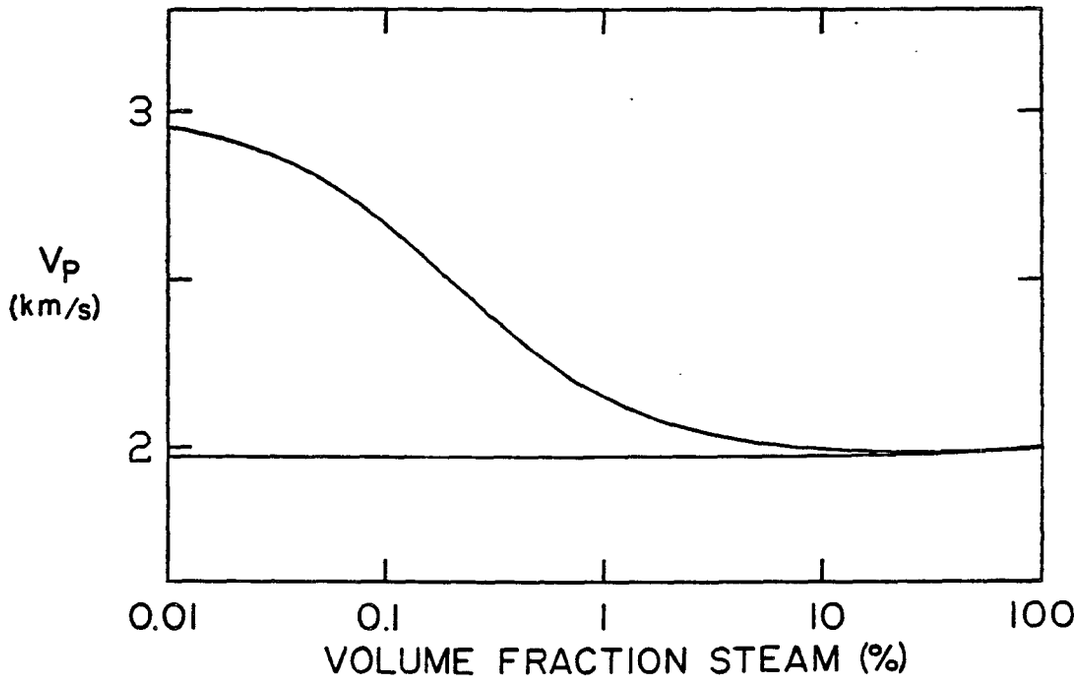

FIG. 5.11. Relaxed and unrelaxed P-wave velocities for a rock containing a mixture of water and steam at a temperature of 200°C. The dry velocity is 2 km/s and the saturated velocity is 3 km/s.

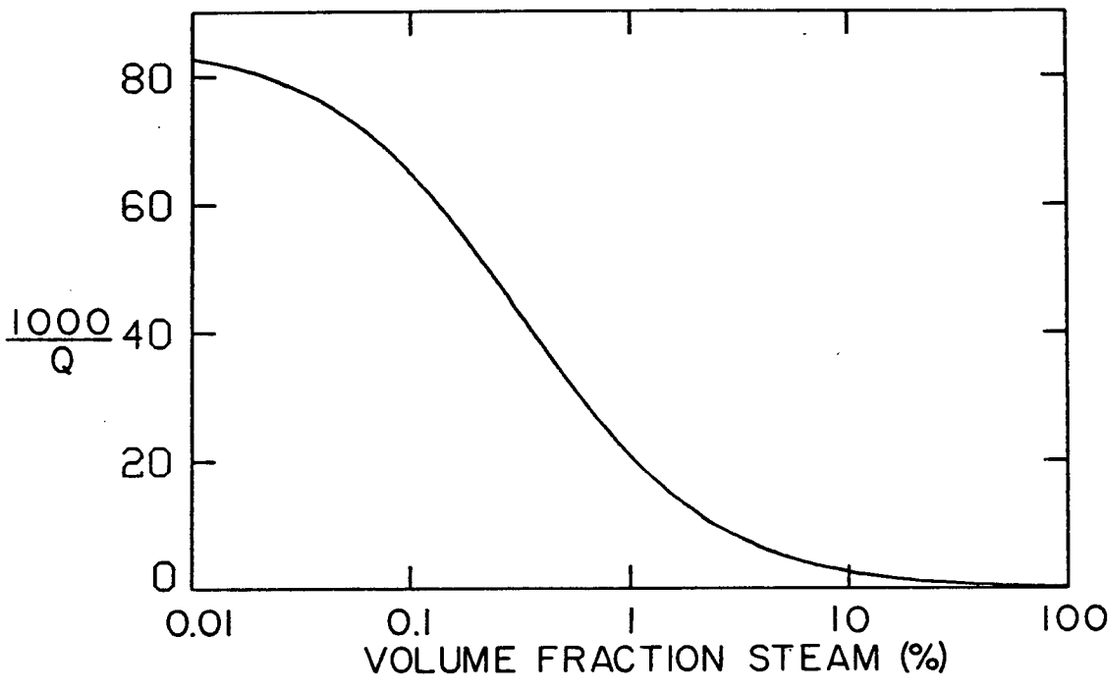

FIG. 5.12. Attenuation for the conditions in figure 5.11.

Another case where phase transitions are expected to play a significant role is in rocks that contain partial melt. Carmichael et al. [1977] give equations of state for several minerals that satisfy measured heat capacities and the observed dependence of melting temperature on pressure up to about 4 GPa (40 kbar). They give empirical relations for (1) the dependence of the specific volume on both temperature and pressure, and (2) heat capacity and the latent heat of fusion at room pressure. The empirical expressions are readily integrated to obtain the Gibbs free energy as a function of temperature and pressure. The Gibbs free energy may be used to compute the melting temperature, and differentiated to yield the heat capacity at any pressure. The resulting set of thermodynamic parameters is guaranteed to be internally consistent; this is important because equations (5.36) and (5.52) involve differences between terms of similar size. Figure 5.13 shows the effective bulk modulus for a mixture of solid and liquid olivine (fayalite), for three different cases: unrelaxed without any phase transitions or heat flow; thermal equilibrium without any phase transitions, and both thermal and phase equilibria. Figure 5.14 shows the attenuation, both with and without phase transitions. In these examples we have neglected the effects of the shear strength of the solid phase. The effect of the shear strength of the rock is to reduce the difference between the relaxed and unrelaxed effective moduli, and thus the attenuation at low melt fractions, unless the melt surrounds the solid grains or is in the form of very thin films. The effects of other melt configurations are treated in detail by Mavko [1979].

Implications for Exploration

Hydrocarbons. Most of the cases where we have predicted significant absorption due to thermal effects are of interest in the exploration for energy resources. The calculations for water and gas mixtures should give an indication of the degree of losses that might be expected in rocks that contain gas. Our results for this case, as shown in figure 5.10, indicate that thermal relaxation will be responsible for a significant amount of absorption when gas is present in small amounts, and that the loss will be strongly dependent on the degree of gas saturation, even in the range where the wave velocities are insensitive to the amount of gas present. The results from figure 5.10 would have been virtually the same had an incompressible liquid

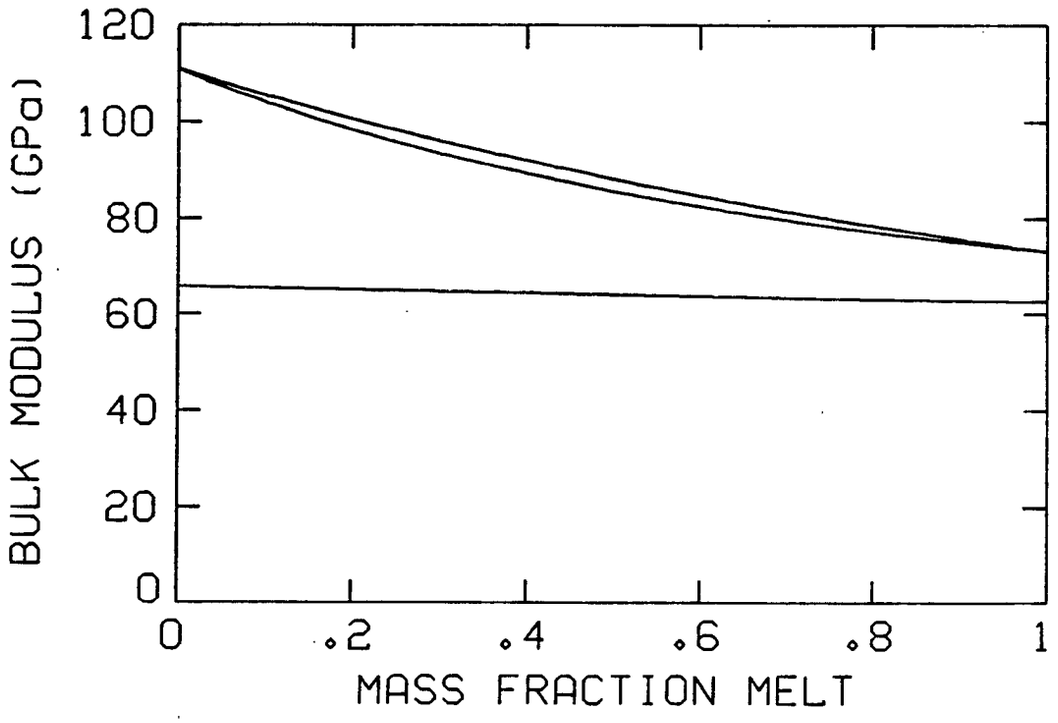

FIG. 5.13. Bulk modulus of olivine as a function of massfraction melt, at a pressure of 2 GPa. Shown are the unrelaxed bulk modulus (top curve), the thermally relaxed without phase transitions, and the completely relaxed bulk modulus including the effects of phase transitions (bottom).

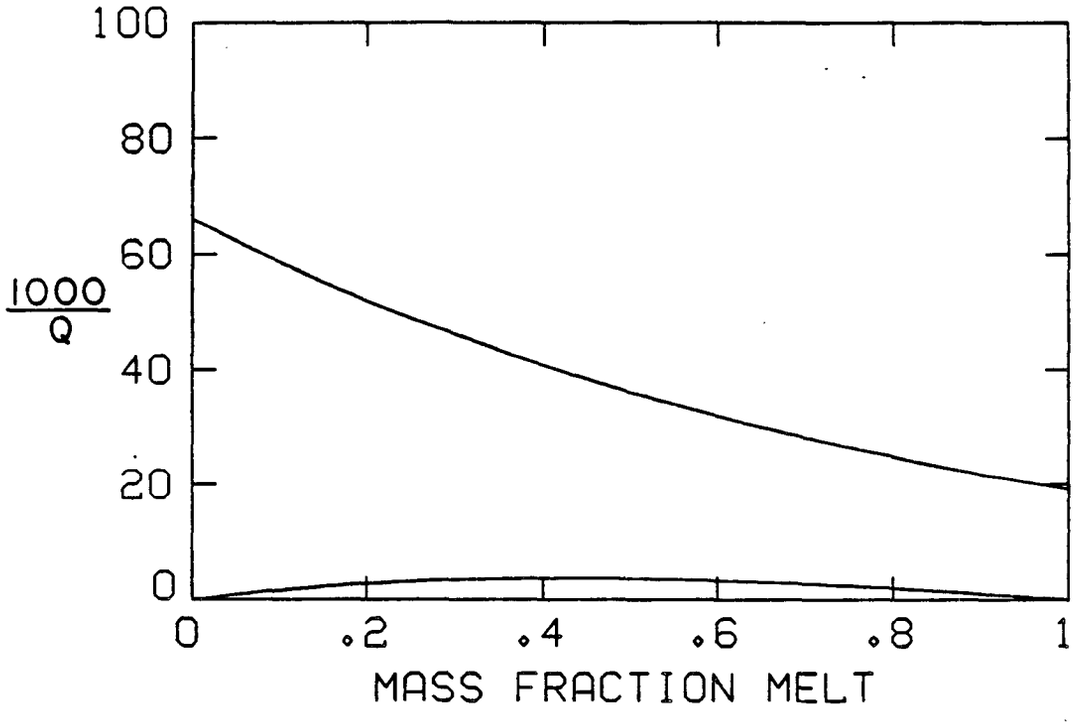

FIG. 5.14. Attenuation for olivine under the same conditions as in figure 5.13. Upper curve is the attenuation when phase transitions are included; the lower curve shows the attenuation caused by heat flow without any phase transitions.

been used instead of water; the loss is controlled primarily by the properties of the gas. As most gases have properties similar to ideal gas, the results from figure 5.10 do apply to any gas-liquid mixtures, as long as the gas does not dissolve in the liquid. Any solubility of the gas in the liquid will have the effect of lowering the relaxed bulk modulus and thus increasing the absorption. This may be the case in most, if not all cases involving hydrocarbons *in situ*, whether the fluid is brine or oil. Consequently, the calculations in figure 5.10 should be considered lower bounds for the absorption due to thermal relaxation. The actual response of oil-gas or brine-gas mixtures may be more like the response of water-steam mixtures (figure 5.12).

It has been noted in the literature that anomalously low amplitudes are sometimes associated with gas zones [Sheriff, 1975; Dobrin, 1976].

Geothermal. Several of the conditions that result in significant thermal losses are related to features of interest in geothermal exploration. Some of the larger concentrations of geothermal energy are associated with recent igneous activity. Observations of P-wave absorption may aid in the location of zones of partial melt at depth, and thus delineate potential sources of heat.

Geothermal energy is utilized in three different forms, each of which is presently of roughly the same economic significance. Low-temperature thermal waters, with temperature at depth ranging from 65°C to 200°C, are useful as a direct source of heat for space heating and various industrial processes. If the pore pressure at depth is anywhere close to hydrostatic, the water will be in the liquid state and boiling will only take place very near the surface. The results from figures 5.6-5.8 are relevant to those circumstances, and imply that the absorption will increase almost linearly with temperature, at temperatures from 50°C to 200°C.

The results of our calculations for liquid water are also applicable to high-temperature geothermal systems. Figure 5.15 shows the boiling temperature of water, as a function of pore pressure. Boiling temperature of 180° is reached at a depth of about 100 m, if the pore pressure is hydrostatic. At higher temperatures the boiling point curve does level off toward the critical point at 374°C and a pressure of 22.1 MPa. It is thus possible that high-temperature water-dominated systems could reach the boiling pressure at depth, even if the pore pressures are close to hydrostatic. This would result

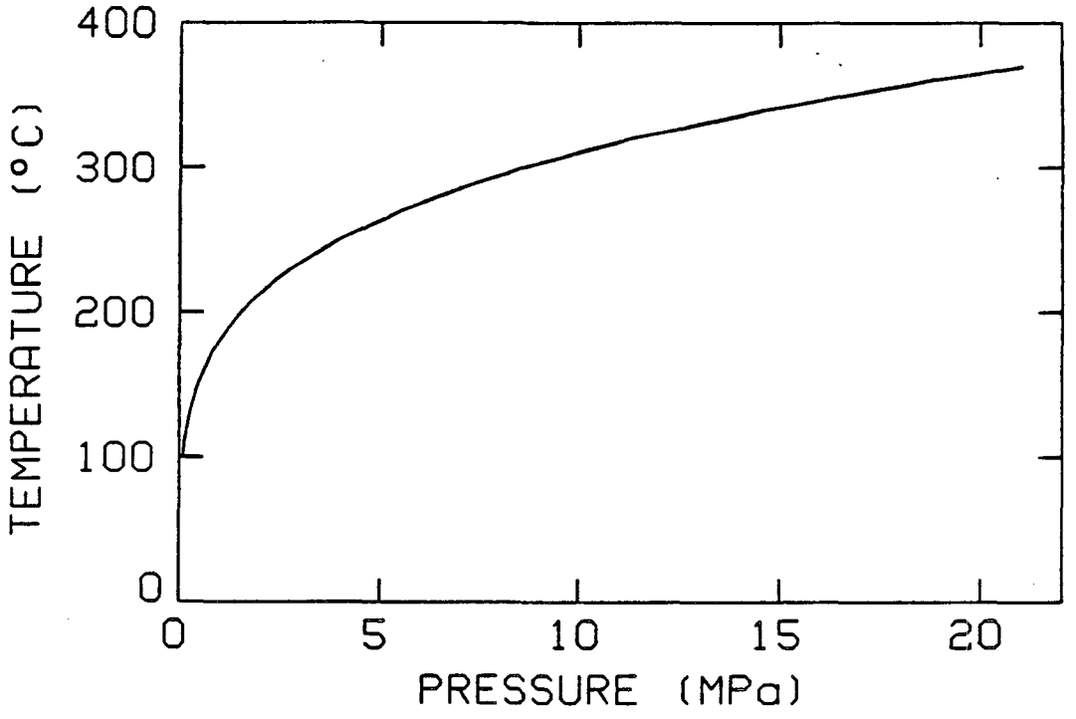

FIG. 5.15. Boiling temperatures of water as a function of pressure.

Chapter VI

FINITE-DIFFERENCE MODELING AND MIGRATION IN MEDIA WITH LATERALLY VARIABLE ATTENUATION AND VELOCITY

The expressions derived in the previous chapters make it possible to describe wave propagation in rocks for monochromatic waves, including the effects of absorption. While the theory for the finite-difference modeling of waves in the frequency domain has been developed in detail [Claerbout, 1971, 1976], its use appears to have been rather limited. As the properties of the earth may be considered time-invariant for the duration of seismic experiments and linear at seismic amplitudes, no generality is lost by Fourier transforming over time. There are several advantages in working in the frequency domain. Each Fourier component of the seismogram may be propagated separately, which can simplify manipulations of large datasets compared to time-domain methods. A time shift over a non-integer number of sampling intervals consists in the frequency domain of a simple multiplication. Perhaps the greatest advantage of the frequency domain is that all time derivatives are evaluated exactly by a simple multiplication. This becomes increasingly important as more accurate equations involving higher time derivatives are used. This also makes it possible to include the effects of anelasticity at little or no additional cost.

Wave-Field Extrapolation

It is shown by Claerbout [1976, p. 196] that the scalar wave equation for constant density

$$P_{zz} + P_{xx} = \frac{1}{v^2} P_{tt} \tag{6.1}$$

where the subscripts denote partial derivatives, becomes

$$R_{zz} + R_{xx} + 2i\bar{m}R_z + (m^2-\bar{m}^2)R = 0 \tag{6.2}$$

when R is defined by

$$R(x,z,\omega) = e^{i\bar{m}z}\,\bar{P}(x,z,\omega) \tag{6.3}$$

$$\bar{P}(x,z,\omega) = \int_{-\infty}^{\infty} P(x,z,t)e^{-i\omega t}\,dt \tag{6.4}$$

$$m = -\frac{\omega}{v} \tag{6.5}$$

$$\bar{m} = -\frac{\omega}{\bar{v}} \tag{6.6}$$

In the derivation of this result, $\bar{v}$ has been assumed to be independent of x and z, while v may be a function of both x and z. Since we are using a minus sign in the forward Fourier transform [Bracewell, 1965], the signs in equations (6.5) and (6.6) are different from those used by Claerbout [1976].

The R_{zz} term is eliminated if each term in equation (6.2) is differentiated with respect to z, multiplied by $i/2\bar{m}$, and added to the original equation. The result is

$$\frac{i}{2\bar{m}}R_{zzz} + \frac{i}{2\bar{m}}R_{xxz} + R_{zz} + 2i\bar{m}R_z + \frac{i}{2\bar{m}}(m^2-\bar{m}^2)R_z \tag{6.7}$$

$$+ (m^2-\bar{m}^2)R + \frac{im}{m}\frac{dm}{dz}R = 0$$

It should be noted that we have not made any approximations yet: equation (6.7) is simply the scalar wave equation in a shifted coordinate frame.

For waves traveling in approximately the same direction as the coordinate frame is shifted, R_{zzz} should be small in relation to the other terms. If it is dropped, the result

$$\frac{i}{2\bar{m}}R_{xxz} + R_{zz} + 2i\bar{m}R_z + \frac{i}{2\bar{m}}(m^2-\bar{m}^2)R_z + (m^2-\bar{m}^2)R + \frac{im}{m}\frac{dm}{dz}Q = 0 \tag{6.8}$$

will be first order in z. The dispersion relation is shown in figure 6.1. As shown in figure 6.1, the dispersion relation for equation (6.8) starts to

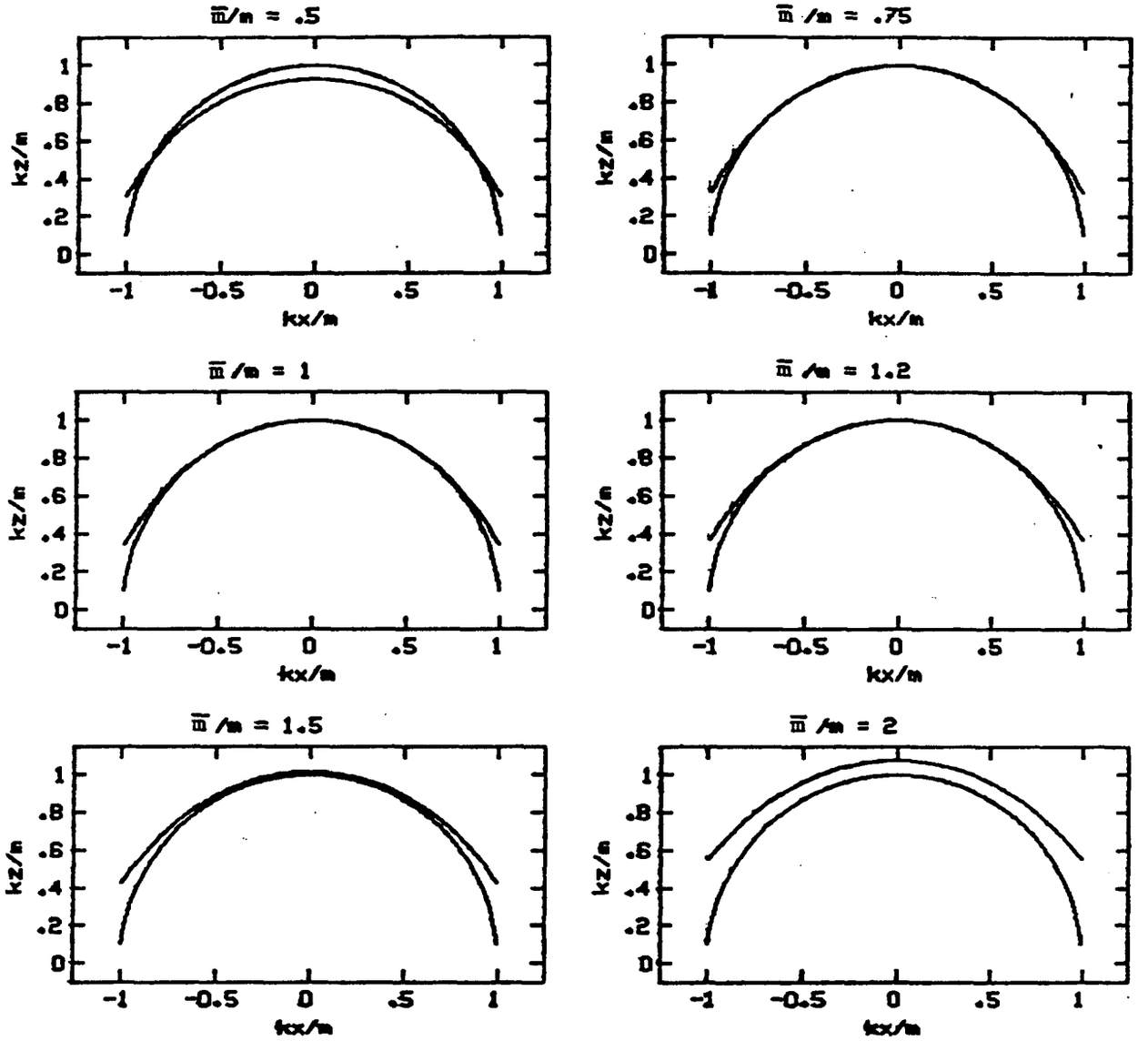

FIG. 6.1. The dispersion relation for equation (6.8). Each plot shows the k_z/m as a function of k_x/m. For comparison the semicircle is also shown. The accuracy of equation (6.8) is quite acceptable for $0.7m < \bar{m} < 1.5m$.

deviate significantly from the correct value when $\bar{m}$ and m differ by more than 50 percent.

In many cases this is not a serious limitation. I have used equation (6.8) extensively to model and migrate seismic sections, without any difficulties. If it is assumed that the coefficients in equation (6.1) are locally constant, one may set $m = \bar{m}$ and then apply a time shift at each depth step. This assumption that the coefficients are locally constant is commonly made, e.g. when a wave equation is derived to satisfy a particular dispersion relation.

Thus one can get the wave field $\bar{P}(z+\Delta z)$ from $\bar{P}(z)$ by setting

$$R(z) = \bar{P}(z) \tag{6.9}$$

and solving

$$\frac{i}{2m(x,z)} R_{xxz} + R_{xx} + 2im(x,z)R_z = 0 \tag{6.10}$$

for $R(z+\Delta Z)$, and then applying the time shift

$$\bar{P}(z+\Delta z) = \exp\left[im(x,z)\Delta z\right]R(z+\Delta z) \tag{6.11}$$

Equation (6.10) is simpler to code than equation (6.8) and has a more accurate dispersion relation, but does not treat the effects of velocity gradients as accurately as equation (6.8). Both equations fit on the finite-difference star described by Claerbout [1976, p. 184-189] and may be solved using the Crank-Nicolson scheme.

Exploding Reflector Model

Most migration and modeling techniques use an imaging principle based on the exploding reflector model. Two basic assumptions are involved. The first is that the the CMP stacked section is equivalent to a zero-offset section. The second assumption is that a zero-offset section may be modeled by placing

sources on all the reflectors at $t = 0$ and continuing the resulting wave field to the surface, using half the true velocity. This has been discussed by various authors [e.g. Stolt, 1978], but it is usually assumed that the velocity depends only on depth. We will explore the extent to which the exploding reflector model is valid when lateral variations in velocity are present. The results may be extended to non-zero offsets; this leads to an accurate method for the computation of synthetic seismograms for all offsets. For simple reflectivity structures this method is very economical.

Theory

We will assume that the reflection seismogram can be approximated by a distribution of point scatterers, imbedded in a variable velocity medium. This assumption is valid when the reflection coefficients are small and independent of the angle of incidence. When this is the case, seismograms can be computed for arbitrary reflectivity structures by superposition of the seismograms resulting from each reflector point. The seismogram, ${}_sS_g$, recorded at g from a source at s, may be considered as a convolution of the shot waveform W (as it would be recorded by the recording instrument), the propagation from the source to the reflector ${}_sP_r$, the reflectivity R and the propagation from the reflector to the geophone ${}_rP_g$. In the frequency domain this may be written as follows:

$$ {}_sS_g = W \; {}_sP_r \; R \; {}_rP_g \tag{6.12} $$

In the case of zero offset reciprocity implies that

$$ {}_sP_r = {}_rP_g \tag{6.13} $$

and

$$ {}_gS_g = W \; R \; {}_rP_g^2 \tag{6.14} $$

Reciprocity may also be used to obtain nonzero offsets when ${}_rP_g$ is known

for all reflector points and surface locations. For a single point scatterer this requires no more computation than the upward continuation of the wave field due to a point source at depth. When the velocity structure is such that ${}_rP_g$ consists of a single spike, with traveltime t_o and amplitude A_g, it is easy to see that ${}_rP_g^2$ is a spike arriving at $2t_o$ with an amplitude A_o^2. Thus one may approximate ${}_rP_g^2$ by stretching ${}_rP_g$ and applying a time-dependent gain to correct for geometric spreading.

The condition that ${}_rP_g$ be a spike is not necessary in all cases - for example, if the rate of dissipation is proportional to frequency (constant Q) a plane-wave pulse is broadened in a homogeneous medium such that the seismogram at any distance is obtained by a stretching and scaling of a single seismogram [Kjartansson, 1979]. Because of the frequency-dependence of the velocity, the scaling factor is not exactly proportional to distance. This does not apply for other dissipation laws, such as that treated by Ricker [1953, 1977].

The observed seismogram is a linear function of the reflectivity in the subsurface (for small reflection coefficents). The convolution of a trace on itself is a non-linear operation and must therefore be performed for each reflector point separately. The time stretching is a linear operation so it can be performed for all the traces and reflectors together, implicitly by using half the true velocity. When a linear operator such as the wave equation is used to compute ${}_rP_g$, a great saving in computational effort can result from superposing the reflectors before the wave extrapolation.

The convolution cannot be replaced by time stretching when more than two raypaths connect the reflector and the surface point. This can happen when $\partial^2 v/\partial x^2 \neq 0$ or when the interfaces between layers of different velocities are curved.

Implementation

Thus, when modeling a zero-offset section on the computer using the exploding reflector model, one can start with a blank upgoing wave field below the lowest reflector, then use equations (6.9), (6.10) and (6.11) to continue the wave field up towards the surface. Since a delta function at t=0 has a

Fourier transform that is simply a constant, independent of frequency, one can then model the exploding reflectors by adding the reflection coefficient to all of the frequencies, at each z-step. The time section is then obtained by inversely Fourier transforming the results at the surface.

Migration of zero-offset data is simply the inverse of the above: one starts by Fourier transforming the time section, and then continuing each frequency down, using either a negative v or Δz. The value of the wave field at t=0 is then extracted at each depth by summing over the real part of all the frequencies. An optional step that removes the effect of the wraparound in the FFT is to then subtract the value of the reflector from the wave field.

Both modeling and migration can be performed by taking one frequency at a time through all the z-steps, or taking all the frequencies through one z-step at a time. It is, however, only possible to subtract the reflectors from the migrated wave field when all the frequencies are taken together. In situations where both the reflector and velocity map, and the Fourier transform of the wave field, are too large to fit in the main memory of the computer, disk input and output are minimized by using some combination of the above -- that is, either taking as many frequencies as will fit into memory through all the z-steps, or keeping as much of the velocity and reflector structure as fits in memory, while taking all the frequencies through that part of the structure. Using this last arrangement we have been able to take full advantage of the speed of the SEP array processor for migrations of several hundred traces of COCORP data [Lynn et al. 1979].

Examples

We will show two such examples. Figure 6.2 shows the exploding reflector seismogram for a point source near a vertical interface. The velocity on the left of the interface is one-third what it is on the right. The depth of the point scatterer is 5 times its distance from the vertical interface. Figure 6.3 shows the result computed using equation (6.3) for the same earth structure. The strongest arrival on figure 6.3 is not present at all in the exploding reflector approximation. Note also that the relative amplitudes are different between the two figures. Figure 6.4 shows the raypaths included in figures 6.2 and 6.3. The velocity structures used in these figures are

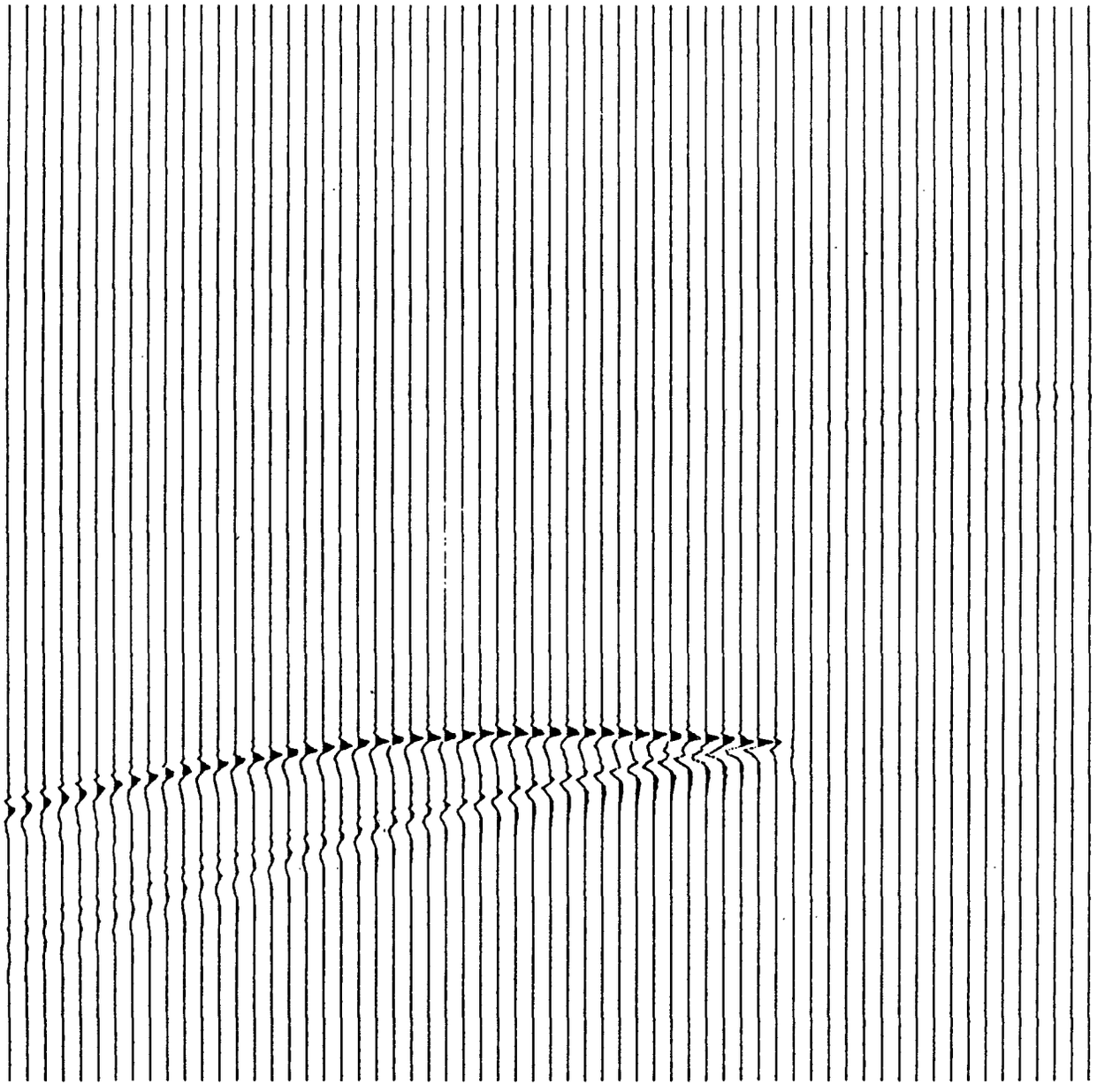

FIG. 6.2. Exploding reflector zero-offset section for a point scatterer at a depth of five times its distance from a vertical velocity contrast of 3 to 1. Computed using monochromatic 45-degree wave equation. Raypaths are shown in figure 6.4a,b.

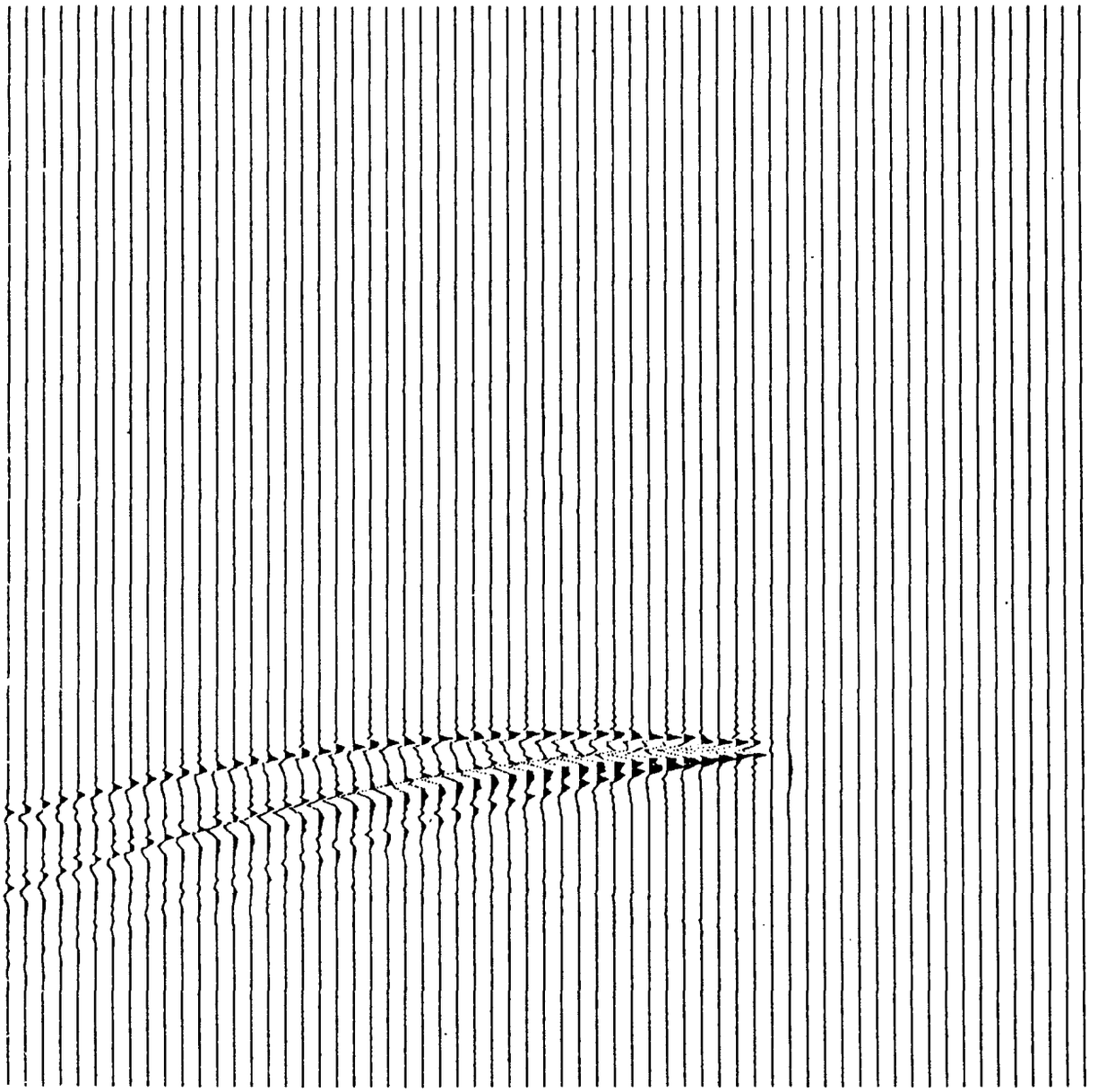

FIG. 6.3. Zero-offset section for same earth model as figure 6.2, computed using equation (6.3). All the raypaths shown in figure 6.4 are now included.

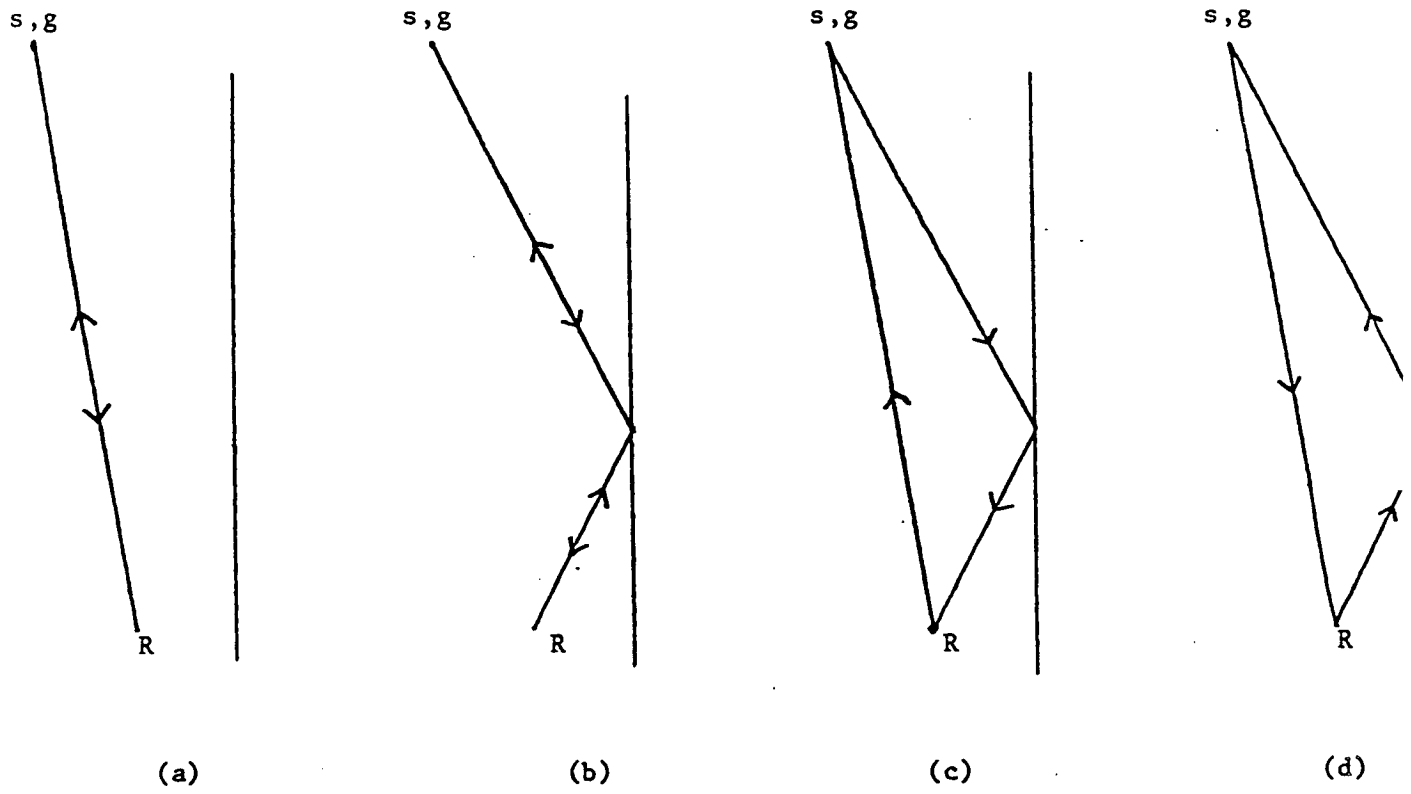

FIG. 6.4. Raypaths for the model in figures 6.2 and 6.3. The exploding reflector model includes only (a) and (b).

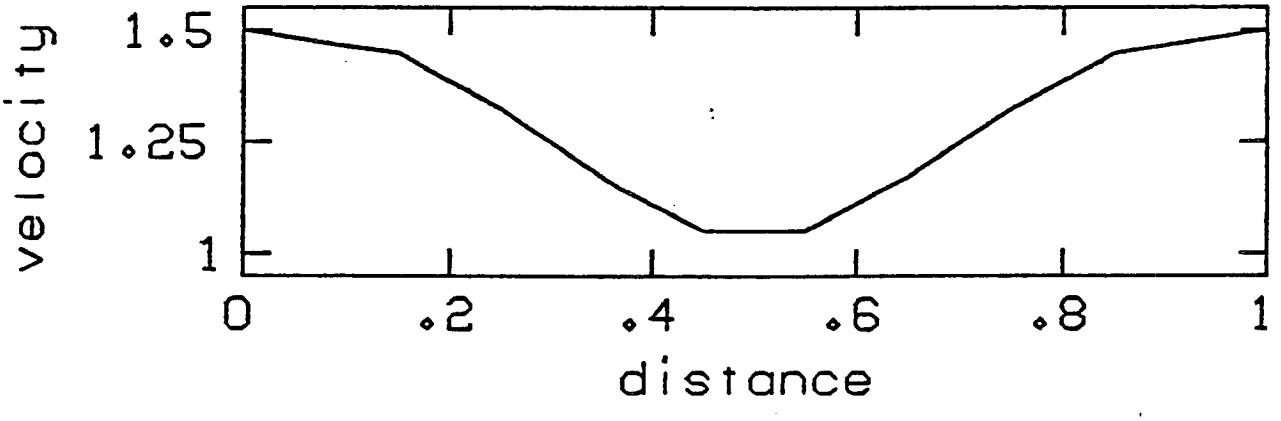

FIG. 6.5. Velocity along the sections in figures 6.6 and 6.7. Velocity is independent of depth.

probably not too realistic from a geologic point of view. Figure 6.5 shows a somewhat more realistic velocity model. For computational convenience we have assumed a velocity that is independent of depth, but very similar effects would be expected for point scatterers below a curved interface between two layers with different velocities, e.g. below a depression in the seafloor. Figure 6.6 shows the exploding reflector result for the velocity function shown in figure 6.5. The source is at a depth that is 1.3 times the width of the computed model. Figure 6.7 shows the correct zero-offset section. As before there are significant differences.

Attenuation

A first-order property of all materials, especially rocks, is the absorption of elastic energy, and the resulting change in the shape of transient waveforms. Most available data is consistent with the assumption that the energy is absorbed by a linear process, and that the energy loss per cycle is independent of frequency. In Chapter II we have seen that these conditions are satisfied by a model that implies a complex, frequency-dependent velocity of the form

$$v = v_0(i\omega)^{\gamma} \tag{6.15}$$

where γ is related to the seismic quality factor Q by

$$\frac{1}{Q} = \tan(\pi\gamma) \tag{6.16}$$

The possible range for γ is $0 < \gamma < \frac{1}{2}$ and for Q is $\infty > Q > 0$. The limiting cases correspond to classical elasticity and Newtonian viscosity. Since the coefficients in the Crank-Nicolson scheme are complex, even for a purely elastic model, the only additional computation, which results from the substitution of equation (6.14) into either (6.5) or (6.6), is in the computation of the coefficients. Appendix B contains FORTRAN listings of an in-core version of a zero-offset diffraction program, which can handle arbitrary velocity and Q structures and the corresponding migration program. Except for the input and output routines, these programs should run on other FORTRAN systems.

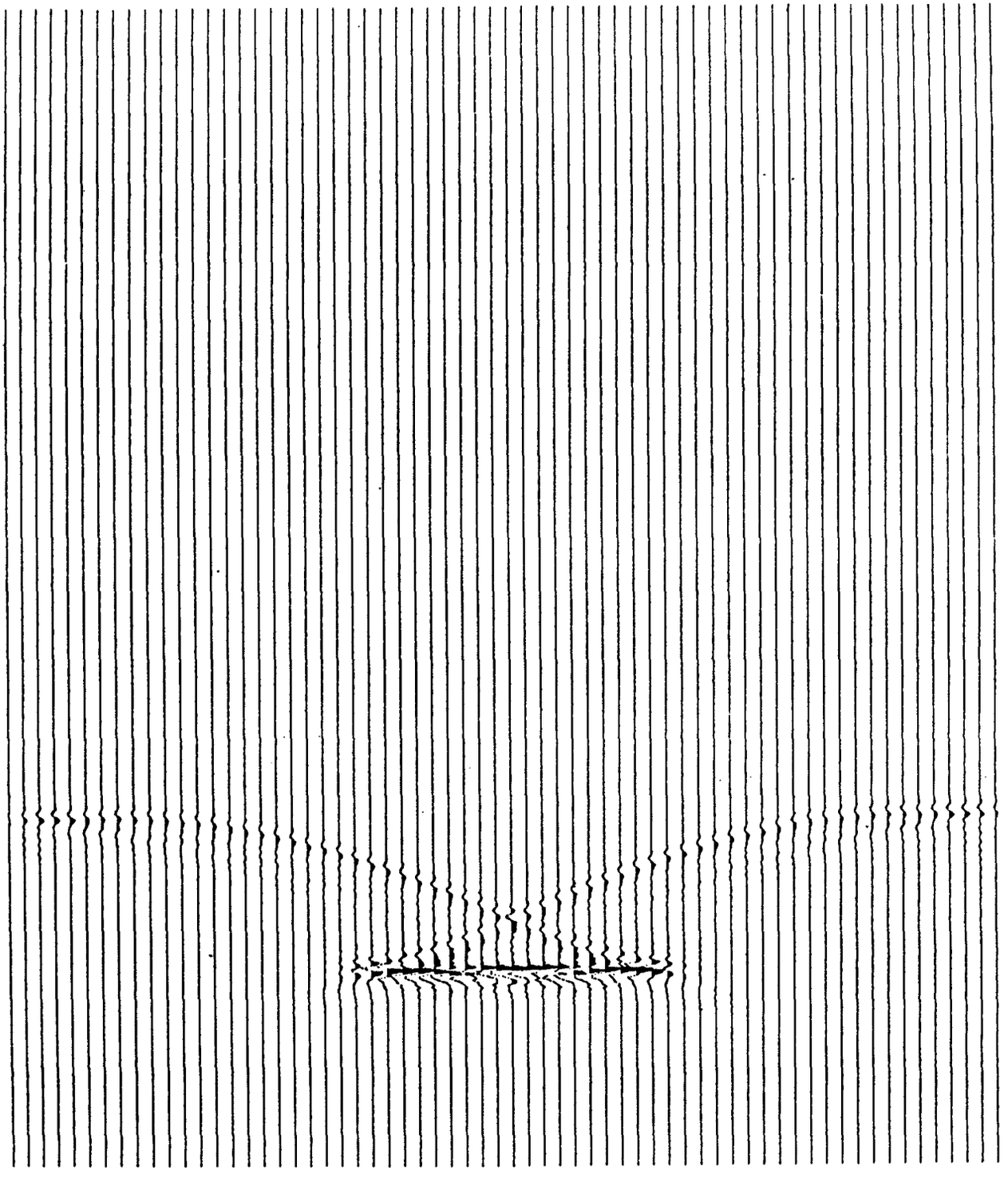

FIG. 6.6. Exploding-reflector-model zero-offset section for a point scatterer at a depth of 1.3 times the width of the section. Velocity is independent of depth and varies as shown in figure 6.5 along the section.

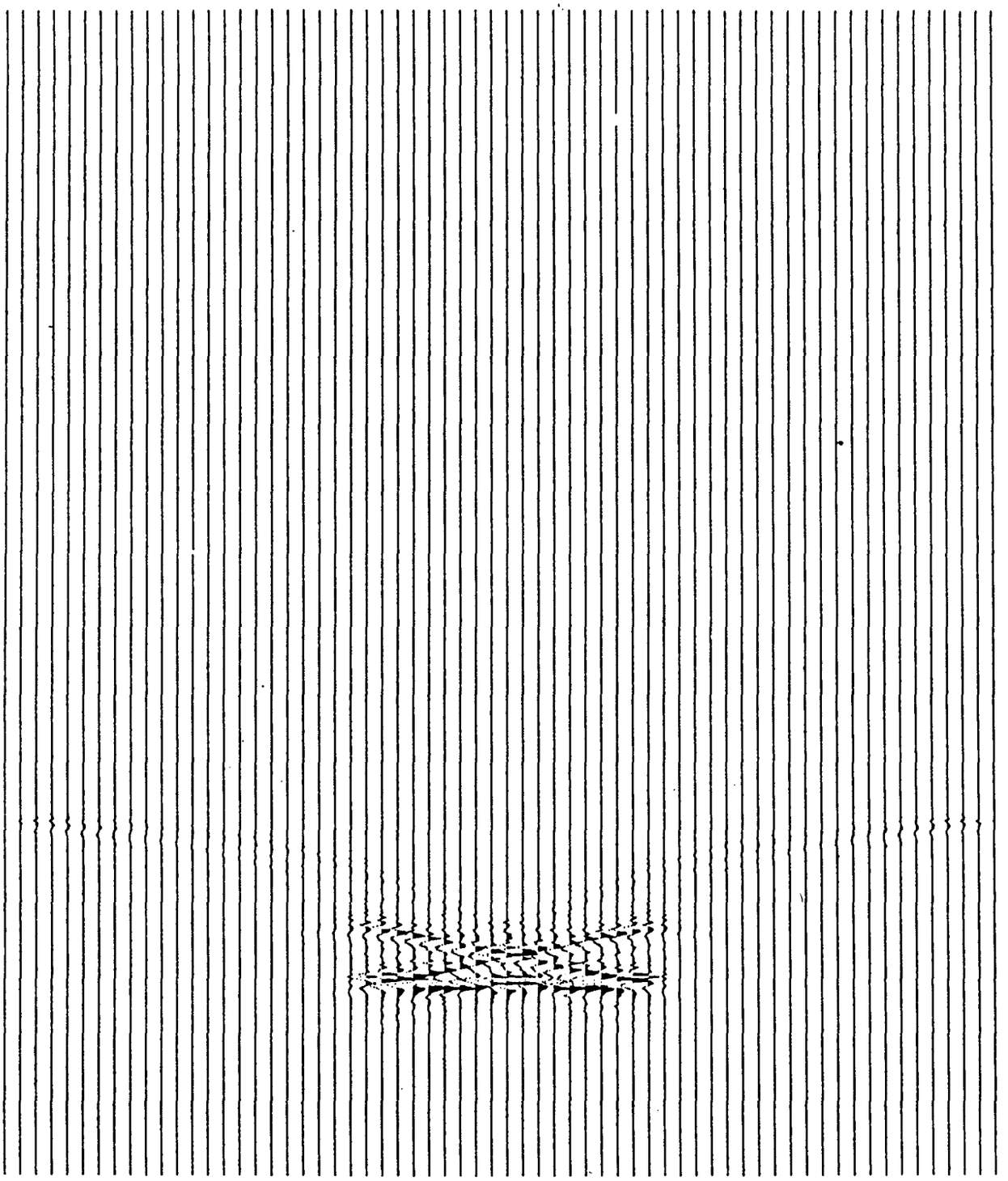

FIG. 6.7. Zero-offset section computed using equation (6.3) for the same earth structure as in figure 6.6.

Figures 6.8-6.11 show examples of outputs produced by these programs, as well as the large dataset array processor versions.

Discussion

It is routine practice [e.g. Burdick and Helmberger, 1978] in the computation of synthetic earthquake seismograms, to compute a seismogram for a purely elastic earth model, and then convolve the result with a response function of the kind presented in Chapter II. This is valid when all the arrivals present on the seismogram have suffered the same amount of attenuation, but is not even approximately valid for reflection seismograms unless it is assumed that all the attenuation takes place in the near-surface layers. Since the waveforms, especially at shorter periods, are often dominated by the attenuation impulse response, it seems worthwhile to include attenuation in the modeling of seismic sections.

Similarly, removal of the attenuation effects, along with the diffractions, in the migration of seismic data, should help isolate the path-independent source waveform, and thus contribute to increasing the resolution of the results. However, the removal of attenuation effects is an inherently unstable process, especially in the presence of noise, so careful filtering of the high frequencies is required, and the results are likely to be sensitive to the quality and processing history of the data. An alternative discussed by Robinson [1979], is to remove only the phase shifts caused by anelasticity dispersion; this may be valuable in obtaining a zero-phase output in deconvolution.

Although an understanding of the seismic attenuation may help us get sharper pictures of the subsurface, that is not the only reason for trying to measure and model it. There are both laboratory [Winkler and Nur, 1979] and theoretical reasons, such as given in Chapter V and by Mavko and Nur [1979], to believe that there is some unique information about the lithology and such parameters as the temperature, porosity, pore pressure, and the amount of saturation that can be extracted from a knowledge of the seismic attenuation parameters, especially when they are integrated with other geophysical information. None of the methods that have been discussed in this chapter are applicable to the problem of estimating Q directly from data. The ability to

compute accurate synthetic seismograms for trial models of the Q structure should be valuable in comparing the various methods for estimating Q and establishing the validity of the results.

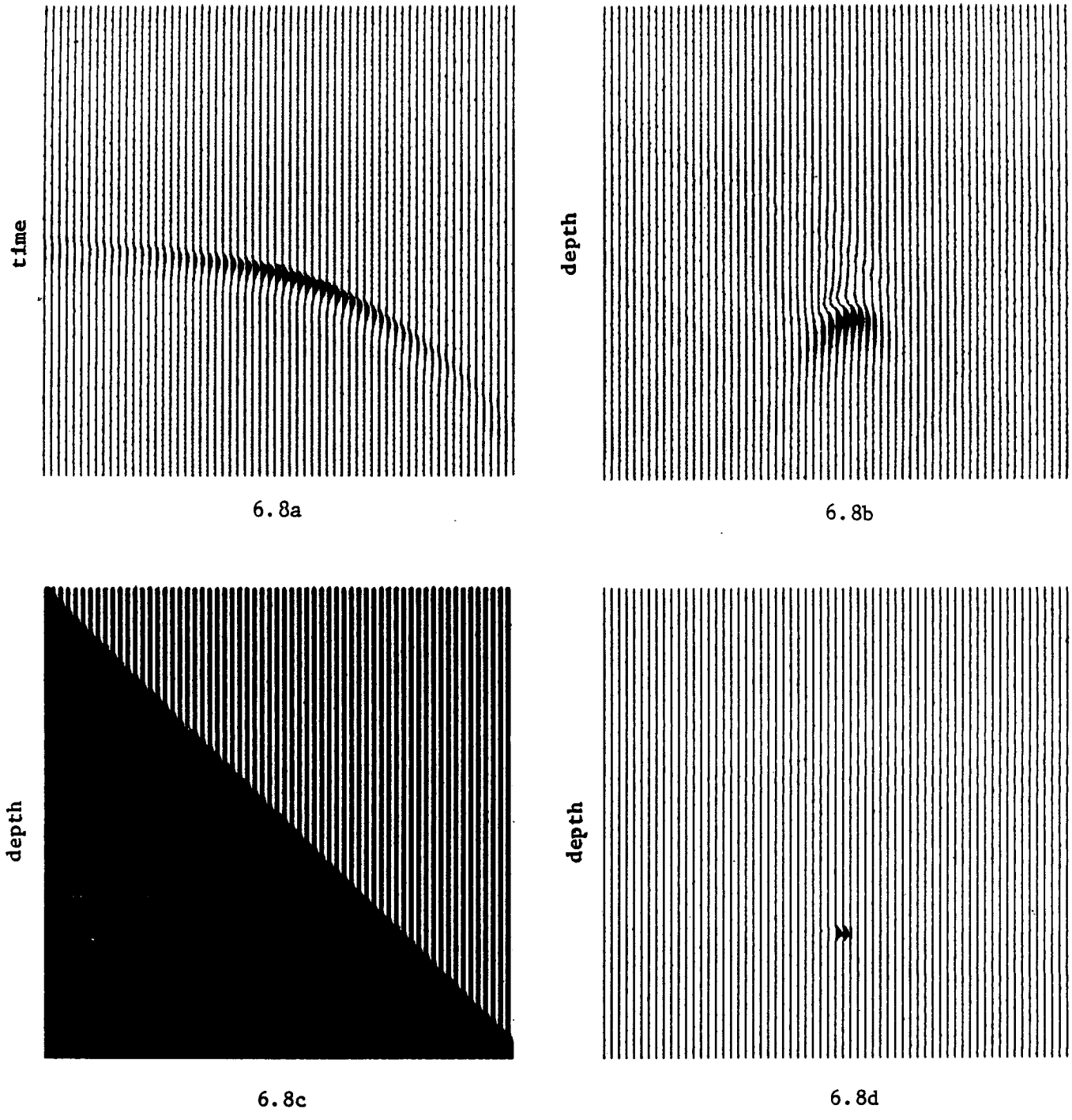

FIG. 6.8. Modeling and migration using the programs listed in appendices. The zero-offset section observed at the surface from the reflector shown in 6.8d, for the velocity structure shown in 6.8c, is shown in 6.8a. Anelasticity with Q = 20 was used. The velocity at a unit frequency is 1 in the upper layer and 2 below. The result of a migration of the section in 6.8a is shown in 6.8b. Most of the loss in resolution is because anelasticity was included in the forward calculation, but not in the migration. Parameters used were as follow: 128 timepoints, 64 traces, 64 depthpoints, Δt of 0.06, Δz of 0.06, and Δx of 0.1.

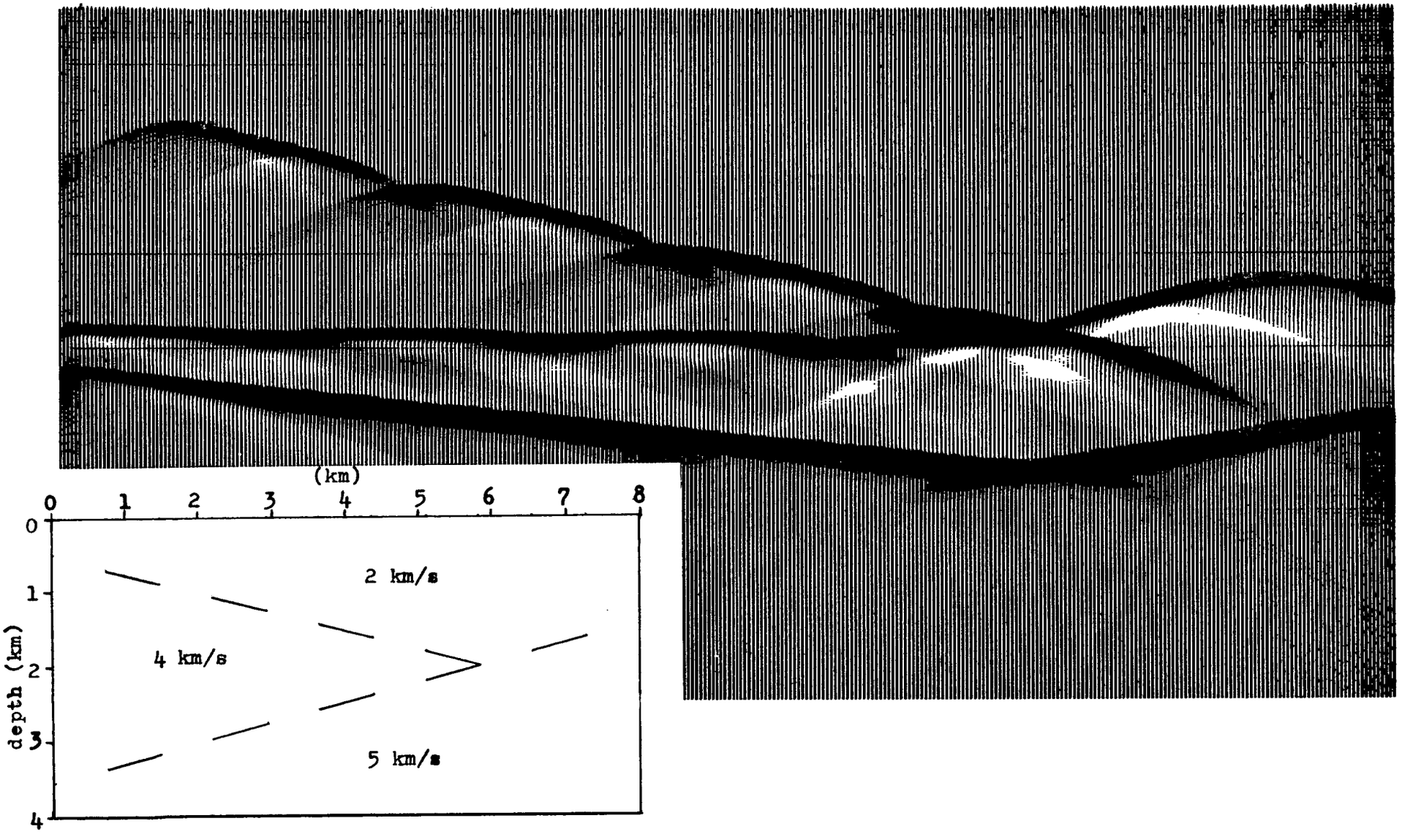

FIG. 6.9. A zero-offset section for the reflector and velocity structure shown, with Q = 40. Total time displayed is four seconds. Velocities shown are for a reference frequency of approximately 1 Hz. The calculation included 330 traces, 320 depth steps and 512 complex frequencies or 1024 timepoints. A gain proportional to $t^{1/2}$ was applied before plotting. The traces are clipped to 1/5 of the maximum. This model was taken from Western Geophysical's depth-migration brochure.

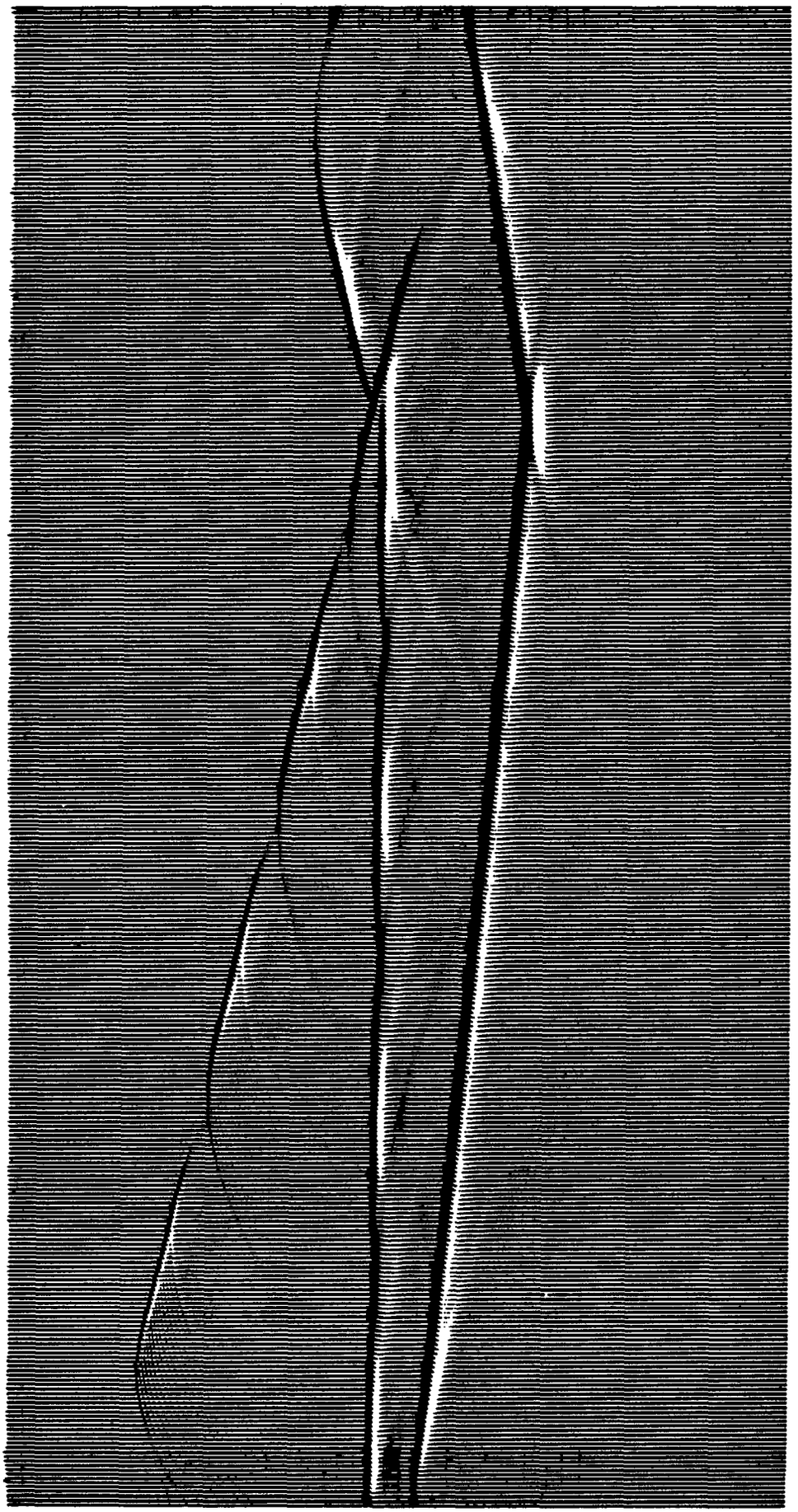

FIG. 6.10. Same results as in figure 6.3, but in order to more realistically simulate the bandwidth of real data the traces have been differentiated with respect to time. The broadening of the waveform, caused by anelasticity, is clearly shown. A gain proportional to $t^{3/2}$ was applied before plotting. The traces are clipped at 1/5 of maximum.

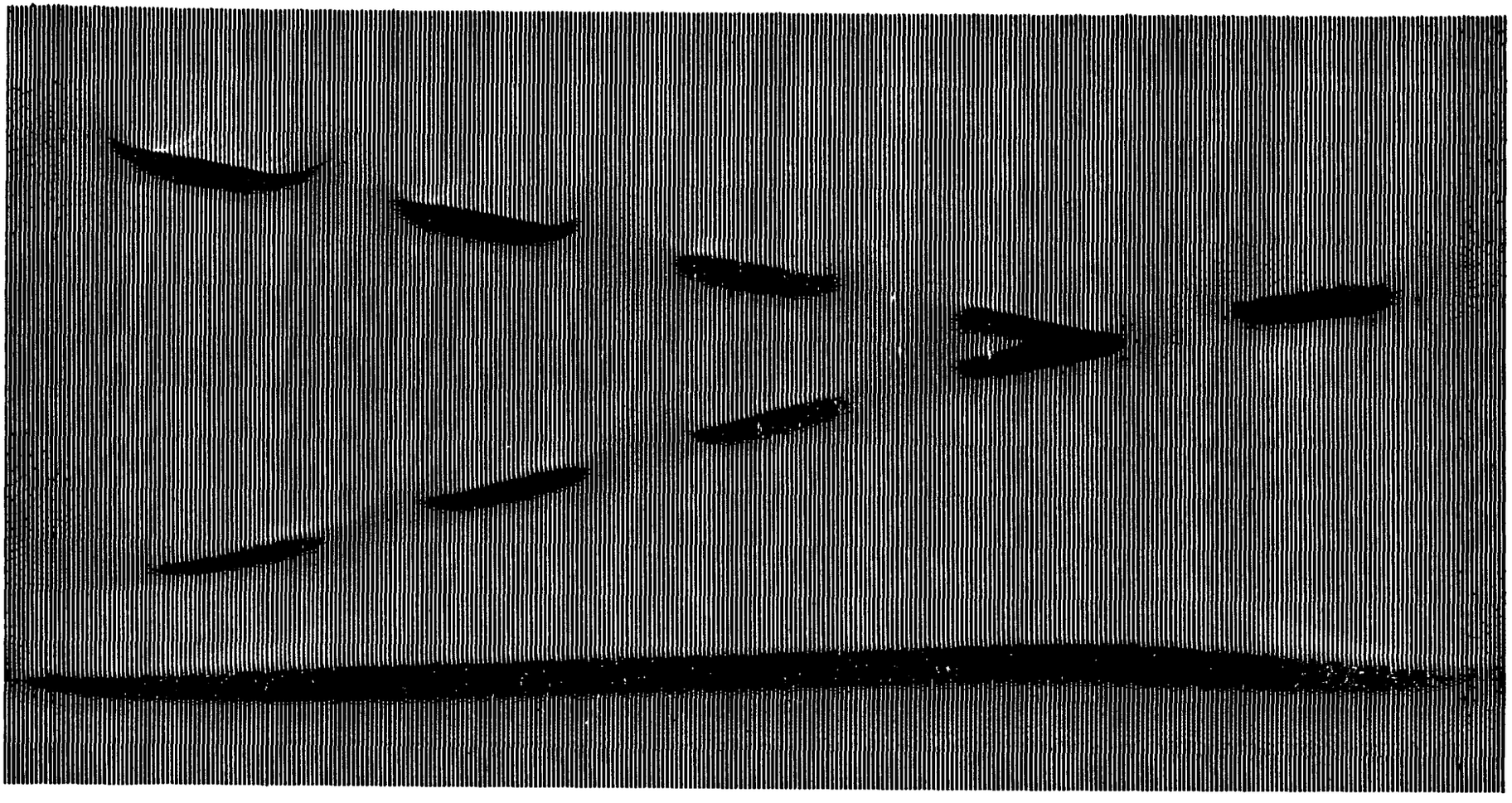

FIG. 6.11. The result of migrating the time section shown in figure 6.3. Total depth displayed is 4.4 km. The vertical smearing is mostly due to the fact that anelasticity was not included in the migration. Some of the lateral smearing is caused by dip-filtering (see Appendix B), and near the ends, absorption at the side boundaries. The plot is clipped at 1/3 of maximum.

Chapter VII

ANALYSIS OF VARIATIONS IN AMPLITUDES AND TRAVELTIMES WITH OFFSET AND MIDPOINT

Lateral variations in rock properties cause complex variations of amplitudes and traveltimes with offset on common-midpoint gathers. A theory for the interpretation and inversion of these complex variations is presented. The application of the theory to seismic data from a producing gas field shows correlations of interpreted velocity and amplitude anomalies with diffractions observed on common-offset sections.

Conventional processing of high quality seismic data involves a high degree of data reduction. The stacking process implies assumptions about the conditions where the data was collected, such as the absence of rapid lateral variations in velocity or absorption. A great deal of information will be lost in stacking when such variations are present, especially if the signal-to-noise ratio is good on the unstacked data. In this report examples of such data are presented along with methods for their inversion.

The dataset used is a seismic line across the Grand Isle gas field off the shore of Louisiana. The data was made available to the Stanford Exploration Project by Dr. Ralph Shuey of Gulf Science and Technology Company in Pittsburgh. Recording parameters for the line are listed in table 7.1. Typical common-midpoint gathers are shown in figures 7.1-7.5, and a common-offset section of the fifth offset is shown in figure 7.6. These plots show a number of interesting features. One of the most striking is the rapid and seemingly irregular changes in the amplitude of the bright spot reflection at 2.3 seconds, with offset.

TABLE 7.1. SHOOTING GEOMETRY
(all dimensions in feet)

Energy source	Airgun
Source depth	30
Shot interval	82
Group interval	164
Near geophone	743
Far geophone	8498
Cable length	7756
Fold	48
Filter	5-144 Hz

These amplitude variations are much too strong to be explained by the angle-dependence of the reflection coefficient, or the destructive and constructive interference between closely spaced reflectors. Many of the amplitude anomalies shown in figure 7.6 correlate for several reflectors: for example, the amplitude variations around midpoint 287 appear to be present on all visible reflectors from about 1.5 seconds down to the bottom of the section. This points towards transmission effects in the overlying rocks as the most plausible explanation. In order to investigate this further, the power in each trace for the interval from 1.5 to 3 seconds was integrated for each midpoint, and for all the offsets. After this was done, it became apparent that some of the offsets had systematically higher or lower amplitudes than the others. In order to remove this effect, each offset was normalized by dividing by the median power for that particular offset. The logarithm of this result is plotted in figure 7.7, as normalized amplitude versus midpoint and offset.

High amplitudes show up dark on the plot; amplitude variations caused by variable reflectivity along the reflectors should show as vertical rectangles on the plot, while variations caused by shot amplitudes should have a 45-degree slope. The black streak on the left side of the plot is caused by two shot locations with no data - the tapes containing garbage. Close inspection reveals a large number of small amplitude fluctuations that are parallel to the streak caused by the bad data; these are undoubtedly caused by variations in the shot amplitude.

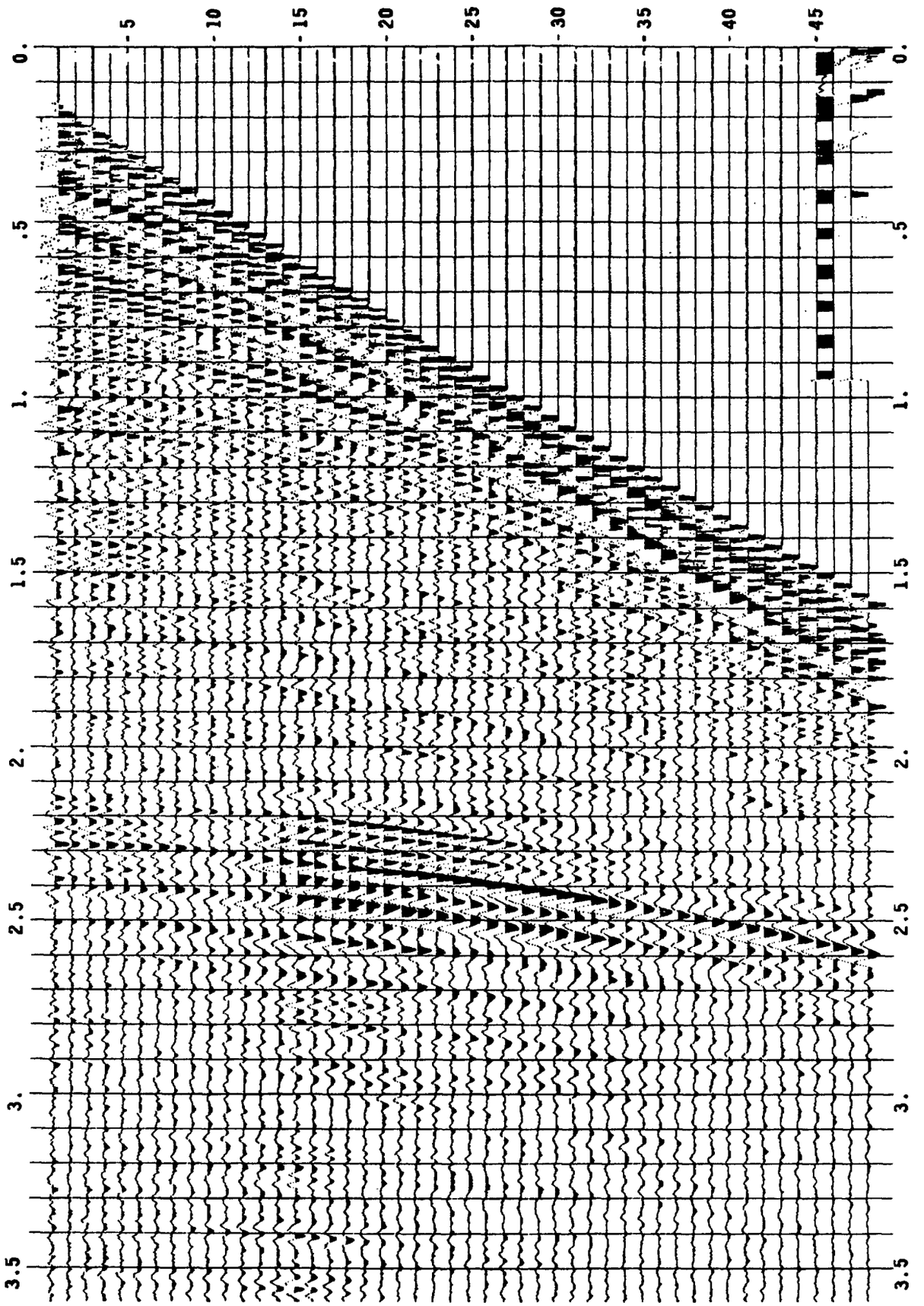

FIG. 7.1. Common-midpoint gather 210. No processing has been applied to the data, except for a display gain proportional to time. Recording parameters are given in table 7.1.

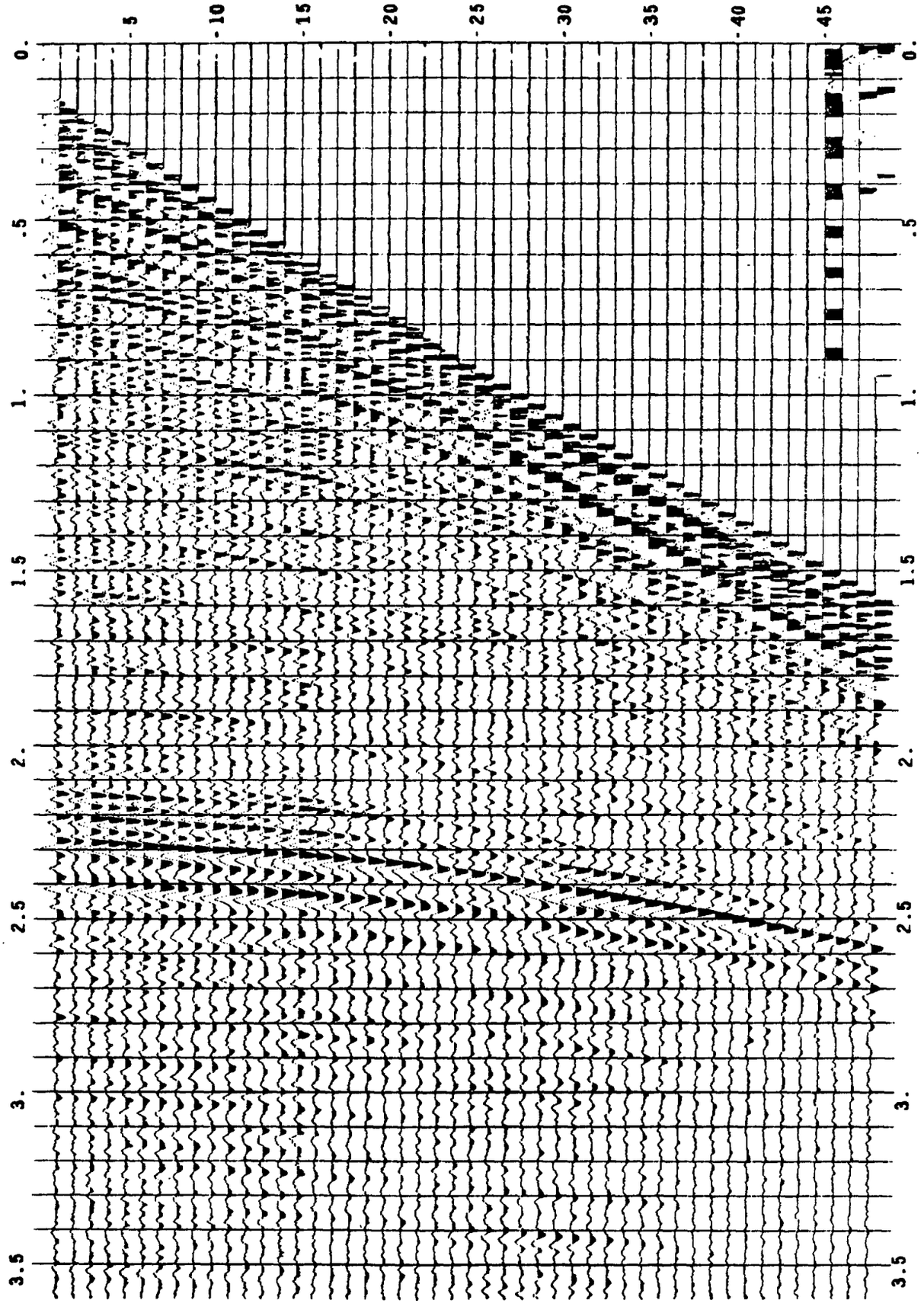

FIG. 7.2. Common-midpoint gather 220. The reflection at 2.3 seconds shows deviations from hyperbolic moveout.

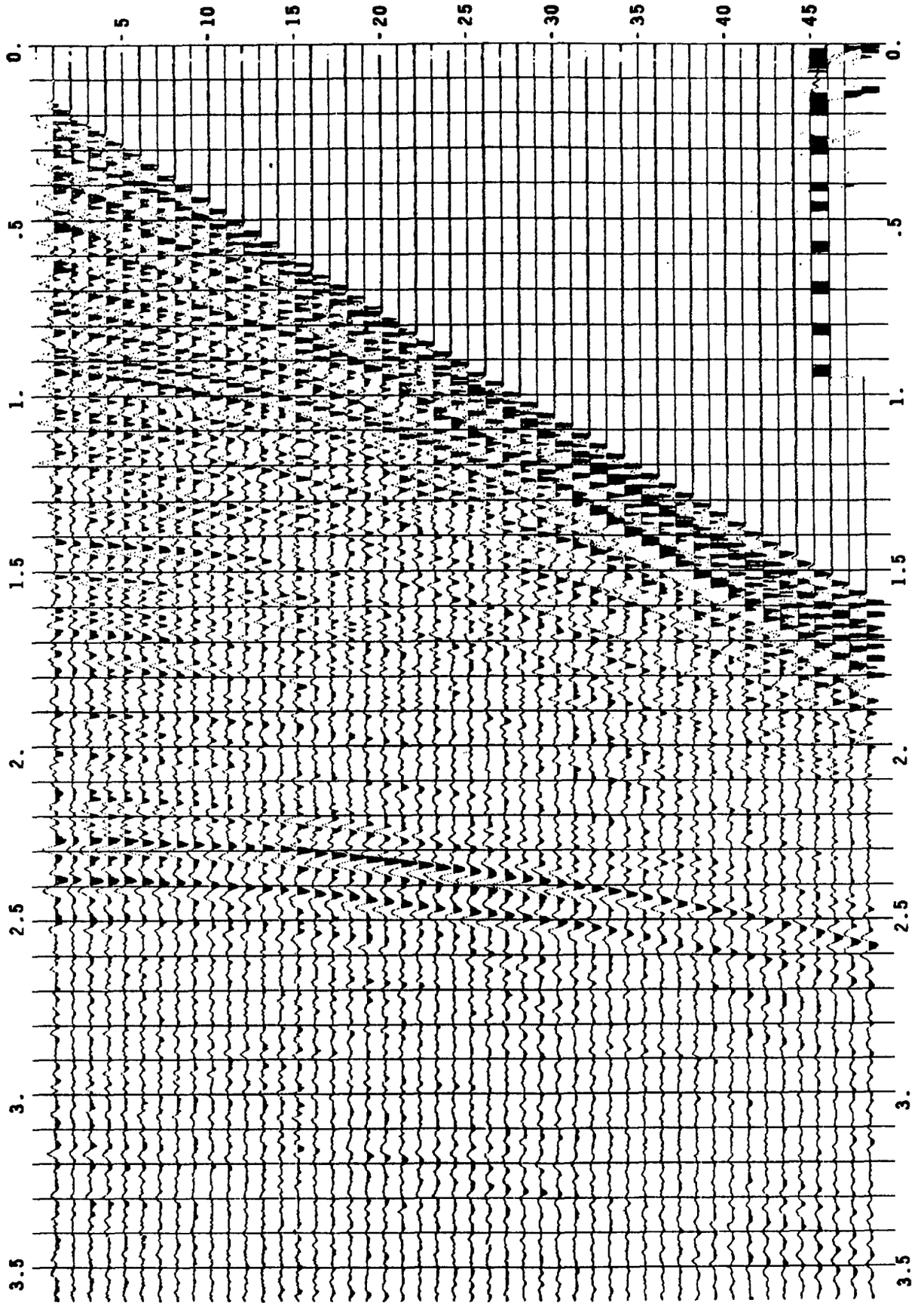

FIG. 7.3. Common-midpoint gather 230. The distance separating figures 7.1 and 7.2, and figures 7.2 and 7.3, and figures 7.4 and 7.5 is 250 meters (820 feet).

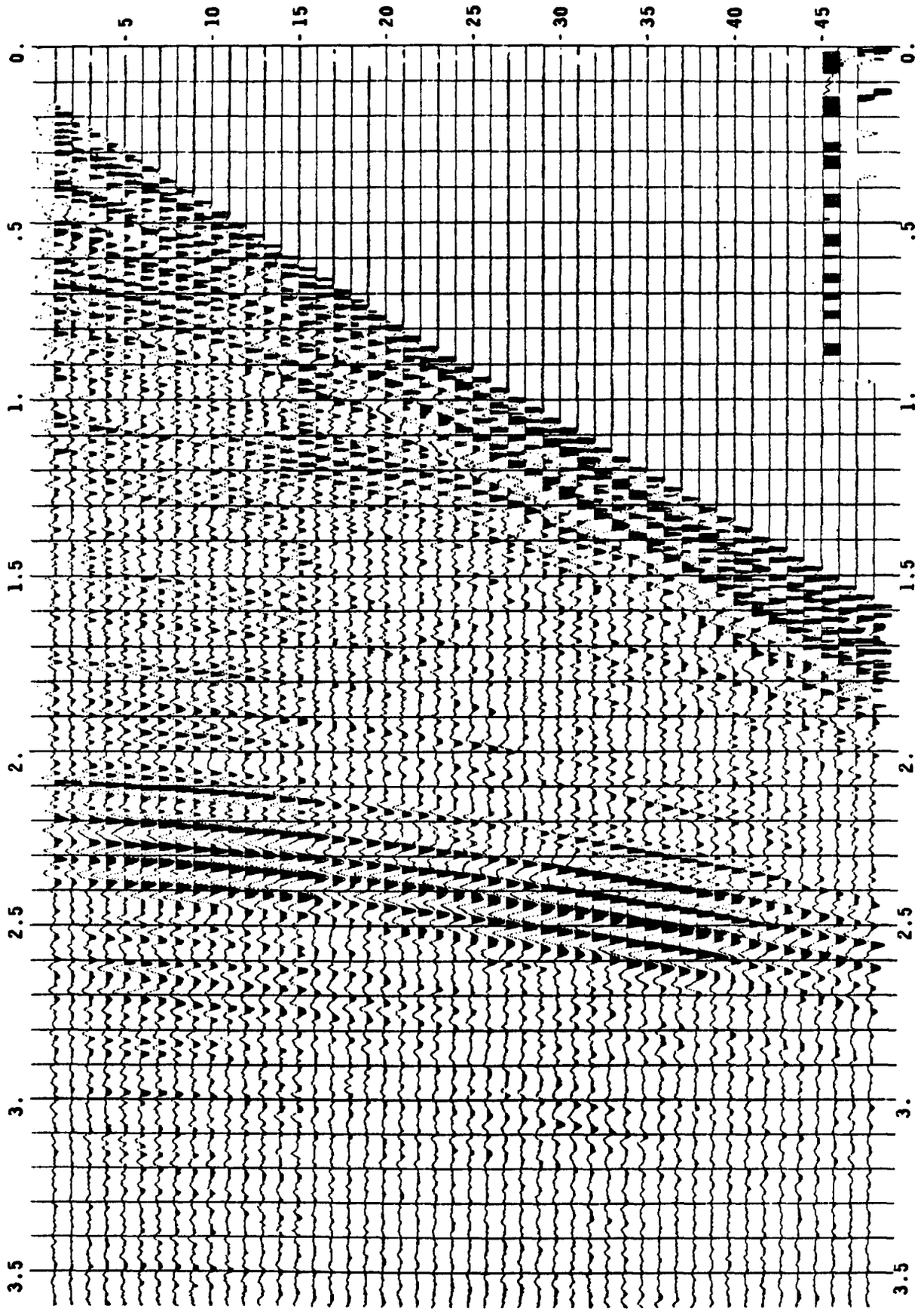

FIG. 7.4. Common-midpoint gather 305.

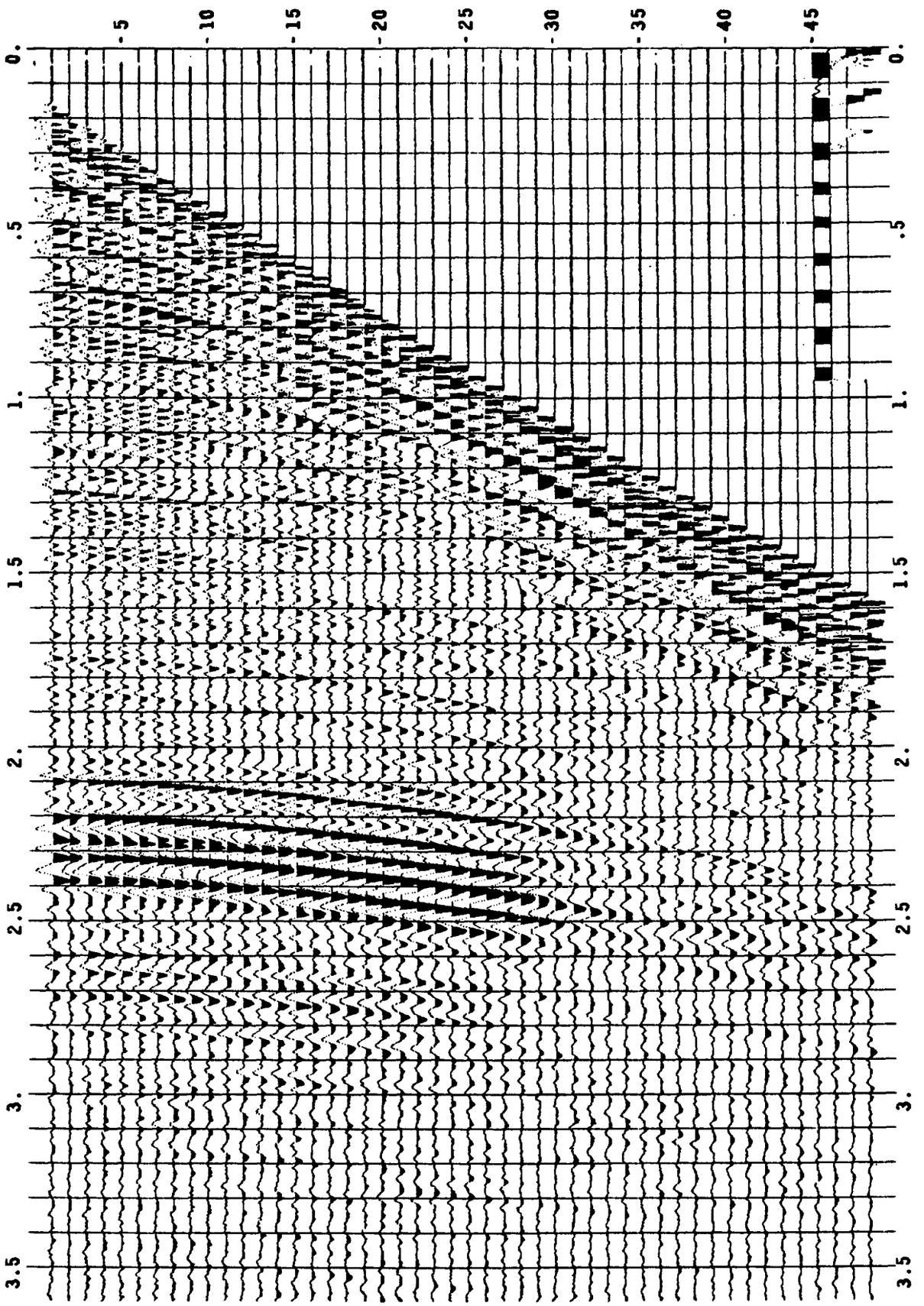

FIG. 7.5. Common-midpoint gather 315.

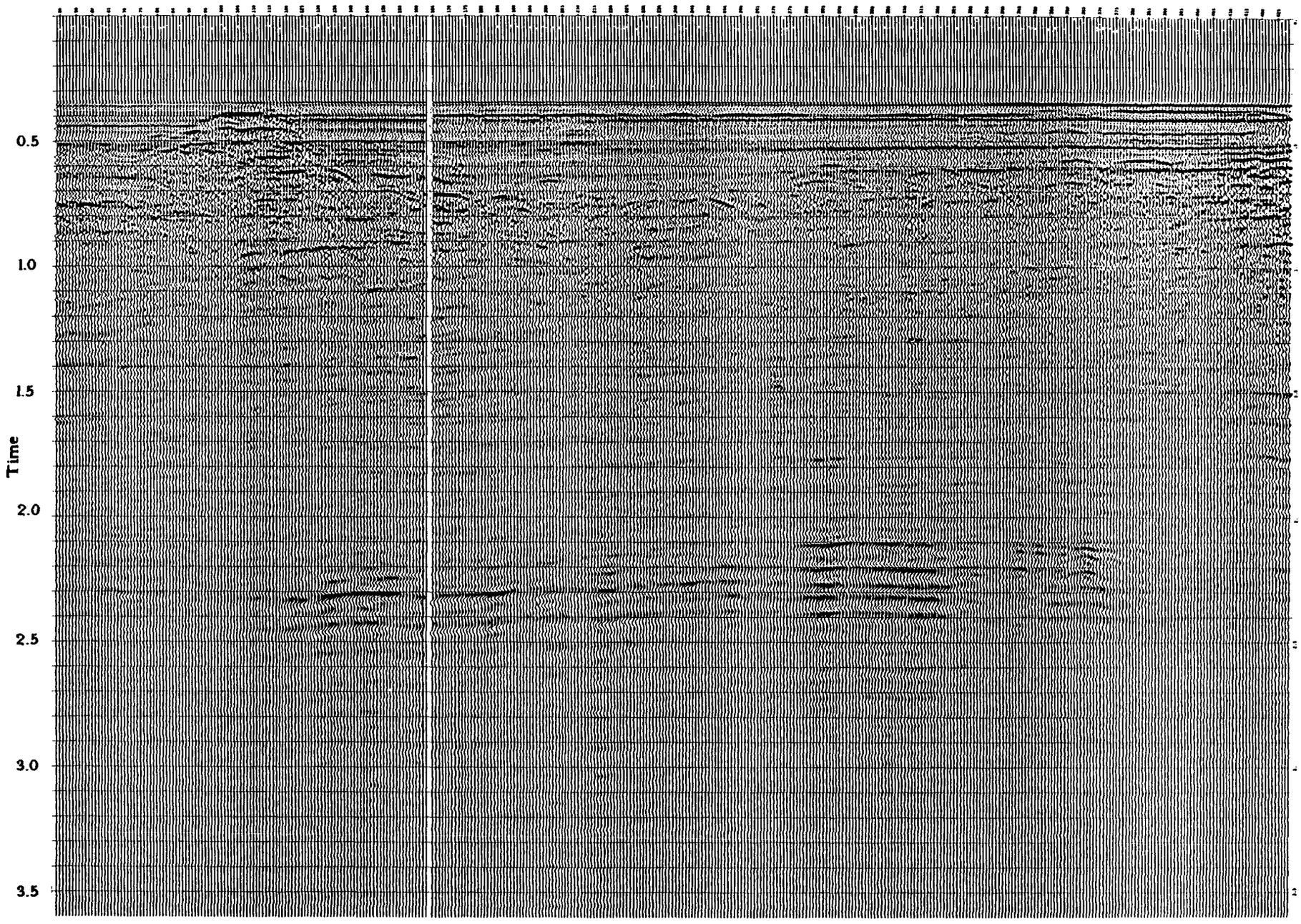

FIG. 6.

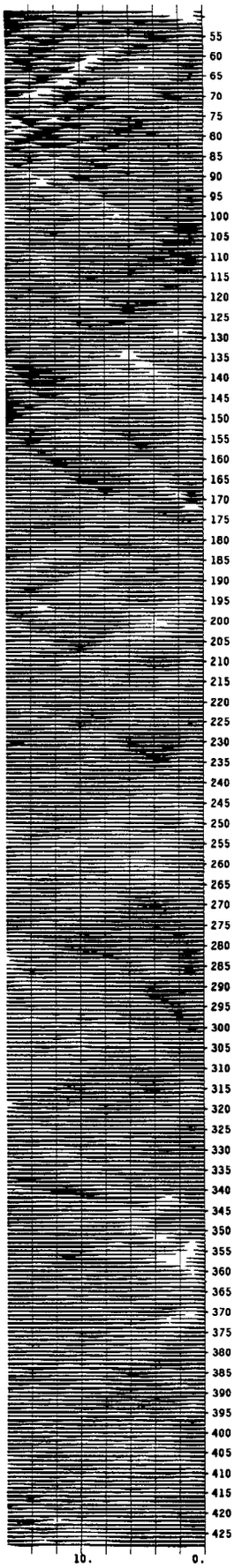

FIG. 16.

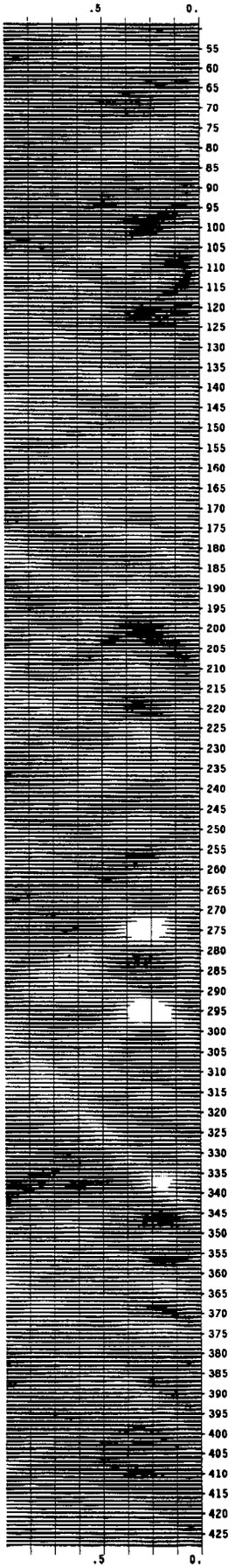

FIG. 15.

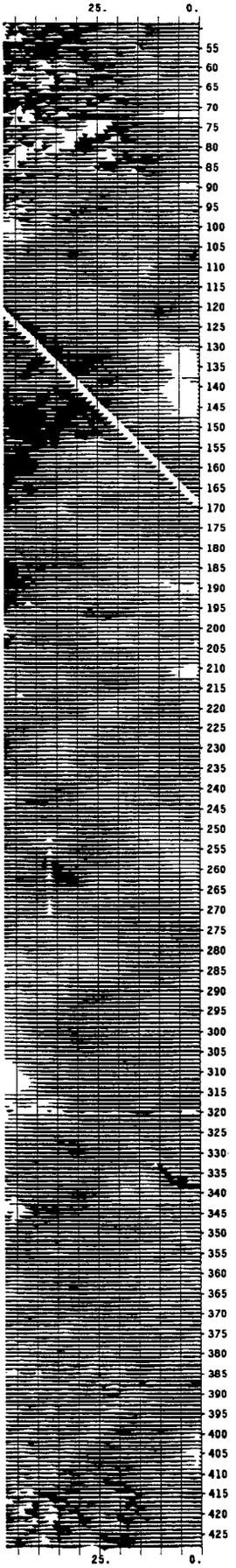

FIG. 9.

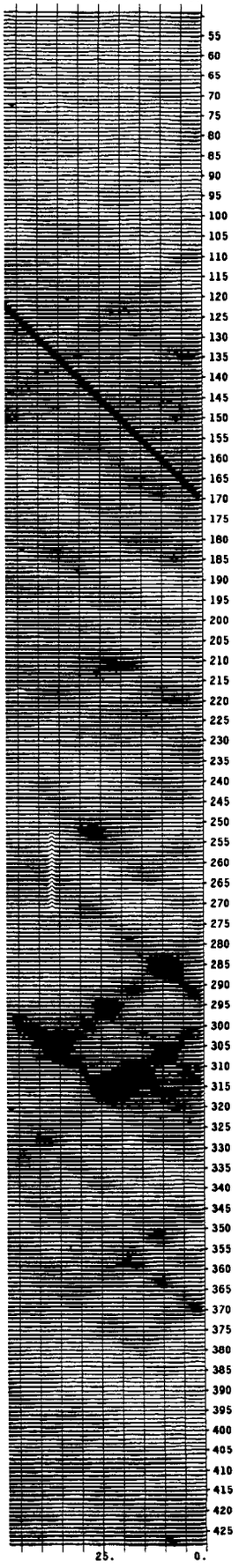

FIG. 7.

FIG. 7.6. A common-offset section for the fifth offset. Shot receiver distance is 320 meters (1070 feet) and trace spacing is 25 meters (82 feet). The amplitude pattern and details of the shape of the bright-spot reflector change from offset to offset. Note the good signal-to-noise ratio and the diffraction patterns in the first second of data.

FIG. 7.7. The logarithm of the power is plotted versus midpoint and offset. The power was integrated over a window that extended after NMO from 1.5 to 3 seconds. Systematic offset dependence was removed by dividing the power at each offset by the median power for that offset.

FIG. 7.9. Traveltime anomalies are shown versus midpoint and offset. The times shown were obtained by crosscorrelation with a sum trace, after time shifts applied as in figure 7.8. The window length was 1.024 seconds. Black indicates delays.

FIG. 7.15. Result of applying the iterative-median inversion to the amplitude data plotted in figure 7.7. The depth scale is relative to the depth of the bright spot which is approximately 8000 feet. The interval from the bright spot to the surface was divided into 16 layers. Black on this plot indicates low amplitudes (high absorption).

FIG. 7.16. Black indicates low velocities. The result of applying the iterative-median inversion to the amplitude data. Slowness is displayed in the same manner as the absorption in figure 7.15.

One potential explanation for the amplitude variations, as they are observed on individual midpoint gathers, is that they are caused by variations in shot strength or by variations of the properties of the sea bottom. Inspection of figure 7.7 shows that this does not suffice to explain some of the larger features visible on the plot. The large amplitudes (dark on the plot) occur in bands that have significantly steeper slope than the shot effects. There is also a bimodal distribution of slopes, since bands that go either left or right with offset occur with about the same frequency.

A closer look at figures 7.1-7.5 shows in addition to the amplitude effects, deviations from hyperbolic moveout. Figure 7.8 shows the gather from figure 7.2, after a time-independent time shift was applied to the traces, as appropriate for an NMO of an event at 2.3 seconds with an RMS velocity of 7000 feet/second. The plot shows deviations in traveltime of almost 20 ms, even though there is excellent match at the far and near offsets. Figure 7.9 shows a plot of time shifts, as determined by crosscorrelations with the sumtrace for each gather, for all the shots and all the offsets, using a one-second time window. This plot shows the same qualitative features as in figure 7.7, but there is a great deal more noise, some of which is probably caused by cycle jumps in the crosscorrelation.

Theory

A theoretical framework for the interpretation of midpoint-offset anomalies of the type we have shown will be presented. Our earth model is shown in figure 7.10. We assume that our observations may be related to some quantity d(h,y) that is the line integral along the raypath of some rock parameter w(z,y). Earth model assumed. The value of the vertical coordinate, z, is zero at the reflector and z_0 at the surface.

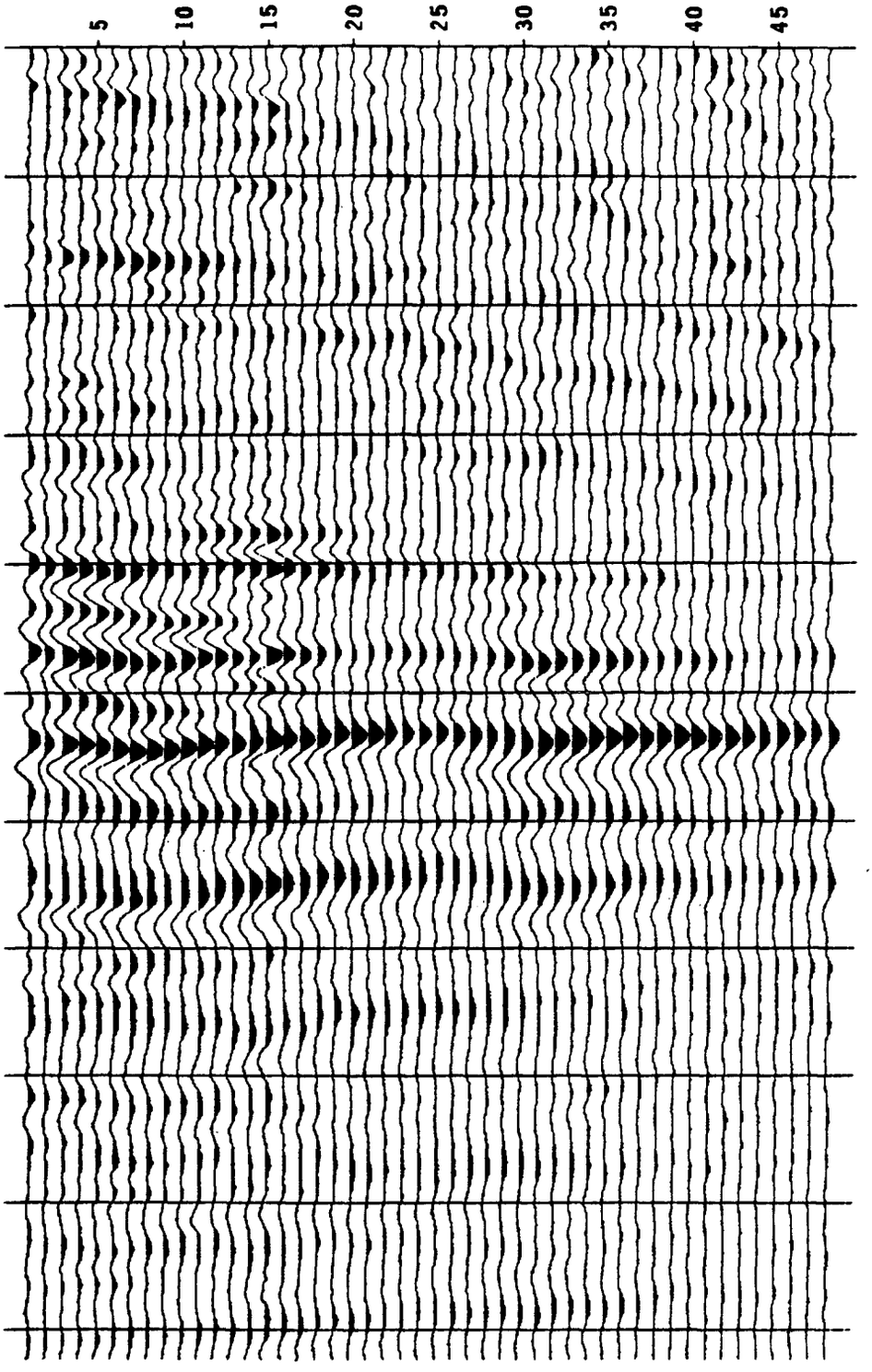

FIG. 7.8. Midpoint gather 220 (same as in figure 7.2) after moveout. Shown is one second window centered at 2.3 seconds, time shifted according to an NMO for an event at 2.3 seconds, using a velocity of 7000 feet/s.

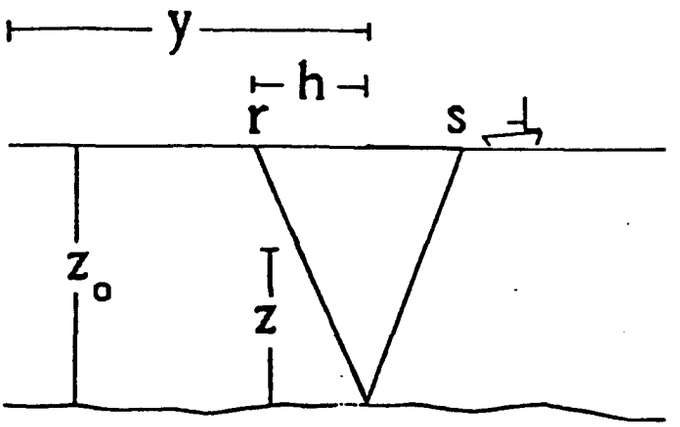

FIG. 7.10. Earth model assumed. The value of the vertical coordinate, z, is zero at the reflector and z_o at the surface.

For example, the traveltime is the integral of the slowness 1/v:

$$t = \int \frac{ds}{v(z,y)} \tag{7.2}$$

Another example is the amplitude decay of a monochromatic wave due to absorption:

$$A = \exp\left[-\int \alpha(z,y)ds\right] \tag{7.2}$$

where A is the amplitude and α is related to the intrinsic quality factor Q by

$$\alpha = \frac{\pi f}{Qv(f)} \tag{7.3}$$

where f is frequency. The dispersion that is a consequence of causality has the effect of making the velocity v slightly dependent on frequency.

For a broad-band source in a medium where Q is independent of frequency, the width of a pulse τ is given by

$$\tau = c \int \frac{ds}{Q(z,y)v(z,y)} \tag{7.4}$$

where c is a constant that depends on the particular measure of pulse width used [Kjartansson, 1979]. These three different types of observations may be treated with the same tools if refractions caused by lateral variations in velocity are neglected. The effects of velocity variations with depth may be accounted for by the application of a coordinate transformation. For velocity variations of a few percent or less, the effect of ray bending on the total path length is small. The assumption of lateral variations on the order of a few percent or less appears well-justified for the present dataset.

If it is further assumed that the measurements are appropriate for primary reflections from a single reflector, or a group of closely spaced reflectors with dips small enough to justify the assumption that the reflector point is directly below the midpoint (migration is not necessary), then we may refer to figure 7.10, and write

$$d(h,y) = \int_0^{z_o} \frac{(h^2+z_o^2)^{\frac{1}{2}}}{z_o} \left[w(z,y-h\frac{z}{z_o}) + w(z,y+h\frac{z}{z_o}) \right] dz \qquad (7.5)$$

Since the average offset effect has been removed through the normalization and NMO of the data in figures 7.7 and 7.9, we may drop the cosine factor in equation (7.5):

$$d(h,y) = \int_o^{z_o} \left[w(z,y-h\,\frac{z}{z_o}) + w(z,y+h\,\frac{z}{z_o}) \right] dz \qquad (7.6)$$

If the function w(z,y) is specified, for example, on a discrete grid, equation (7.6) may be used to model the observations. Figure 7.11 shows the result of a forward calculation from the model shown in figure 7.12. Linear interpolation between adjacent y points in each layer was used. The general character of the synthetic is quite similar to that of the data. Equation (7.6) may be Fourier-transformed over the midpoint coordinates; the result is

$$D(h,k_y) = 2 \int_o^{z_o} \cos(h\,\frac{z}{z_o}\,k_y)\; W(z,k_y)\,dz \qquad (7.7)$$

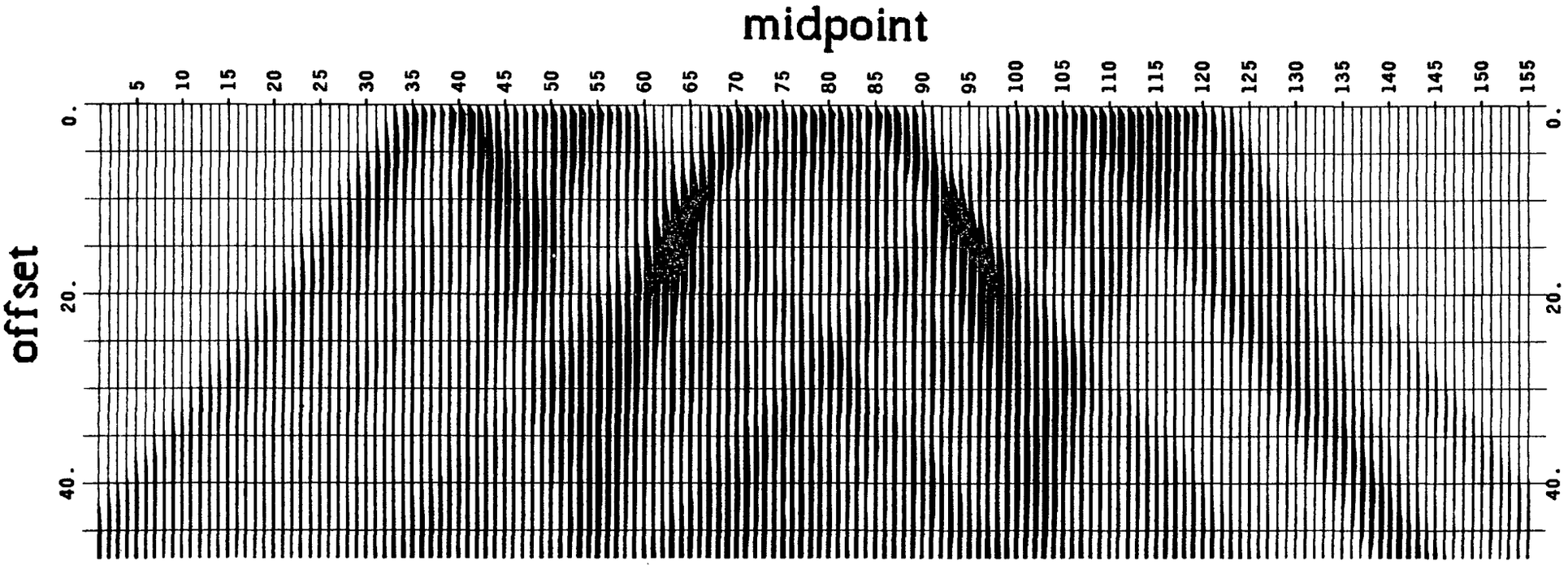

FIG. 7.11. A synthetic midpoint-offset display, computed by evaluating the integral in equation (7.6) numerically, for the structure shown in figure 7.12.

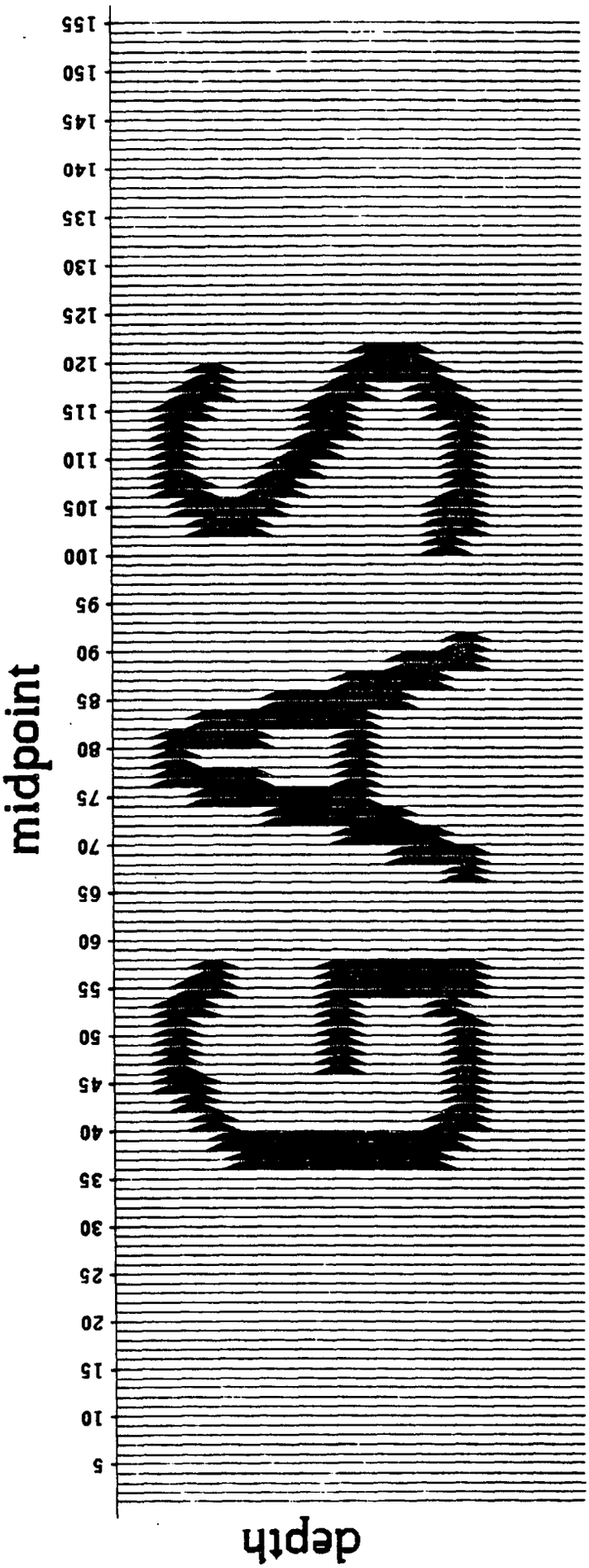

FIG. 7.12. The structure used to compute the synthetic in figure 7.11. The interval from the reflector to the surface is divided into 26 layers.

The form of the integrand in (7.7) is a Fourier transform from the z-domain to the h-domain, except for the integration limits. Thus it is readily seen that the component of the observations which changes most slowly with offset is controlled by the material closest to the reflector, and that the near offsets provide information about the long wavelength components of W, while the far offsets provide the short spatial wavelength information.

Observations at a particular offset h are most sensitive to wavelengths in depth on the order of hk_y/z_o. This implies that measurements do not contain information about velocity layers with tangent of dip less than z_o/h_m, where h_m is the maximum half-offset. The maximum observable dip is similarly limited by the near-offset.

Equation (7.7) may be solved numerically if the interval from the reflector to the surface is divided into n_z layers and the integral replaced by a sum. The result is a set of simultaneous equations of the form

$$\bar{d} = \bar{\bar{A}}\bar{w} \tag{7.8}$$

where $\bar{d}$ is a vector of n_h observations for a particular k_y, and $\bar{w}$ is a vector of n_z values of the function $W(z,k_y)$. The $\bar{\bar{A}}$ matrix is given by

$$a_{ij} = 2\,\Delta z \cos\left(\frac{\Delta z}{z_o}\,\Delta h k_y ij\right) \tag{7.9}$$

Equation (7.8) may be solved for $\bar{w}$ using standard least-square methods. In the process of implementing the solution we found it necessary to constrain the solution, since the matrix $\bar{\bar{A}}^T\bar{\bar{A}}$ is highly singular for low k_y values for the reasons discussed above, even when n_z is less than n_h. General methods for introducing constraints into the matrix $\bar{\bar{A}}$ are discussed by Claerbout [1976]. We chose to minimize the norm N given by

$$N = \bar{e}^T\bar{e} + \gamma\bar{d}^T\bar{d} \tag{7.10}$$

where

$$\bar{e} = \bar{\bar{A}}\bar{w} - \bar{d} \tag{7.11}$$

and γ is chosen empirically. The norm N is minimized by solving

$$(\bar{\bar{A}}^T\bar{\bar{A}} + \gamma\bar{\bar{I}}) = \bar{\bar{A}}^T\bar{d} \qquad (7.12)$$

Figure 7.13 shows the results from applying the wavenumber domain (WD) inversion to the synthetic in figure 7.11. Comparison with figure 7.12 shows that much of the low-dip information has been lost, while the steeply dipping components of the original model were recovered reasonably well. When the wavenumber-domain inversion was applied to the data from figures 7.7 and 7.9, the output was severely contaminated by the impulse responses of the spikes in the data, some of which were caused by instrument errors or cycle jumps in the crosscorrelations. One possible way to deal with this would be to run the inversion, compute a synthetic from the result, compare the synthetic to the data, and set data where the residual exceeds a selected threshold equal to the computed value, and then repeat the process as often as needed. Convergence should be very rapid.

Another possible solution would be to apply an iterative solution technique to the data in the time domain and, rather than minimizing the sum of the residuals squared or the L_2 norm, minimize the sum of the absolute values, the L_1 norm. The L_1 norm gives much better results than the L_2 norm when dealing with data of uneven quality [Claerbout and Muir, 1973; Claerbout, 1976]. The method that we have chosen may be considered a modification of either the Simultaneous Iterative Reconstruction Technique (SIRT) that has been used in the field of medical tomography [Dines and Lytle, 1979], or the Gauss-Seidel method used by Wiggins, et al. [1976] to determine residual statics corrections. These methods proceed as follows: A model is used to compute a synthetic, which is then subtracted from the data to get the residual error. Then the mean residual for all data that are affected by each model parameter is divided by the number of layers and added to that model point. This procedure is repeated several times. Our modification of this algorithm consists simply of replacing the mean in the second step by a median. This has proved very effective in eliminating the undesired effects of spikes in the data. Figure 7.14 shows the result of applying the median - iterative method (MI) to the synthetic in figure 7.11. The result is similar to the result of the WD inversion shown in figure 7.13, except that some of the artifacts related to

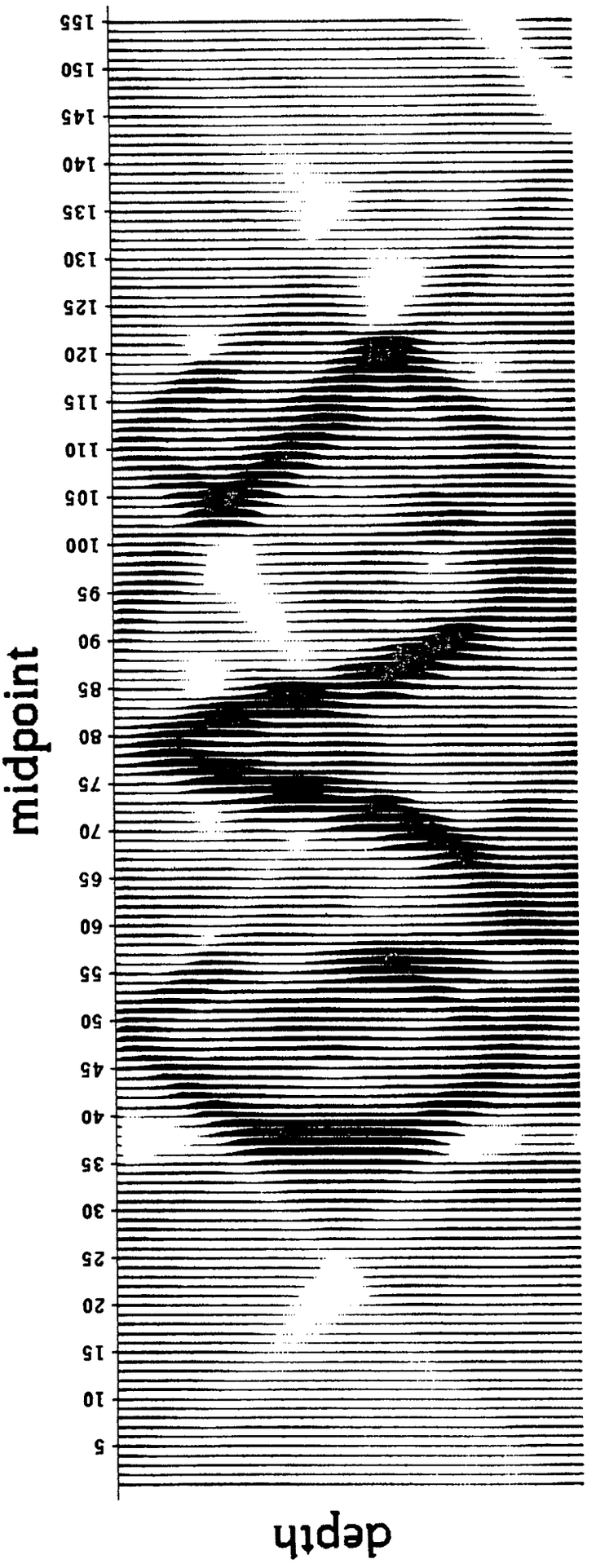

FIG. 7.13. Result of applying the wavenumber-domain inversion to the synthetic in figure 7.11. The interval from the reflector was divided into 40 layers. Note that the components of the original model with dips outside the range of dips used in the calculation of the model have been lost.

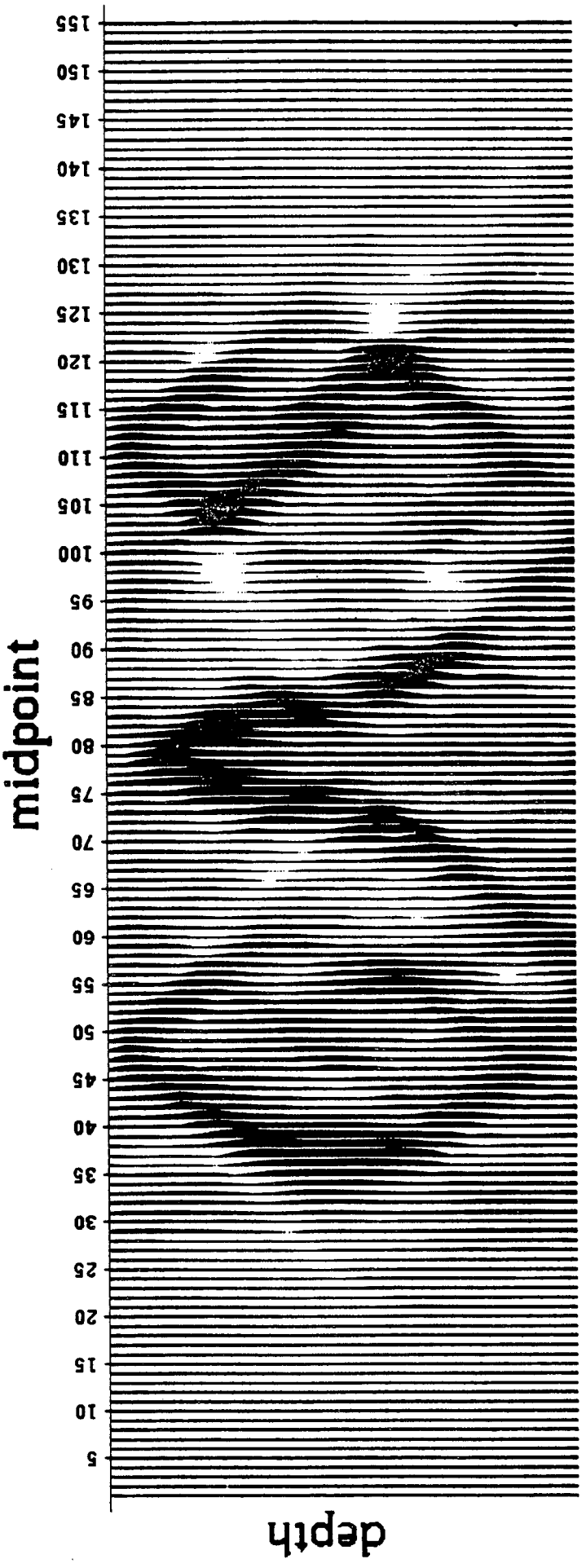

FIG. 7.14. Result of applying the iterative-median inversion to the synthetic in figure 7.11.

the ends of the data on figure 7.13 are absent on figure 7.14. The combined effect of the model calculation and the inversion is in both cases to filter out dips that are outside the range of dips for the rays that sampled the model.

Inversion of Field Data

We applied the MI inversion to the amplitude data in figure 7.7, as well as to the traveltime data. The application of the inversion to the amplitude data rests on two assumptions, that the amplitude fluctuations are caused by absorption, and that the waves are sufficiently band-limited so that equation (7.2) is applicable. Since the data were not deconvolved, it is to be expected that the combined effects of water bottom multiples and shot waveform would result in a highly peaked spectrum and amplitude decay similar to that of a monochromatic wave. This assumption could be made more appropriate by using only the power in a narrow spectral window. Besides absorption, the most likely candidates for the cause of the amplitude fluctuations are scattering and focusing effects caused by lateral variations in velocity. It is difficult to see how scattering could account for amplitude changes by a factor of three, at frequencies as low as 25 Hz. All the reflectors above the bright spot are weak in comparison to the bright spot; consequently all of the transmission coefficients should be close to unity. Focusing from small scale velocity structures can easily result in large amplitude variations. As a working hypothesis we are assuming that the effects of raybending on amplitudes may be neglected. The validity of this assumption remains to be tested.

Figure 7.15 shows the result of the inversion of the amplitude data. The most noteworthy feature of this display is the band of alternating peaks and lows that start near the surface around midpoint 100, reach a depth of about one-quarter the depth to the reflector around midpoint 200, and get gradually shallower toward the right side of the section. Inspection of figure 7.6 shows a series of diffractions at corresponding locations. These diffractions are much less noticeable on the conventional stacked section than on the unstacked data. Since the field data does not carry information about components of the earth model that dip less than the rays at maximum offset, the long wavelength components of the velocity structure are not shown.

We are unable to conclude anything about magnitude of attenuation; only changes over distances less than a cable length are indicated. One constraint that must be satisfied, however, is that the attenuation be non-negative. From laboratory data [Winkler and Nur, 1979], it is known that attenuation is very sensitive to small changes in the state of the rocks and the pore fluids, and can easily change to several times its minimum value.

Figure 7.16 shows the result of applying the inversion to the traveltime data shown in figure 7.9. The noise level is considerably greater than in the amplitude inversion, but the same general features are shown. A clear correlation between peaks in slowness and low attenuation values is evident from the inversions. This is somewhat surprising since higher velocities tend to be associated with lower attenuation in rocks under most, but not all conditions. Laboratory results [Winkler and Nur, 1979; Winkler, 1979; Frisillo and Stewart, 1979] show that attenuation first increases, reaches a peak, and then decreases as gas or air is introduced into a liquid-saturated rock, while P-wave velocity drops with increasing gas saturation. If focusing effects have significant effects on the amplitude anomalies, the tendency would be for the rays that cross through high-velocity lenses to diverge. Further work is needed to determine to what extent this can explain the observed amplitude anomalies.

The main exception from this correlation is the large shallow anomaly around midpoint 110, that shows both time delays and low amplitudes for rays crossing it. This is as would be expected on the basis of the laboratory data if this region contained a diffuse pocket of gas, perhaps connected by faults with the producing gas reservoir that gives rise to the bright-spot reflection.

We have not calibrated the output of the inversions. Most of the observed features appear to be localized and have dimensions that are similar to the spatial resolution of the data. This is in part because the low dip components of the anomalies have been lost. The observed variations in traveltimes are actually quite small - about 10 milliseconds out of a total traveltime of more than 2 seconds, thus a 5% change in velocity over one-tenth of the path could account for the observed effects. A typical amplitude anomaly may be about a factor of 3 in amplitude at 25 Hz; this implies an average

differential Q of about 150 for the whole path or 15 if the attenuation takes place over one-tenth of the path.

Conclusions

The results of this study show that a substantial amount of information is carried in the unstacked seismic data, in both the amplitudes and travel-times of events. The amplitudes carry information about both velocity and intrinsic absorption; the relative importance of the two contributions is still uncertain. Several different techniques are available to analyze this information: we have demonstrated that a relatively simplistic approach can give valuable results when applied to high-quality seismic data. There are a number of ways to improve on some of the assumptions that we have made, and this should result in a corresponding improvement of the results. The velocity and attenuation information thus obtained should be useful, both in the geologic interpretation of the prospects and to improve the stacking and migration of the data.

Appendix A

VISCOELASTIC MODELS

In the literature on viscoelasticity, it is common to describe the behavior of materials through networks of springs and dashpots, often characterized by either relaxation or retardation spectra. It has been claimed that only attenuation models given in terms of such networks are physically realizable, and models derived by other means have been termed "ad hoc" [e.g. Minster, 1978a].

While it is possible to give physical models for attenuation that can not be modelled by spring-dashpot networks, [e.g. Nur and Mavko, 1979], the formulation of viscoelastic models in terms of relaxation spectra is often useful. Gross [1953] has summarized the relationships between the various functions that have been used to characterize viscoelastic materials. In his notation the retardation frequency density function, N(s), is related to the creep function according to

$$\Psi(t) = -\int_0^\infty N(s)e^{-ts}\,ds \qquad \text{(A-1)}$$

and the relaxation frequency density function, $\bar{N}(s)$, is related to the relaxation function according to

$$\bar{\Psi}(t) = \int_0^\infty \bar{N}(s)e^{-ts}\,ds \qquad \text{(A-2)}$$

Kanamori and Anderson [1977] used a a relaxation function of the form

$$\bar{N}(s) = As^{-1} \qquad s_1 < s < s_2 \qquad \text{(A-3)}$$

$$\bar{N}(s) = 0 \qquad \text{elsewhere}$$

to derive an absorption band NCQ model. The constant Q model may be specified

by

$$\bar{N}(s) = \frac{M_0 \sin(2\pi\gamma)}{\pi} (st_0)^{2\gamma} s^{-1} \qquad (A\text{-}4)$$

Using the definition of the gamma function and the identity

$$\Gamma(z)\Gamma(1-z) = \frac{\pi}{\sin(\pi z)} \qquad (A\text{-}5)$$

the constant Q relaxation function (2.20) is readily obtained. Since the constant Q model is mathematically a special case of the power law models of Strick [1967] and Azimi et al. [1968], it follows that those models also have spring-dashpot representations.

Appendix B

LISTING OF FINITE-DIFFERENCE PROGRAMS

```
c       The programs listed here were used to obtain the results
c       shown in figure 6.8. These programs should be portable,
c     except for the input-output routines.
c
c     Finite-difference modeling program, that
c     uses the monochromatic wave equation:
c
c        i
c      ---- Q     +    Q     +     2 m i  Q        =   0
c      2 m    xxz        xx                 z
c
c     Velocity, anelasticity and reflectivity may be
c     arbitrary functions of x and z.
c     An improved approximation for the second derivative
c     is used (variable beta), see FGDP, p. 222.
c     A zero-offset time section is obtained by inversely
c     Fourier transforming the output of this program.
c     Dip filtering is included (see FGDP, p. 225).
c
c        Einar Kjartansson, September 1978.
c
      complex wave(64,64),t(64),d(64),a(64),b(64),e(64),f(64)
      complex aa(64),bb(64)
      complex cv0(64), cexp,cmplx
      complex m,shift,cc3,cc1,rr3,rr1,bab,ra,dipflt
      complex abp(64),cbp(64)
      real q1(64),vel(64),ref(64),gam(64)
      equivalence (a(2),abp(1))  ,  (a(1),cbp(2))
c
c     Read in parameters and set constants.
c
      call rdparm(nom,nx,nz,dom,dx,dz,vis)
      rr1 = (0.,.5)/dz
      rr3 = (0.,2.)*dx*dx/dz
      dipflt = (0.,1.)*vis
      beta = .14
c
c     Clear upgoing wave field.
c
      do 20 iom = 1,nom
         do 20 ix = 1,nx
20          wave (ix,iom) = (0.,0.)
c
c     Take the wave field up through the structure.
c
      do 100 izinv = 1,nz
         iz = nz - izinv + 1
c
```

```
c       Get velocity, 1/Q and reflectivity.
c
        call rdvst(iz,nx,vel)
        call rdqst(iz,nx,ql)
        call rdrst(iz,nx,ref)
        do 40 ix = 1,nx
           gampi =  atan(ql(ix))
           cv0(ix) = cexp((0.,-.5)*gampi)/vel(ix)
40         gam(ix) = gampi/3.141592654
        do 100 iom = 2,nom
           om = (iom-1)*dom
c
c          Apply time shift and
c          compute coefficients.
c
           do 50 ix = 1,nx
              m = -om**(1.-gam(ix))*cv0(ix)
              shift = cexp((0.,1.)*m*dz)
              t(ix) = shift*(wave(ix,iom)+ref(ix))
           m = m + dipflt/vel(ix)
              cc3 = rr3*m
              cc1 = rr1/m + beta*cc3
              aa(ix)= (.5,0.) - cc1
              a(ix) = aa(ix)- (1.,0.)
              bb(ix)  = cc1 + cc1 - (1.,0.) - cc3
50            b(ix) = bb(ix) + (2.,0.)
c
c          Absorbing side condition.
c
           bab = m*cmplx(0.,dx*.25)
           ra = ((1.,0.)+bab) / ((1.,0.)-bab)
           b(1) = b(1) + ra*a(1)
           bb(1) = bb(1) + ra*aa(1)
           b(nx) = b(nx) + ra*a(nx)
           bb(nx) = bb(nx) + ra*aa(nx)
c
c          Solve Crank-Nicolson matrix equation.
c
           d(1) = bb(1)*t(1) + aa(2)*t(2)
              d(nx) = bb(nx)*t(nx) + aa(nx-1)*t(nx-1)
           do 70 ix = 2, nx-1
70            d(ix) = bb(ix)*t(ix)+aa(ix-1)*t(ix-1)+aa(ix+1)*t(ix+1)
           call cvtri(abp,b,cbp,nx,t,d,e,f)
           do 100 ix = 1,nx
100           wave(ix,iom) = t(ix)
c
c    Output the result.
c
     call wrwave(nx,nom,wave)
     stop
     end
```

```
c
c
c     Finite-difference migration program, that
c     uses the monochromatic wave equation:
c
c
c        i
c      ---- Q     +    Q     +     2 m i  Q         =   0
c      2 m    xxz         xx                  z
c
c
c     Velocity may be an arbitrary function of x and z.
c     Anelasticity is not included in this program.
c     An improved approximation for the second derivative
c     is used (variable beta), see FGDP, p. 222.
c     The input to this program is the Fourier tranform of a
c     zero-offset section.
c     Dip filtering is included (see FGDP, p. 225).
c
c        Einar Kjartansson, September 1978.
c
c     Bullet proof version, E.K. april 1979.
c
      complex wave(64,64),t(64),d(64),a(64),b(64),e(64),f(64)
      complex aa(64),bb(64),ref(64)
      complex  cexp,cmplx
      complex shift,cc3,cc1,rr3,rr1,bab,ra,dipflt
      complex abp(64),cbp(64)
      equivalence (a(2),abp(1)) , (a(1),cbp(2))
      real m,vel(64)
c
c     Read in parameters and set constants.
c
      call rdparm(nom,nx,nz,dom,dx,dz,vis)
      rr1 = (0.,.5)/dz
      rr3 = (0.,2.)*dx*dx/dz
      dipflt = (0.,1.)*vis
      beta = .14
c
c     Read the Fourier transform of the surface wave field.
c
      call rdwave(nx,nom,wave)
c
c     Continue the wave field down.
c
      do 150 iz = 1,nz
c
c        Get the velocity and clear the reflector sum.
c        The velocity is taken to be negative in migration.
c
         call rdvst(iz,nx,vel)
         do 40 ix = 1,nx
40          ref(ix) = (0.,0.)
         do 100 iom = 2,nom
```

```
            om = (iom-1)*dom
c
c           Apply time shift and
c           compute coefficients.
c
            do 50 ix = 1,nx
               m = om/vel(ix)
               shift = cexp((0.,1.)*m*dz)
               t(ix) = shift*wave(ix,iom)
                  m = m + dipflt/vel(ix)
               cc3 = rr3*m
               cc1 = rr1/m + beta*cc3
               aa(ix)= (.5,0.) - cc1
               a(ix) = aa(ix)- (1.,0.)
               bb(ix)  = cc1 + cc1 - (1.,0.) - cc3
50             b(ix) = bb(ix) + (2.,0.)
c
c           Absorbing side condition.
c
            bab = m*cmplx(0.,dx*.25)
            ra = ((1.,0.)+bab) / ((1.,0.)-bab)
            b(1) = b(1) + ra*a(1)
            bb(1) = bb(1) + ra*aa(1)
            b(nx) = b(nx) + ra*a(nx)
            bb(nx) = bb(nx) + ra*aa(nx)
c
c           Solve Crank-Nicolson matrix equation.
c
            d(1) = bb(1)*t(1) + aa(2)*t(2)
            d(nx) = bb(nx)*t(nx) + aa(nx-1)*t(nx-1)
            do 70 ix = 2, nx-1
70          d(ix) = bb(ix)*t(ix) + aa(ix-1)*t(ix-1) + aa(ix+1)*t(ix+1)
            call cvtri(abp,b,cbp,nx,t,d,e,f)
            do 100 ix = 1,nx
c
c              Sum to get wave field at t = 0.
c
               ref(ix) = ref(ix) + t(ix)
100            wave(ix,iom) = t(ix)
         do 110 ix = 1,nx
c
c           Subtract wave field at t = 0 to remove wraparound.
c
            ref(ix) = ref(ix)/nom
            do 110 iom = 1,nom
110            wave(ix,iom) = wave(ix,iom) - ref(ix)
150      call wrref(iz,nx,ref)
      stop
      end
```

```
      subroutine rdparm(nom,nx,nz,dom,dx,dz,vis)
c           Suboutine to generate parameters.
      nom = 64
      nx = 64
      nz = 64
      dt = .06
      dom = 2.*3.141592654/(nom*dt)
      dx = .1
      dz = .06
      vis = dom
      return
      end
      subroutine rdvst(iz,nx,vel)
c           Subroutine to generate velocity model
      real vel(nx)
      do 10 ix = 1,nx
10    vel(ix) = 1.
      do 20 ix = 1,iz
20    vel(ix) = 2.
      return
      end
      subroutine rdqst(iz,nx,ql)
c           Subroutine to generate Q model
      real ql(nx)
      do 10 ix = 1,nx
10    ql(ix) = 1./20.
      return
      end
      subroutine rdrst(iz,nx,ref)
c           Subroutine to generate reflector structure.
      real ref(nx)
      if (iz .ne. 48 ) goto 20
      do 10 ix = 1,nx
      xx = (nx + 1.)*.5 - ix
10    ref(ix) = exp(-1.*xx*xx)
      return
20    do 30 ix = 1,nx
30    ref(ix) = 0.
      return
      end
      subroutine rdwave(nx,nom,wave)
c           Subroutine to read in the Fourier transformed wave field.
      complex wave(64,64)
      integer uopen, uread
      logical*1 fn(100)
      call fname('.frq',fn)
      if = uopen(fn,0)
      do 10 iom = 1,nom
10    ir = uread(if,wave(1,iom),512)
      return
      end
      subroutine wrwave(nx,nom,wave)
c           Subroutine to write on disk the wave field.
      complex wave(64,80)
```

```
      integer uwrite,ucreat
      logical*1 fn(100)
      call fname('.frq',fn)
      if = ucreat(fn,"0664)
      do 10 iom = 1,nom
10    ir = uwrite(if,wave(1,iom),512)
      return
      end
      subroutine wrref(iz,nx,ref)
c          Subroutine to write reflector structure on disk.
      complex ref(nx)
      real rref(64)
      logical*1 fn(100)
      integer ucreat,uwrite
      if (iflag .eq. 1) goto 20
      iflag = 1
      call fname('.rst',fn)
      if = ucreat(fn,"0644)
20    do 30 ix = 1,nx
30    rref(ix) = ref(ix)
      nw = uwrite(if,rref,nx*4)
      return
      end
      subroutine cvtri(a,b,c,n,t,d,e,f)
c     Solve a tridiagonal matrix equation with
c     complex and variable coefficients
      implicit complex ( a-h,o-z)
      dimension t(n),d(n),f(n),e(n),a(n),b(n),c(n)
      n1 = n-1
      e(1) = -a(1)/b(1)
      f(1) = d(1)/b(1)
      do 10 i = 2,n1
      den = b(i)+c(i)*e(i-1)
      e(i) = -a(i)/den
10    f(i) = (d(i) - c(i)*f(i-1))/den
      t(n) = (d(n)- c(n)*f(n1))/(b(n)+c(n)*e(n1))
      do 20 j = 1,n1
      i = n-j
20    t(i) = e(i) *t(i+1) + f(i)
      return
      end
```

REFERENCES

Anderson, D.L., H. Kanamori, R.S. Hart and H.-P. Liu, The earth as a seismic absorption band, ***Science***, ***196***, 1104-1106, 1977.

Armstrong, B.H. Background internal friction of heterogenous solids (abstract), ***Geophysics***, ***44***, 334, 1979.

Azimi, S.A., A.V. Kalinin, V.V. Kalinin and B.L. Pivovarov, Impulse and transient characteristics of media with linear and quadratic absorption laws, ***Phys. Solid Earth (Engl. Ed.)***, ***1968***, 88-93, 1968.

Balch A.H. and F.R. Smolka, Plane and spherical transient Voigt waves, ***Geophysics***, ***35***, 745-761, 1970.

Bland, D.R., ***The Theory of Linear Viscoelasticity***, Pergamon Press, New York, 1960.

Bless, S.J. and T.J. Ahrens, Measurements of the longitudinal modulus of Pierre clay shale at varying strain rates, ***Geophysics***, ***42***, 34-40, 1977.

Boltzmann, L., Zur Theorie der elastiche Nachwirkung, ***Annalen der Physik und Chemie***, ***Erganzung***, ***7***, 624-654, 1876.

Boore, D.M., K.L. Larner and K. Aki, Comparison of two independent methods for the solution of wave-scattering problems: response of a sedimentary basin to vertiacally incident SH waves, ***J. Geophys. Res.***, ***76***, 558-569, 1971.

Born, W.T., The attenuation constant of earth materials, ***Geophysics***, ***6***, 132-148, 1941.

Bracewell, R., ***The Fourier Transform and its Applications***, 381 pp., McGraw-Hill, New York, 1965.

Brennan, B.J. and F.D. Stacey, Frequency dependence of elasticity of rock -- test of seismic velocity dispersion, ***Nature***, ***268***, 220-222, 1977.

Brown, R.J.S., and J. Korringa, On the dependence of the elastic prproperties of a porous rock on the compressibility of the pore fluid, ***Geophysics***, ***40***, 608-616, 1975.

Carmichael, I.S.E., J. Nicholls, F.J. Sperra, B.J. Wood, and S. A. Nelson, High-temperature properies of silicate liquids: applications to the equilibration and ascent of basic magma, ***Phil. Trans. R. Soc. Lond. A.***, ***286***, 373-421, 1977.

Claerbout, J.F., Coarse grid calculations of waves in inhomogeneous media with application to delineation of complicated seismic structure, ***Geophysics***,

35,, 407-418, 1970.

Claerbout J.F., and F. Muir, Robust modeling with erratic data, *Geophysics*, *38*,, 826-844, 1973.

Claerbout, J.F., ***Fundamentals of Geophysical Data Processing***, McGraw-Hill, New York, 1976.

Clark, G.B. and G.B. Rupert, Plane and spherical waves in a Voigt medium, *J. Geophys. Res.*, *71*, 2047-2053, 1966.

Clark, S.P., ***Handbook of Physical Constants***, Geol. Soc. Am. mem 97, New York, 1966.

Collins, F. and C.C. Lee, Seismic wave attenuation characteristics from pulse experiments, *Geophysics*, *21*, 16-40, 1956.

Collins, F., Plane compressional Voigt waves, *Geophysics*, *25*, 483-504, 1960.

Dines, K.A. and Lytle, R.J., Computerized gephysical tomography, ***Proceedings of the IEEE***, *67*, 1065-1073, 1979.

Dobrin, M.B., ***Introduction to Geophysical Prospecting***, 3rd edition, McGraw-Hill, New York, 630p, 1976.

Domenico, S.N., Effect of water saturation on seismic reflectivity of sand reservoirs encased in shale, *Geophysics*, *39*, 759769, 1974.

Domenico, S.N., Effect of brine-gas mixture on velocity in an unconsolidated sand reservoir, *Geophysics*, *41*, 882-894, 1976.

Dutta, N.C., and H. Ode, Attenuation and dispersion of compressional waves in fluid-filled rocks with partial gas saturation (White model) - Part I: Biot theroy, *Geophysics*, *44*, 1777-1788, 1979.

Eshelby, J.D., The determination of the elastic field of an ellipsoidal inclusion, and related problems, *Proc. Roy. Soc., Ser. A*, *241*, 376-396, 1957.

Frisillo, A.L., and T.J. Stewart, Effect of partial gas/brine saturations on ultrasonic absorption in sandstone (abstract), ***Stanford University publications in Geological Sciences***, *17*, 24, 1979.

Futterman, W.I., Dispersive body waves, *J. Geophys. Res.*, *67*, 5279-5291, 1962.

Gassmann, F., Elastic waves through a packing of spheres, *Geophysics*, *16*, 673-685, 1951b

Gassmann, F., Uber die Elastizitat poroser Medien, ***Vierteljarhsschrift der Naturforsechenden Gesellshaft in Zurich***, *96*,, 1-21, 1951a.

Gladwin, M.T. and F.D. Stacey, Anelastic degradation of acoustic pulses in

rock, *Phys Earth Planet. Int.*, *8*, 332-336, 1974.

Gordon, R.B. and L.A. Davis, Velocity and attenuation of seismic waves in imperfectly elastic rock, *J. Geophys. Res.*, *73*, 3917-3935, 1968.

Gretener, P.E.F., An analysis of the observed time discrepancies between continuous and conventional well velocity surveys, *Geophysics*, *26*, 1-11, 1961.

Gross, B., *Matematical Structure of the Theories of Viscoelasticity*, 74 pp.,Hermann, Paris, 1953.

Hanks, T.C., Earthquake stress drops, ambient tectionc stresses and stresses tat drive plate motions, *Pure Appl. Geophys.*, *115*, 441-458, 1977.

Hill, D.P., Structure of Lomg Valey Caldera, California, from a seismic refraction experiment, *J.Geophys. Res.*, *81*, 745-753, 1976.

Jaramillo, E.E. and J.D. Colvin, Transient waves in a Voigt medium, *J. Geophys. Res.*, *75*, 5767-5773, 1970.

Johnston, D.H. and N. Toksoz, Attenuation of seismic waves in dry and satruated rocks (abstract), *Geophysics*, *42* 1511, 1977.

Jonscher, A.K., The "universal" dielectic response, *Nature*, *267*, 673-679,1977.

Jordan, T.H. and S.A. Sipkin, Estimation of the attenuation operator for multiple ScS waves, *Geophys. Res. Lett.*, *4*, 167-170, 1977.

Kanamori, H. and D.L. Anderson, Importance of physical dispersion in surface wave and free oscillation problems: review, *Rev. Geophys. Space. Phys.*, *15*, 105-112, 1977.

Keenan, J.H., F.G. Keyes, P.G. Hill, and J. G. Moore, *Steam Tables*, John Wiley, New York, 1969.

Kelly, D.C., *Thermodynamics and Statistical Physics*, p. 142-143, Academic Press, New York, 1973.

Kjartansson, E., Constant Q - wave propagation and attenuation, *J.Geophys. Res.*, *84*, 4737-4748, 1979.

Kjartansson, E., Thermal relaxation, an attenuation mechanism for porous rocks (abstract), *EOS Trans. AGU*, *59*, 324, 1978.

Knopoff, L., Q, *Rev. Geophys. Space Phys.*, *2*, 625-660, 1964.

Kogan, S.Y., A brief review of seismic wave absorption theories II *Phys. Solid Earth (Engl. Ed.)*, *1966*, 678-683, 1966.

Kolsky, H., The propagation of stress pulses in viscoelastic solids, *Phyl.*

Mag., *1*, 693-710, 1956.

Korringa, J., R.J. Brown, D.D. Thompson and R.J. Runge, Self-consistent imbedding and the ellipsoidal model for porous rocks, *J.Geophys. Res.*, *84*, 5591-5598, 1979.

Liu, H.-P., D.L. Anderson and H. Kanamori, Velocity dispersion due to anelasticity; implications for seismology and mantle composition, *Geophys. J. Roy. Astron. Soc.*, *47*, 41-58, 1976.

Lockner, D.A., J.B. Walsh and J.D. Byerlee, Changes in seismic velocity and attenuation during defromation of grainite, *J. Geophys. Res.*, *82*, 5374-5378, 1977.

Lomnitz, C., Creep measurements in igneous rocks, *J. Geol.*, *64*, 473-479, 1956.

Lomnitz, C., Linear dissipation in solids, *J. Appl. Phys.*, *28*, 201-205, 1957.

Lomnitz, C., Application of the logarithmic creep law to stress wave attenuation in the solid earth, *J. Geophys. Res. 67*, 365-368, 1962.

Lundquist, G., Evidence for a frequency dependent Q (abstract), *EOS Trans. AGU*, *58*, 1182, 1977.

Lynn, H.B, Migration and interpretation of deep crustal seismic reflection data, Ph.D. dissertation, Stanford University, Stanford, Calif., 1979.

Lynn, H.B., L. Gagnon, E., Kjartansson, and D. Seeburger, Migrations and interpretations in latrally varying media, Wind River Thrust, Wyoming, paper presented at 49th annual meeting of the SEG, New Orleans, Nov 6th, 1979.

Majer, E.L., and T.V. McEvilly, Seismological investigations at the Geysers geothermal field, *Geophysics*, *44*, 246-269, 1979.

Mavko, G.M., Frictional attenuation: an inherent amplitude dependence, *J. Geophys. Res.*, *84*, 4769-4776, 1979.

Mavko, G.M., and A. Nur, The effect of nonelliptical cracks on the compressibility of rocks, *J.Geophys. Res.*, *83*, 4459-4468, 1978.

Mavko, G.M., and A. Nur, Wave attenuation in partially saturated rocks, *Geophysics*, *44*, 161-178, 1979.

Mavko, G.M., E. Kjartansson and K. Winkler, Seismic wave attenuation in rocks, *Rev. of Geophys. and Space Phys.*, *17*, 1155-1164, 1979.

Mavko, G.M., Velocity and attenuation in partially molten rocks, submitted to *J. Geophys. Res.* 1979.

McDonal, F.J., F.A. Angona, R.L. Mills, R.L. Sengbush, R.G. van Nostrand and J.E. White, Attenuation of shear and compressional waves in Pierre shale,

Geophysics, *23*, 421-439, 1958.

McKavanagh, B.M. and F.D. Stacey, Mechanical hysteresis in rocks at low strain amplitudes and seismic frequencies, *Phys. Earth Plan. Int.*, *8*, 246-250, 1974.

Mindlin, R.D., and H. Deresiewicz, Elastic spheres in contact under varying oblique forces, *J. Appl. Mech.*, *20*, 327-344, 1953.

Minster J.B., Transient and impulse responses of a one-dimensional linearly attenuating medium - I. Analytical results, *Geophys. J. Roy. Astron. Soc.*, *52*, 479-501, 1978a.

Minster J.B., Transient and impulse responses of a one-dimensional linearly attenuating medium - II. A parametric study, *Geophys. J. Roy. Astron. Soc.*, *52*, 503-524, 1978b.

Munasinghe, M. and G.W. Farnell, Finite difference analysis of Rayleigh wave scattering at vertical discontinuities, *J. Geophys. Res.*, *78*, 2454-2466, 1973.

Nur, A., and G. Simmons, The effect of saturation on velocity in low porosity rocks, *Earth. Plan. Sci. Lett.*, *7*, 183-193, 1969.

O'Connell, R.J. and B. Budiansky, Measures of dissipation in viscoelastic media, *Geophys. Res. Lett.*, *5*, 5-8 1978.

O'Connell, R.J., and B.Budinasky, Seismic velocities in dry and saturated cracked solids, *J.Geophys. Res.*, *79*, 5412-5426, 1974.

Pandit, B.I. and J.C. Savage, An experimnetal test of Lomnitz's theory of internal friction in rocks, *J. Geophys. Res.*, *78*, 6097-6099, 1973.

Pandit, B.I., and C.C. Tozer, Anamalous propagation of elastic energy within the moon, *Nature*, *226*, 335, 1970.

Reiter, L. and M.E. Monfort, Variataions in initial pulse width as a function of anelastic properies and surface geology in central California, *Bull. Seismol. Soc. Am.*, *67*, 1319-1338, 1977.

Ricker, N., The form and laws of propagation of seismic wavelets, *Geophysics*, *18*, 10-40, 1953.

Ricker, N., *Transient Waves in Visco-Elastic Media*, 278 pp., Elsevier, Amsterdam, 1977.

Robinson, J.C., A technique for the continous representation of dispersion in seismic data, *Geophysics*, *44*, 1345-1251, 1979.

Savage, J.C., Attenuation of elastic waves in granular mediums, *J. Geophys.*

Res., *70*, 3935-3942, 1965.

Savage, J.C., Thermoelastic attenuation of elastic waves by cracks, *J. Geophys. Res.*, *71*, 3929-3938, 1966.

Savage, J.C., Comments on paper by R.B. Gordan and L.A. Davis, "Velocity and attenuation of seismic waves in imperfectly elastic rock", *J. Geophys. Res.*, *74*, 726-728, 1969.

Savage, J.C. and H.S. Hasegawa, Evidence for a linear attenuation mechanism, *Geophysics*, *32*, 1003-1014, 1967.

Schoenberger, M. and F.K. Levin, Apparent atteunuation due to intrabed multiples, II, *Geophysics*, *43*, 730-737, 1978.

Sheriff, R.E., Factors affecting seismic amplitudes, *Geophys. Pros.*, *23*, 125-138, 1975.

Simmons, G. and W.F. Brace, Comparison of static and dynamic measurements of compressibility of rocks, *J. Geophys. Res.*, *70*, 5649-5656, 1965.

Strick, E., The determination of Q, dynamic viscosity and creep curves from wave propagation measurements, *Geophys. J. Roy. Astron. Soc.*, *13*, 197-218, 1967.

Strick, E., A predicted pedestal effect for pulse propagation in constant-Q solids, *Geophysics*, *35*, 387-403, 1970.

Strick, E., An explanation of observed time discrepancies beween continuous and conventional well velocity surveys, *Geophysics*, *36*, 285-295, 1971.

Tittmann, B.R., Intermal friction measurements and their implications in seismic Q structure models of the earth's crus, in *The Earth's Crust*, Geophys. Monog. Series, Vol. 20, ed. by J.Heacock, 197-213, 1978.

Tittmann, B.R., M. Abdel-Gawad, and R.M. Housley, Elastic velocity and Q measurements on Apollo 12, 14, 15 rocks, *Proc. Lunar Sci. Conf. 3rd*, 2565-2575, 1972.

Vaisnys, J.R., Propgataion of acoustic waves through a system undergoing phase transformations, *J. Geophys. Res.*, *73*, 7675-7683, 1968.

Voigt, W., Uber innere Ribung fester Korper, insbesondere der Metalle, *Annalen der Physik und Chemie, Neue Folge*, *47*, 671-693, 1892.

Walsh, J.B., Seismic wave attenuation in rock due to friction, *J. Geophys. Res.*, *71*, 2591-2599, 1966.

Walsh, J.B., The effect of cracks on the compressibility of rock, *J. Geophys. Res.*, *70*, 381-389, 1965.

Weast, R.C. ed., *Handbook of Chemistry and Physics*, 46th edition, The Chemical

Rubber Company, Cleveland, 1966.

White, J.E., Computed seismic speeds and attenuation in rocks with partial gas saturation, ***Geophysics***, ***40***, 224-232, 1975.

Wiggins, R., K. Larner and R.,D. Wisecup, Residual statics analysis as a general linear inverse problem, ***Geophysics***, ***41***, 922-938, 1976.

Winkler, K. and A. Nur, Pore fluids and seismic attenuation in rocks, ***Geophys. Res. Lett.***, ***6***, 1-4, 1979.

Winkler, K., A. Nur and M. Gladwin, Friction and seismic attenuation in rocks, ***Nature***, ***277***, 528-531, 1979.

Winkler, K., The effects of pore fluids and frictional sliding on seismic attenuation, Ph.D. dissertation, 188pp., Stanford Univ., Stanford, Calif., 1979.

Wong, T.-F., and W.F. Brace, Thermal expansion of rocks: some measurements at high pressure, ***Tectonophysics***, ***57***, 95-117, 1979.

Zener, C.M., ***Elasticity and Anelasticity of Metals***, Univ. of Chicago Press, 1948.